Arctic Report Card 2024

The rapid pace and complexity of Arctic change demand new and strengthened Arctic adaptation and global reductions of fossil fuel pollution.

DOI: 10.25923/b7c7-6431

T.A. Moon, M.L. Druckenmiller and R.L. Thoman; Eds.

December 2024

Twila A. Moon, Matthew L. Druckenmiller, Richard L. Thoman; Editors
Cynthia Garcia; NOAA Coordinating Editor
Sandy Lucas; NOAA Federal Advisor

arctic.noaa.gov/Report-Card

How to Cite Arctic Report Card 2024
Citing the complete report or Executive Summary:
Moon, T. A., M. L. Druckenmiller, and R. L. Thoman, Eds., 2024: *Arctic Report Card 2024*, https://doi.org/10.25923/b7c7-6431.

Citing an essay (example):
Mudryk, L. R., A. Elias Chereque, C. Derksen, K. Luojus, and B. Decharme, 2024: Terrestrial Snow Cover. *Arctic Report Card 2024*, T. A. Moon, M. L. Druckenmiller, and R. L. Thoman, Eds., https://doi.org/10.25923/4bb3-3f87.
(Note: Each essay has a unique DOI assigned)

Front cover photo credits
Center: *Sun sets over Utqiaġvik, Alaska, in spring.* Credit: Matthew L. Druckenmiller, NSIDC
Bottom Right: *Caribou above Harrison Creek, Alaska Steese National Conservation Area.* Credit: Jim Herriges, BLM
Bottom Left: *Seward Peninsula, Alaska.* Credit: Gerald (JJ) Frost, Alaska Biological Research, Inc.

Funding Acknowledgments for the Arctic Report Card
Financial support for Arctic Report Card 2024 was provided by NOAA's Global Ocean Monitoring and Observing (GOMO) Arctic Research Program, including content editing funded through the Cooperative Institute for Earth System Research and Data Science (CIESRDS) via NOAA Cooperative Agreement NA22OAR4320151 (Druckenmiller and Moon) and by the Cooperative Institute for Climate, Ocean, and Ecosystem Studies (CICOES) under NOAA Cooperative Agreement NA20OAR4320271 (Thoman). The editors thank the Arctic Monitoring and Assessment Programme (AMAP) Secretariat for organizing the independent peer review and all the reviewers. The editors also recognize the contribution of coordinating editor Cynthia Garcia from the Arctic Research Program in NOAA's GOMO, who coordinated and managed the various elements of the ARC's production process, and the entire ARC production team for the professionalism, dedication, and enthusiasm in producing each year's Report.

Table of Contents

2024 Headlines

The rapid pace and complexity of Arctic change demand new and strengthened Arctic adaptation and global reductions of fossil fuel pollution.

The Arctic continues to warm at a faster rate than the global average. The 2024 Arctic Report Card highlights record-breaking and near-record-breaking observations that demonstrate dramatic change, including Arctic tundra transformation from carbon sink to carbon source, declines of previously large inland caribou herds, and increasing winter precipitation. Observations also reveal regional differences that make local and regional experiences of environmental change highly variable for people, plants and animals. Adaptation is increasingly necessary and Indigenous Knowledge and community-led research programs are essential to understand and respond to rapid Arctic changes.

Headlines

In the air

- Arctic annual surface air temperatures ranked second warmest since 1900.
- Autumn 2023 and summer 2024 were especially warm across the Arctic with temperatures ranking 2nd and 3rd warmest, respectively.
- An early August 2024 heatwave set all-time record daily temperatures in several northern Alaska and Canada communities.
- The last nine years are the nine warmest on record in the Arctic.
- Summer 2024 across the Arctic was the wettest on record.
- Arctic precipitation has shown an increasing trend from 1950 through 2024, with the most pronounced increases occurring in winter.

In the ocean

- In September 2024, the extent of sea ice, which has a profound influence on the Arctic environment, was the sixth-lowest in the 45-year satellite record.
- All 18 of the lowest September minimum ice extents have occurred in the last 18 years.
- Arctic Ocean regions that are ice-free in August have been warming at a rate of 0.5°F (0.3°C) per decade since 1982.
- In most of the shallow seas that ring the Arctic Ocean, August mean sea surface temperatures were 3.6-7.2°F (2-4°C) warmer than 1991-2020 averages, though the Chukchi Sea was 1.8-7.2°F (1-4°C) cooler than average.
- Long-term ocean primary productivity—plankton blooms—continue to increase in all Arctic regions, except for the Pacific Arctic, throughout the observational record of 2003-24. However, in 2024, lower-than-average values were dominant across much of the Arctic.
- Ice seal populations remain healthy in the Pacific Arctic, though the ringed seal diet is shifting from Arctic cod to saffron cod with warming waters.

On land

- When including the impact of increased wildfire activity, the Arctic tundra region has shifted from storing carbon in the soil to becoming a carbon dioxide source. Circumpolar wildfire emissions have averaged 207 million tons of carbon per year since 2003.
- The Arctic remains a consistent methane source.
- Alaskan permafrost temperatures were the second warmest on record.
- Warmer temperatures impact caribou movements and survival through direct summer heat and changes in winter snow and ice conditions, with regional variations in population declines and recoveries.
- Arctic migratory tundra caribou populations have declined by 65% over the last 2-3 decades. While the generally smaller coastal herds of the western Arctic have seen some recovery over roughly the last decade, previously large inland herds are continuing a long-term decline or remain at the lowest populations noted by Indigenous elders.
- Summer heat impacts on caribou herds are projected to increase over the next 25-75 years, requiring shared knowledge between scientists and northern communities for management strategies.
- Snow accumulation during the 2023/24 winter was above average across both the Eurasian and North American Arctic.
- Despite above-average snow accumulation, the snow season was the shortest in 26 years over portions of central and eastern Arctic Canada. Arctic snow melt is occurring 1-2 weeks earlier than historical conditions throughout May and June.
- Greenland Ice Sheet mass loss lowest since 2013.
- Tundra greenness, a measure of expanding tundra vegetation cover and biomass due to warming temperatures, ranked second highest in the 25-year satellite record.

Indigenous Knowledge and partnerships

- Indigenous hunters are the original researchers of their homelands, with observation and monitoring skills integral to traditional practices.
- The Ittaq Heritage and Research Centre in Kangiqtugaapik (Clyde River), Nunavut, Canada operates the Angunasuktiit program, teaching traditional hunting and harvesting to new generations.
- Supporting Indigenous leadership in Arctic research requires sustained support of Indigenous ways of life and knowledge generation.

Executive Summary

https://doi.org/10.25923/b7c7-6431

T. A. Moon[1], M. L. Druckenmiller[1], and R. L. Thoman[2,3]

[1]National Snow and Ice Data Center, Cooperative Institute for Research in Environmental Sciences, University of Colorado Boulder, Boulder, CO, USA
[2]Alaska Center for Climate Assessment and Policy, University of Alaska Fairbanks, Fairbanks, AK, USA
[3]International Arctic Research Center, University of Alaska Fairbanks, Fairbanks, AK, USA

The Arctic continues to warm faster than the globe overall and in 2024, for the 11th year in a row, Arctic temperature anomalies were higher than the global average. With 2024 on track to be the world's hottest year on record, on the heels of a 2023 record, heightened Arctic warming is even more alarming. The 2024 Arctic Report Card (ARC2024) brings forward direct observations of record-breaking and near-record breaking conditions that combine with stark regional differences to make local and regional experiences of environmental change highly variable for people, plants, and animals. The geographic designation of the Arctic has many definitions (e.g., here are a few). Each ARC2024 essay notes the geography of focus for the observations discussed. ARC2024 provides an annual update on eight Arctic *Vital Signs*, from ocean primary productivity and surface temperatures to tundra greenness and snow cover, and examines three *Indicator* topics on Alaska ice seals, North American caribou, and Arctic lands as sources of global heat-trapping carbon emissions. The ARC2024 *Frostbite* contributed by the Ittaq Heritage and Research Centre in Kangiqtugaapik (Clyde River), Nunavut is a powerful reminder that Arctic Indigenous hunters and harvesters are the region's original researchers, developing complex and nuanced knowledge frameworks that are vital for Arctic Indigenous peoples and contribute to local to global research and observations.

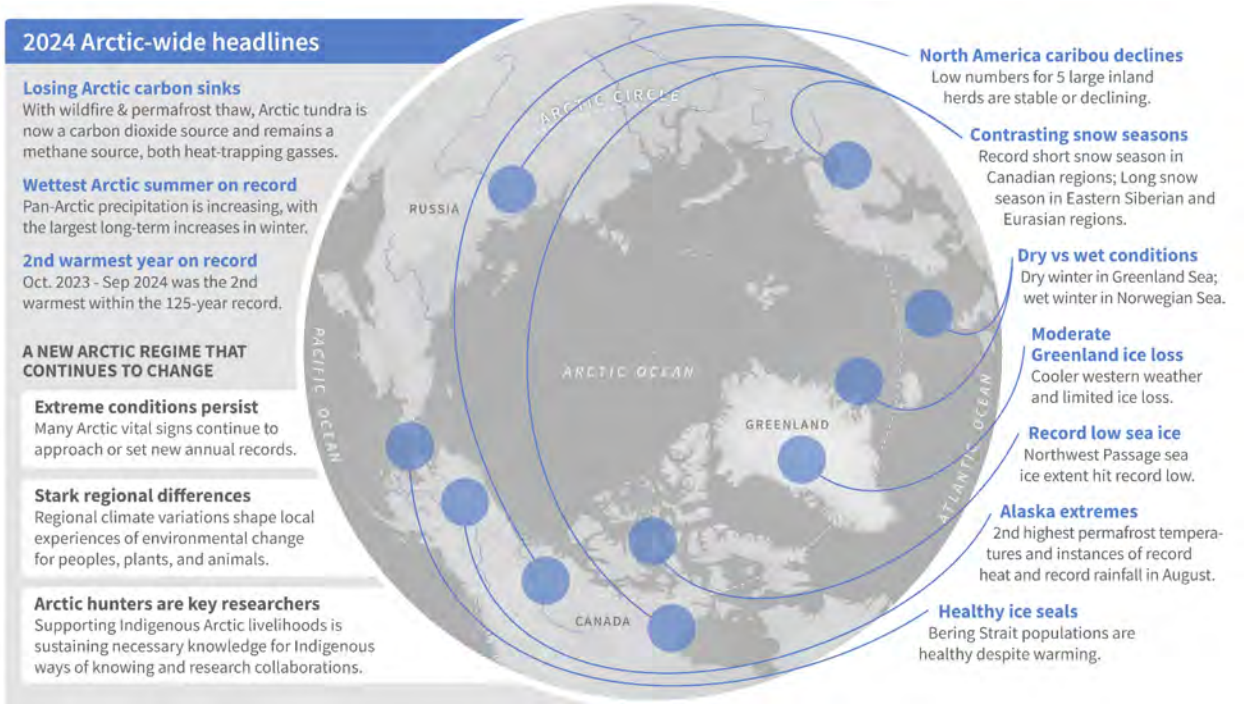

Fig. 1. A sample of notable events and important topics from across the Arctic.

Fig. 2. The ARC2024 map provides a general geographic reference for many locations mentioned in this year's report.

The multidecadal records for many *Vital Signs* suggest that the Arctic exists now within a "new regime", with recent observations that are not always setting new annual records but are still consistently within a more extreme range compared to past baseline records. For example, though the minimum sea ice extent for 2024 was only the sixth lowest on record (beginning in 1979), the last 18 September extents are the 18 lowest within those 45 years. At the same time, the extent of thicker, older ice, which is an important habitat for many species, has remained very low since 2007. Similarly, sea surface temperatures in the Arctic did not climb to record levels in 2024, yet a long-term warming trend is clear and most Arctic Ocean marginal seas were ~2-4°C (3.6-7.2°F) warmer in August 2024 than the 1991-2020 baseline. One more example from the marine environment is overall high primary productivity, including sharp increases in some seas during the 2003-24 observational record.

Framing the Arctic as in a "new regime" underscores that the region today is dramatically changed from even a decade or two ago, yet it must not imply that the Arctic climate has stabilized under human-caused warming. Projections of climate change for the next several decades are clear: change will continue. Every year the Arctic Report Card includes observations that bring sometimes surprising and often sobering news about the Arctic environment. This year, the *Indicator* essay on carbon cycling notes that permafrost warming trends continue, with Alaska observations showing the 2nd warmest permafrost temperatures on record. The essay also discusses a multidecadal increase in wildfires across North American permafrost regions, with wildfires now an urgent, annual concern for Arctic residents.

These changes together are pushing the Arctic into uncharted territory; the Arctic tundra region has shifted to being a global source of carbon dioxide (CO_2) rather than a carbon sink, and the region continues to be a methane (CH_4) source as well. Both powerful heat-trapping gasses, the transition to acting as a source for both CO_2 and CH_4 is of global concern as societies struggle to rein in emissions and align with the international Paris Agreement goal to limit warming. Common understandings of the timing and character of Arctic seasons are also now challenged. For example, over the past 15 years, Arctic snow melt has commonly occurred 1-2 weeks earlier in May and June for both North America and Eurasia as compared to historical conditions.

Focusing on annual and long-term averages, however, can mask another key characteristic of the Arctic today: stark regional differences that can make it challenging to plan for certain weather conditions and create strongly contrasting experiences of Arctic change. Even with above average snow accumulation for the 2023/24 winter and a longer than average snow season in Eurasian Arctic regions, portions of central and eastern Arctic Canada had the shortest snow season in the 26-year record. Despite the Arctic experiencing the second warmest summer on record overall, weather patterns brought cooler conditions to western Greenland and the Greenland Ice Sheet experienced only modest ice loss. Losing only 55 ± 35 Gt of ice mass during September 2023-August 2024, this was the lowest annual ice loss since 2013. Late fall (October-December) 2023 saw drier conditions than usual over the East Greenland and Barents Seas, while just southeast of this area conditions were wetter than usual over northern Eurasia. Tundra greenness is another good example. While the 2024 circumpolar average greenness value was the second highest in the 25-year record, continuing a recent sequence of high greenness values, smaller zones across the Siberian tundra were anomalously brown.

The Arctic works as a complex, connected system. Some system connections are easier to see. For example, the Chukchi Sea west of Alaska experienced cooler than normal spring and summer air temperatures, low sea surface temperature for August 2024, and the persistence of an unusually long-lived zone of sea ice, which was formed by strong convergence and deformation in spring. There is little doubt that these conditions fed into each other, revealing how regional air temperatures, water temperatures, and ocean dynamics shape ice conditions that in turn have consequences for marine life and coastal communities. But we must refrain from extrapolating any one year's apparent connections to predict long-term system change; instead we must follow the story of long-term observations. For example, ice seal populations, including ringed, bearded, spotted, and ribbon seals, across the Bering to Chukchi Seas remain healthy despite dramatic long-term warming and sea ice loss within their habitat. Yet, ringed seal diets are showing an increase in saffron cod and decrease in Arctic cod, which is predicted with warmer water. We do not yet know how seals' adaptive capacities are being limited or enhanced by the complex ecological changes and shifts they are experiencing. Continued monitoring and collaboration across topics, organizations, and communities is necessary.

The Arctic environment of 2024 is already dramatically changed from decades past and change will continue for decades to come. For some plants and animals, these changes may prove devastating. North American migratory tundra caribou numbers have decreased by 65% since a peak in the 1990s and early 2000s. While the generally smaller coastal herds of the western Arctic have seen some recovery over roughly the last decade, previously large inland herds are continuing a long-term decline or remain at the lowest populations noted by Indigenous elders. The ability of caribou to adapt to climate change by moving to new regions can also be limited by roads and development. Herds like the Bathurst Herd in north central Canada are under serious threat, a grave concern for local peoples whose food security has been tied to these animals since time immemorial.

Arctic residents are responding in the moment to the changes underway, and the deep observational skills of those like the Indigenous hunters in the Kangiqtugaapik region are helping their communities understand, prepare, and take action. While we can hope that many plants and animals will find pathways for adaptation, as ice seals in the Bering Strait have so far, hope is not a pathway for preparation or risk reduction. Only the strongest actions on mitigating heat-trapping gas emissions, with almost all human-produced emissions created outside of the Arctic, will allow us to minimize risk and damage into the future. Support for observations, collaboration, and adaptation is required in every scenario. In our connected Earth system, we all have a role to play to minimize risk, support adaptation, and foster collaboration to realize the best possible outcomes within the challenging pathway ahead.

December 7, 2024

Surface Air Temperature

https://doi.org/10.25923/mjhx-3j40

T. J. Ballinger[1], A. Crawford[2], M. C. Serreze[3], S. Bigalke[4], J. E. Walsh[1,5], B. Brettschneider[6], R. L. Thoman[1,5], U. S. Bhatt[7], E. Hanna[8], H. Motrøen Gjelten[9], S. -J. Kim[10], J. E. Overland[11], and M. Wang[11,12]

[1]International Arctic Research Center, University of Alaska Fairbanks, Fairbanks, AK, USA
[2]Department of Environment and Geography, University of Manitoba, Winnipeg, MB, Canada
[3]National Snow and Ice Data Center, Cooperative Institute for Research in Environmental Sciences, University of Colorado Boulder, Boulder, CO, USA
[4]Department of Geography, Portland State University, Portland, OR, USA
[5]Alaska Center for Climate Assessment and Policy, University of Alaska Fairbanks, Fairbanks, AK, USA
[6]National Weather Service Alaska Region, NOAA, Anchorage, AK, USA
[7]Geophysical Institute, University of Alaska Fairbanks, Fairbanks, AK, USA
[8]Department of Geography and Lincoln Climate Research Group, University of Lincoln, Lincoln, UK
[9]Norwegian Meteorological Institute, Oslo, Norway
[10]Korea Polar Research Institute, Incheon, Republic of Korea
[11]Pacific Marine Environmental Laboratory, NOAA, Seattle, WA, USA
[12]Cooperative Institute for Climate, Ocean, and Ecosystem Studies, University of Washington, Seattle, WA, USA

Headlines

- Arctic (60-90° N) annual surface air temperatures for October 2023-September 2024 ranked 2nd warmest since 1900.
- Autumn 2023 and summer 2024 were especially warm across the Arctic with temperatures ranking 2nd and 3rd warmest, respectively.
- An early August 2024 heatwave produced record daily temperature maxima in several northern Alaska and Canada communities.

Overview

Rising surface air and ocean temperatures characterize the changing Arctic (Ballinger et al. 2023; Timmermans and Labe 2023; see essay *Sea Surface Temperature*). The increase in Arctic (60-90° N) surface air temperature continues to exceed that for the planet as a whole (90° S-90° N), a phenomenon termed Arctic Amplification. Recent studies have shown that, after accounting for natural variability, the Arctic is warming approximately three times faster than the global mean based on observational data and climate model simulations since 1980 (Sweeney et al. 2023; Zhou et al. 2024). There are many documented physical indicators of a warming Arctic. Recent decades have witnessed springtime snow cover declines on Arctic lands (see essay *Terrestrial Snow Cover*), summer sea ice losses (see essay *Sea Ice*), and Greenland Ice Sheet mass loss (see essay *Greenland Ice Sheet*). Extreme events are also becoming more frequent (Overland 2024) and their character is changing over time (e.g., Arctic cold extremes are warming at twice the rate as pan-Arctic annual temperatures since 1979; Polyakov et al. 2024). The warming Arctic has palpable ecological impacts at various spatial scales, which have been

documented in past and present Arctic Report Cards; for example, western Alaska salmon (Schoen et al. 2023) and western Arctic caribou (see essay *Migratory Tundra Caribou in a Warmer Climate*) populations have shown sensitivity to rising temperatures.

As with Surface Air Temperature essays in previous Arctic Report Cards, the sections that follow offer a historical perspective on this past year's Arctic air temperatures and highlight notable seasonal anomaly patterns and extremes.

Annual and seasonal air temperatures in context

Air temperatures at the annual scale are described in terms of the water year (i.e., October 2023-September 2024 represents 2024). Three-month seasons are therefore referenced as follows: autumn 2023 (October-December), winter (January-March), spring (April-June), and summer (July-September) 2024. These seasons span the annual cycles of the Vital Sign variables consistently described in the Arctic Report Card.

Annual Arctic and global surface air temperature anomalies (i.e., departures from average) from NASA's GISTEMP version 4 dataset (see *Methods and data*) are shown in Fig. 1a. This past year was the Arctic's 2nd warmest on record since 1900 with anomalies of 1.20°C above the 1991-2020 mean. While 2024 is on track to be the warmest year on record globally since at least 1900, Arctic temperature anomalies continue to be larger. This is the 11th consecutive year in which Arctic regional temperature departures exceeded those of the Earth as a whole. This past decade has been the Arctic's warmest, and has been characterized by several new annual and seasonal records.

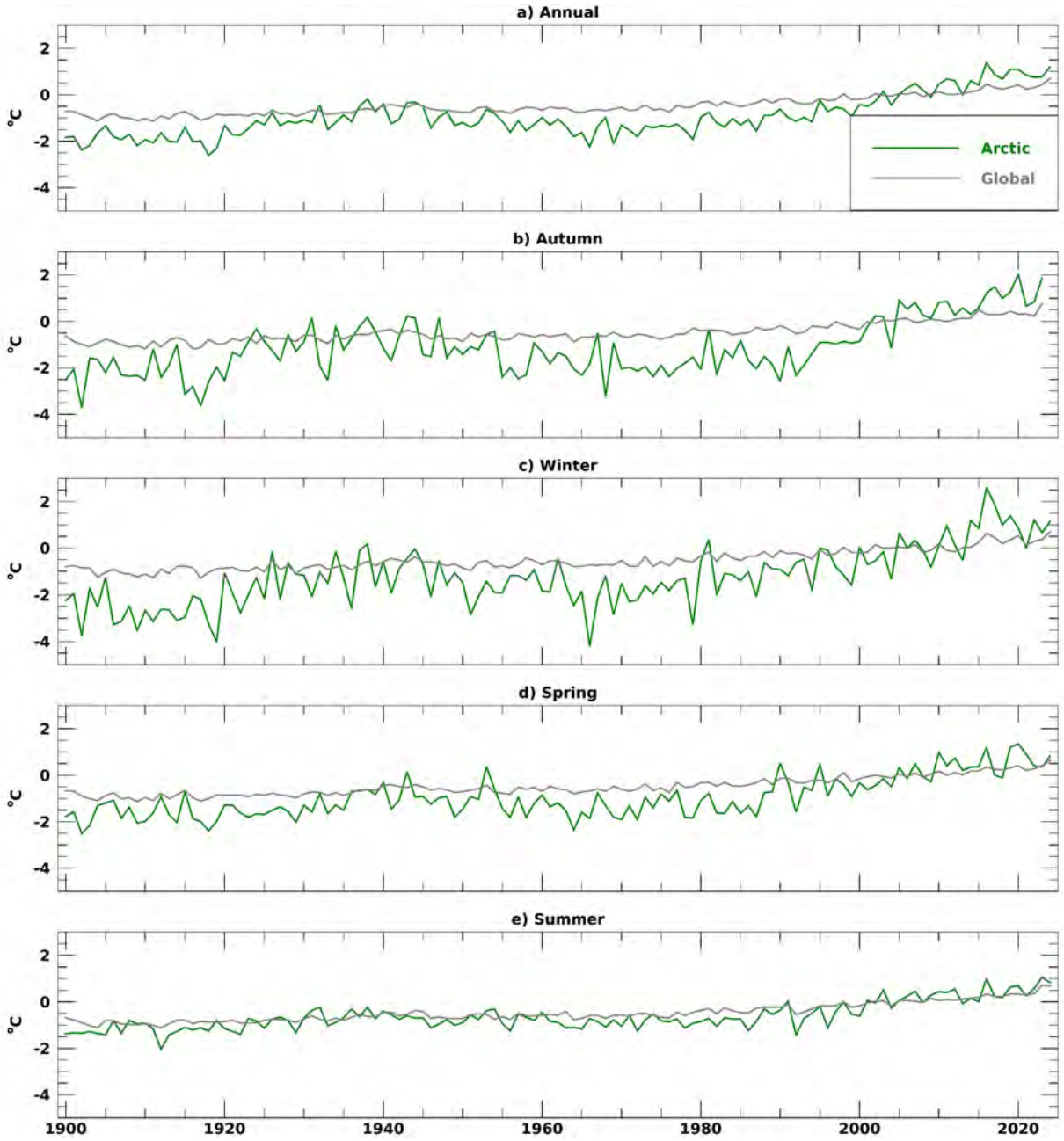

Fig. 1. Time series of (a) annual, (b) autumn, (c) winter, (d) spring, and (e) summer surface air temperature anomalies (°C) relative to the 1991-2020 mean and averaged across Arctic (60-90° N) and Global (90° S-90° N) land and ocean areas. Annual time series in a) reflect the water year average (i.e., October 2023-September 2024 represents the 2024 SAT value). Source: NASA GISTEMP v4 data are obtained from the NASA Goddard Institute for Space Studies.

Arctic seasonal temperature anomalies were also comparatively higher than the global average (Fig. 1b-d). This is striking given that seasonal global temperature records were also set during autumn 2023, and winter and spring 2024. Seasonal temperature departures were some of the warmest in the Arctic since 1900, with autumn at 1.86°C (2nd warmest), winter at 1.14°C (6th warmest), spring at 0.82°C (6th warmest), and summer at 0.83°C (3rd warmest).

The annual and seasonal air temperature anomalies display a clear and rather consistent depiction of Arctic Amplification (Fig. 1). Several mechanisms and feedbacks underlie Arctic Amplification, and some have seasonally-dependent expressions. Poleward heat and moisture transport driven by weather pattern variability can contribute to warm extremes year-round, whereas albedo feedbacks involving the amount and quality of snow and ice cover are constrained by sunlight that is prevalent in the warm season and absent at the highest northern latitudes during winter months (Cohen et al. 2020). During autumn and winter, when Arctic Amplification is strongest, the accumulation of heat in the Arctic Ocean is released to the overlying atmosphere driving warmer air temperatures (Taylor et al. 2022). Patterns of seasonal air temperature anomalies align with some of these processes responsible for Arctic Amplification.

Seasonal air temperature anomaly patterns

Seasonal air temperature anomaly patterns are shown in Fig. 2. Autumn 2023 was characterized by positive anomalies covering much of the high latitude Eurasian and North American Arctic lands. Of note is a +4-6°C area over much of northern and western Canada, the North Slope of Alaska, and the eastern Beaufort Sea (Fig. 2a). Autumn anomalies of 6°C, representing record high temperatures since 1950, covered much of the Canadian Archipelago and adjacent northern mainland coasts of Nunavut and the Northwest Territories. Below-average sea-level pressure (SLP) prevailed over the North American high latitudes during this time, suggesting more frequent storms produced warm air advection that contributed to the positive anomalies (Fig. 3a). Above-average sea surface temperature and delayed sea ice formation in the Beaufort Sea and Canadian Arctic Archipelago also may have contributed to warmer conditions. This warm pocket in high-latitude North America was punctuated by periods of extremes, including a series of record and above-freezing daily maximum temperatures observed at Clyde River, Baffin Island during 29 November to 3 December (ECCC 2024). Few areas were characterized by negative anomalies with an exception of Scandinavia where -2 to -3°C air temperature anomalies prevailed over much of Norway, Sweden, and Finland along with drier conditions (see essay *Precipitation*).

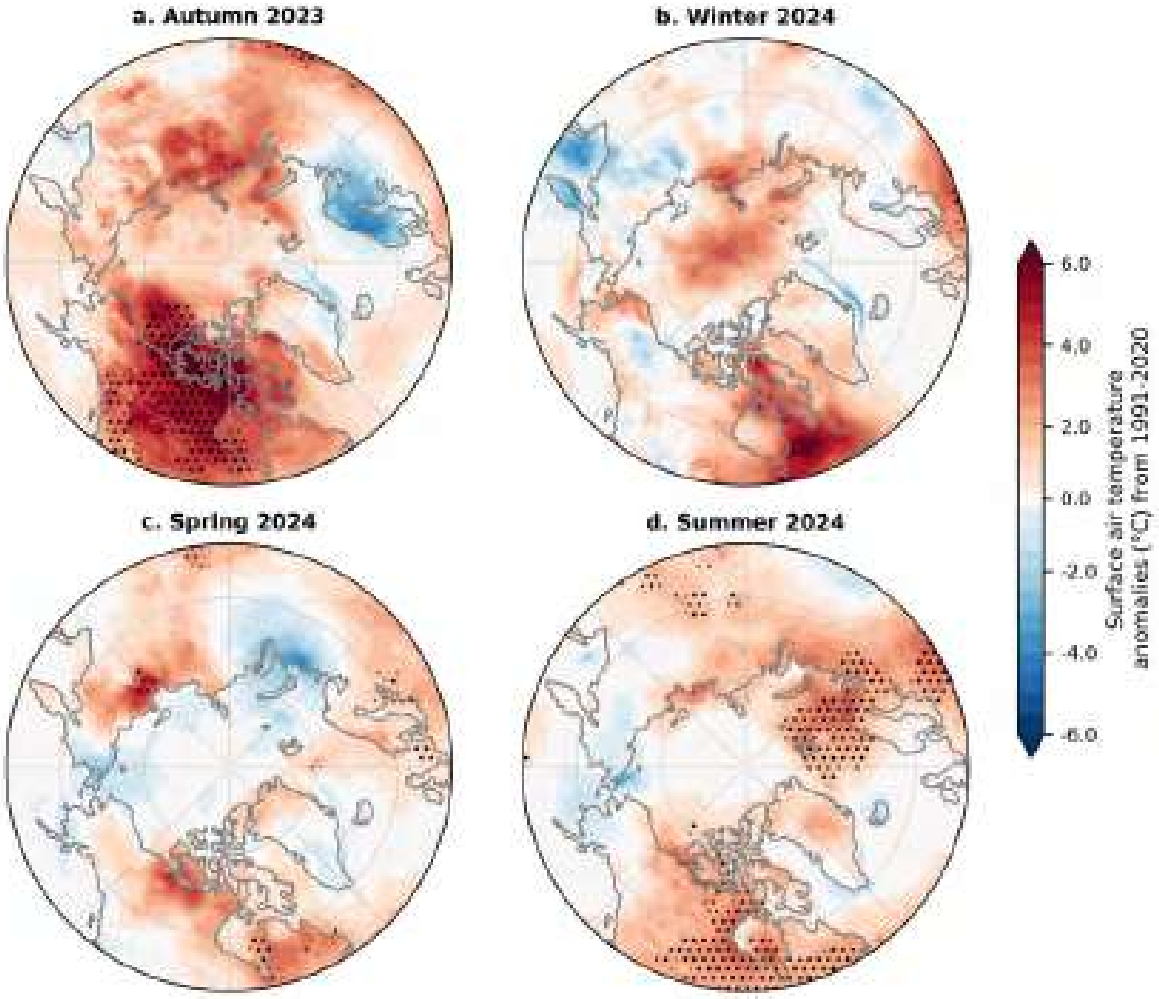

Fig. 2. Seasonal surface air temperature anomalies (°C) for (a) autumn 2023, (b) winter 2024, (c) spring 2024, and (d) summer 2024. Temperature anomalies are shown relative to their 1991-2020 means. Stippled areas indicate record high seasonal temperatures since 1950. Source: ERA5 reanalysis air temperature data are obtained from the Copernicus Climate Change Service.

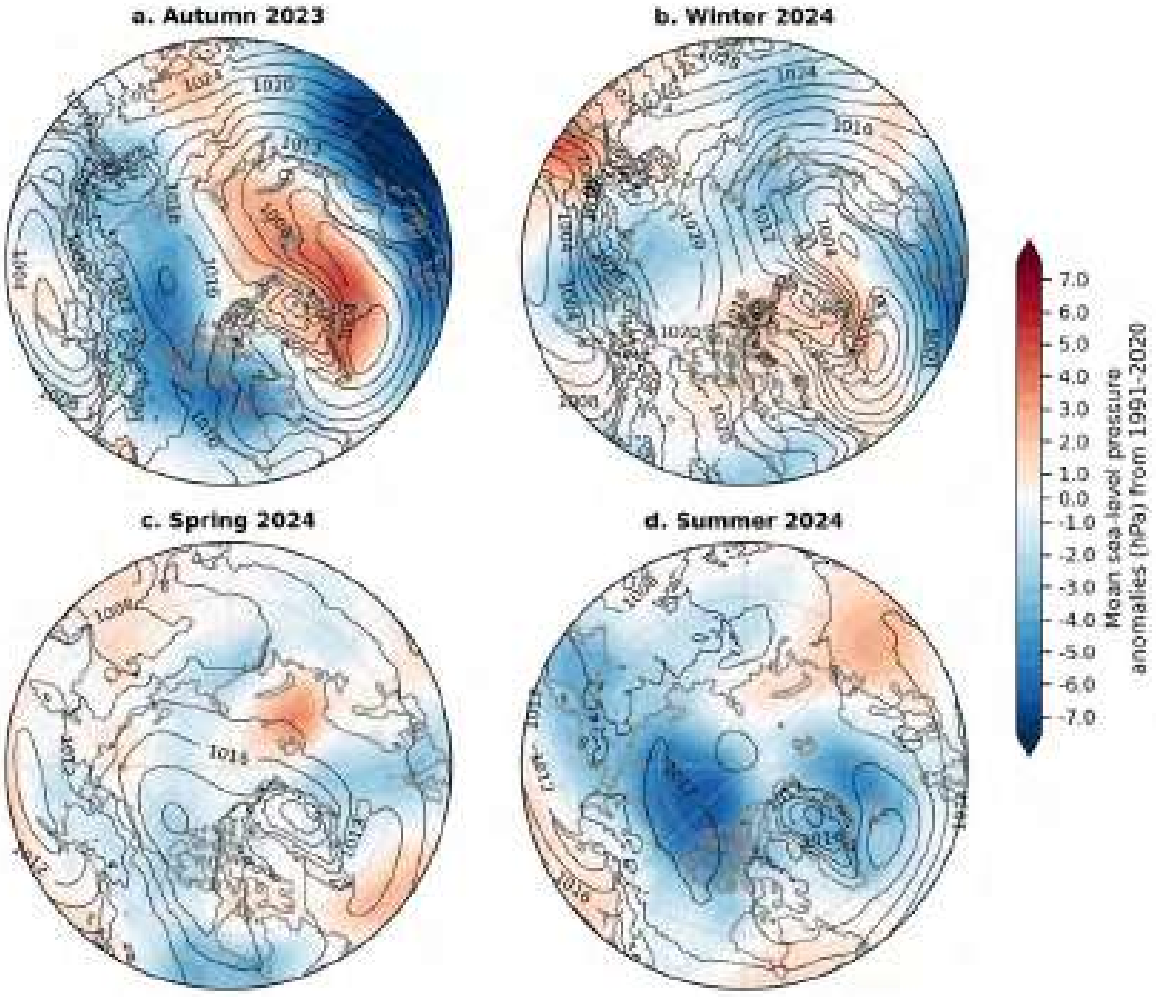

Fig. 3. Seasonal sea-level pressure (SLP) anomalies (shading) and raw values (isobars) (both in hPa) for (a) autumn 2023, (b) winter 2024, (c) spring 2024, and (d) summer 2024. SLP anomalies are shown relative to their 1991-2020 means. Source: ERA5 reanalysis SLP data are obtained from the Copernicus Climate Change Service.

Winter 2024 saw positive anomalies over the Central Arctic Ocean (~3-4°C) with smaller magnitude anomalies generally found over Arctic lands (Fig. 2b). Exceptions include the North Slope of Alaska, northern Baffin Island, northern Quebec, and Severnaya Zemlya, where the largest positive anomalies (~5-6°C) occurred. The latter two areas were associated with negative pressure anomalies to the west (Fig. 3b) that enhanced warm air advection from the south. The largest cold anomalies appeared within the Kamchatka Peninsula and the Sea of Okhotsk and relatively small temperature anomalies over Eurasia appear linked to a cold February over the region. Overall, the pan-Arctic temperature pattern in winter shows fewer large warm or cold extremes relative to the preceding autumn.

Spring 2024 featured continued positive anomalies of 2-4°C over northern Canada and eastern Siberia (Fig. 2c). Small negative temperature anomalies extended offshore from the northeastern and northwestern Russian coastlines. In contrast to autumn 2023 and winter 2024, air temperatures over the Arctic Ocean during spring were average to slightly below average, linked to a relatively weak SLP anomaly pattern over the region (Fig. 3c).

Continued warmth across parts of northern Canada and northern Eurasia characterized summer 2024. Record high air temperatures since 1950 were found in Nunavut, northern portions of Manitoba, Ontario, and Quebec, and across much of Hudson Bay where seasonal departures were 2-3°C above the 1991-2020 mean. An early August heat wave produced multiple high temperature records in northern Alaska and the northern Canadian provinces. This included 31.7°C (89°F) at Deadhorse on Alaska's North Slope and 34.8°C (95°F) in Inuvik, Northwest Territories (Thoman 2024). Notable areas with record temperature anomalies were also found in the eastern Arctic, namely extending from northern Scandinavia and across the Norwegian Sea and Barents Sea to the northern Svalbard coast. A few areas, including the western Chukchi Sea, central Bering Sea, and adjacent lands were marked by negative temperature anomalies associated with an extensive area of lower-than-normal SLP across the western Arctic (Fig. 3d).

Methods and data

The NASA Goddard Institute for Space Studies surface temperature analysis version 4 (GISTEMP v4) is used to describe long-term Arctic (60-90° N) and Global (90° S-90° N) surface air temperatures since 1900 (Fig. 1). GISTEMP v4 air temperatures over lands are obtained from the NOAA Global Historical Climatology Network version 4 (GHCN v4) dataset and ocean surface temperatures are taken from the NOAA Extended Reconstructed Sea Surface Temperature version 5 (ERSST v5) dataset. The GISTEMP product is described in detail in Hansen et al. (2010) and Lenssen et al. (2019).

We use ERA5 reanalysis (Hersbach et al. 2020) two-meter (i.e., surface) air temperature and sea-level pressure fields in Figs. 2 and 3, respectively, to provide spatial context to recent Arctic temporal variability shown in Fig. 1. Temporal comparison of GISTEMP v4 and ERA5 Arctic surface air temperature time series shows minimal interannual differences during the last four decades (Ballinger et al. 2023). All values and fields are presented as anomalies with respect to the 1991-2020 mean.

References

Ballinger, T. J., and Coauthors, 2023: Surface air temperature. *Arctic Report Card 2023*, R. L. Thoman, T. A. Moon, and M. L. Druckenmiller, Eds., https://doi.org/10.25923/x3ta-6e63.

Cohen, J., and Coauthors, 2020: Divergent consensuses on Arctic amplification influence on midlatitude severe winter weather. *Nat. Climate Change*, **10**, 20-29, https://doi.org/10.1038/s41558-019-0662-y.

ECCC, 2024: Past weather and climate: Historical data. Environment and Climate Change Canada, Station climate IDs 2400800 and 2400802, accessed 4 September 2024, https://climate.weather.gc.ca/historical_data/search_historic_data_e.html.

Hansen, J., R. Ruedy, M. Sato, and K. Lo, 2010: Global surface temperature change. *Rev. Geophys.*, **48**, RG4004, https://doi.org/10.1029/2010RG000345.

Hersbach, H., and Coauthors, 2020: The ERA5 global reanalysis. *Quart. J. Roy. Meteor. Soc.*, **146**, 1999-2049, https://doi.org/10.1002/qj.3803.

Lenssen, N. J. L., G. A. Schmidt, J. E. Hansen, M. J. Menne, A. Persin, R. Ruedy, and D. Zyss, 2019: Improvements in the GISTEMP uncertainty model. *J. Geophys. Res.-Atmos.*, **124**, 6307-6326, https://doi.org/10.1029/2018JD029522.

Overland, J. E., 2024: Emergence of Arctic extremes. *Climate*, **12**, 109, https://doi.org/10.3390/cli12080109.

Polyakov, I. V., T. J. Ballinger, R. Lader, and X. Zhang, 2024: Modulated trends in Arctic surface air temperature extremes as a fingerprint of climate change. *J. Climate*, **37**, 2381-2404, https://doi.org/10.1175/JCLI-D-23-0266.1.

Schoen, E. R., K. G. Howard, J. M. Murphy, D. E. Schindler, P. A. H. Westley, and V. R. von Biela, 2023: Divergent responses of western Alaska salmon to a changing climate. *Arctic Report Card 2023*, R. L. Thoman, T. A. Moon, and M. L. Druckenmiller, Eds., https://doi.org/10.25923/f2hv-5581.

Sweeney, A. J., Q. Fu, S. Po-Chedley, H. Wang, and M. Wang, 2023: Internal variability increased Arctic amplification during 1980-2022. *Geophys. Res. Lett.*, **50**, e2023GL106060, https://doi.org/10.1029/2023GL106060.

Taylor, P. C., and Coauthors, 2022: Process drivers, inter-model spread, and the path forward: A review of amplified Arctic warming. *Front. Earth Sci.*, **9**, 758361, https://doi.org/10.3389/feart.2021.758361.

Thoman, R., 2024: Update: August 2024 Arctic Heatwave. Alaska and Arctic Climate Newsletter, https://alaskaclimate.substack.com/p/update-august-2024-arctic-heatwave.

Timmermans, M. -L., and Z. Labe, 2023: Sea surface temperature. *Arctic Report Card 2023*, R. L. Thoman, T. A. Moon, and M. L. Druckenmiller, Eds., https://doi.org/10.25923/e8jc-f342.

Zhou, W., L. R. Leung, and J. Lu, 2024: Steady threefold Arctic amplification of externally forced warming masked by natural variability. *Nat. Geosci.*, **17**, 508-515, https://doi.org/10.1038/s41561-024-01441-1.

November 14, 2024

Precipitation

https://doi.org/10.25923/xf7c-p592

M. C. Serreze[1], S. Bigalke[2], R. Lader[3], A. Crawford[4], and T. J. Ballinger[3]

[1]National Snow and Ice Data Center, Cooperative Institute for Research in Environmental Sciences, University of Colorado Boulder, Boulder, CO, USA
[2]Department of Geography, Portland State University, Portland, OR, USA
[3]International Arctic Research Center, University of Alaska Fairbanks, Fairbanks, AK, USA
[4]Department of Environment and Geography, University of Manitoba, Winnipeg, MB, Canada

Headlines

- Summer (July-September) 2024 precipitation averaged across the pan-Arctic (poleward of 60° N) was at a record high.
- During 1950 through 2024, annual Arctic precipitation has increased, and the increase is most pronounced in winter.
- During October-December 2023 there was below-average precipitation over the East Greenland and Barents Seas and above-average precipitation extending from the U.K. eastward into Eurasia.

Introduction

Patterns of Arctic precipitation vary strongly both regionally and seasonally, with very dry (even polar desert conditions) over much of the Canadian Arctic Archipelago and central Arctic Ocean contrasting with much wetter conditions over the Atlantic side of the Arctic. Locally, precipitation is strongly boosted by forced uplift of air masses by orography (orographic precipitation). Interannual variability in Arctic precipitation relates to variations in the passage of cyclones and their warm and cold fronts, as well as convective precipitation, which is caused by rising warm, moist air and mostly restricted to land areas in summer when there is strong surface heating but can also occur over the ice-free ocean in some circumstances. Reflecting such variability, the October 2023-September 2024 water year for the Arctic region poleward of 60° N was characterized by large regional anomalies in precipitation, notably in autumn and summer. During 1950-2024, pan-Arctic precipitation exhibits an upward trend in annual means, and is seasonally most pronounced for autumn and winter. In this essay, water year seasons are defined as autumn (October-December), winter (January-March), spring (April-June), and summer (July-September).

Precipitation at a glance

The prominent features of the 2023/24 water year were: 1) large positive precipitation anomalies in autumn over the Alaska panhandle and from the U.K. extending eastward across Europe, paired with negative anomalies over the East Greenland and Barents Seas; 2) a band of heavy precipitation events in winter extending north from the Gulf of Alaska, across eastern Alaska and into the East Siberian Sea; and 3) summer dryness over large parts of the Eurasian and North American continents, but with wet conditions over central and northern Alaska and Scandinavia. Overall, pan-Arctic (north of 60° N)

precipitation for the 2023/24 water year in the ERA5 reanalysis was the 11th highest over the 1950 to 2024 record. Corresponding ranks for autumn, winter, spring, and summer are 17th, 17th, 20th and 1st.

Figure 1 shows seasonal precipitation totals derived from ERA5 during the 2023/24 water year expressed as anomalies with respect to the 1991-2020 means. A notable feature of autumn is the especially wet conditions over the Alaska panhandle, pointing to orographic uplift. Another interesting feature is a dipole pattern, pairing positive precipitation anomalies from the U.K. to southern Norway with negative anomalies extending from the East Greenland Sea into the Norwegian and Barents Seas. The origins of this pattern are two-fold. First, the main center of extratropical cyclone formation was shifted to the south and east, lying over the North Sea and Scandinavia instead of around Iceland. Second, storms that did form around Iceland were steered almost due east (instead of the more normal northeast), striking northern Europe instead of the Norwegian and Barents Seas. Elsewhere, autumn anomalies were generally small, except for a wet area southeast of Greenland.

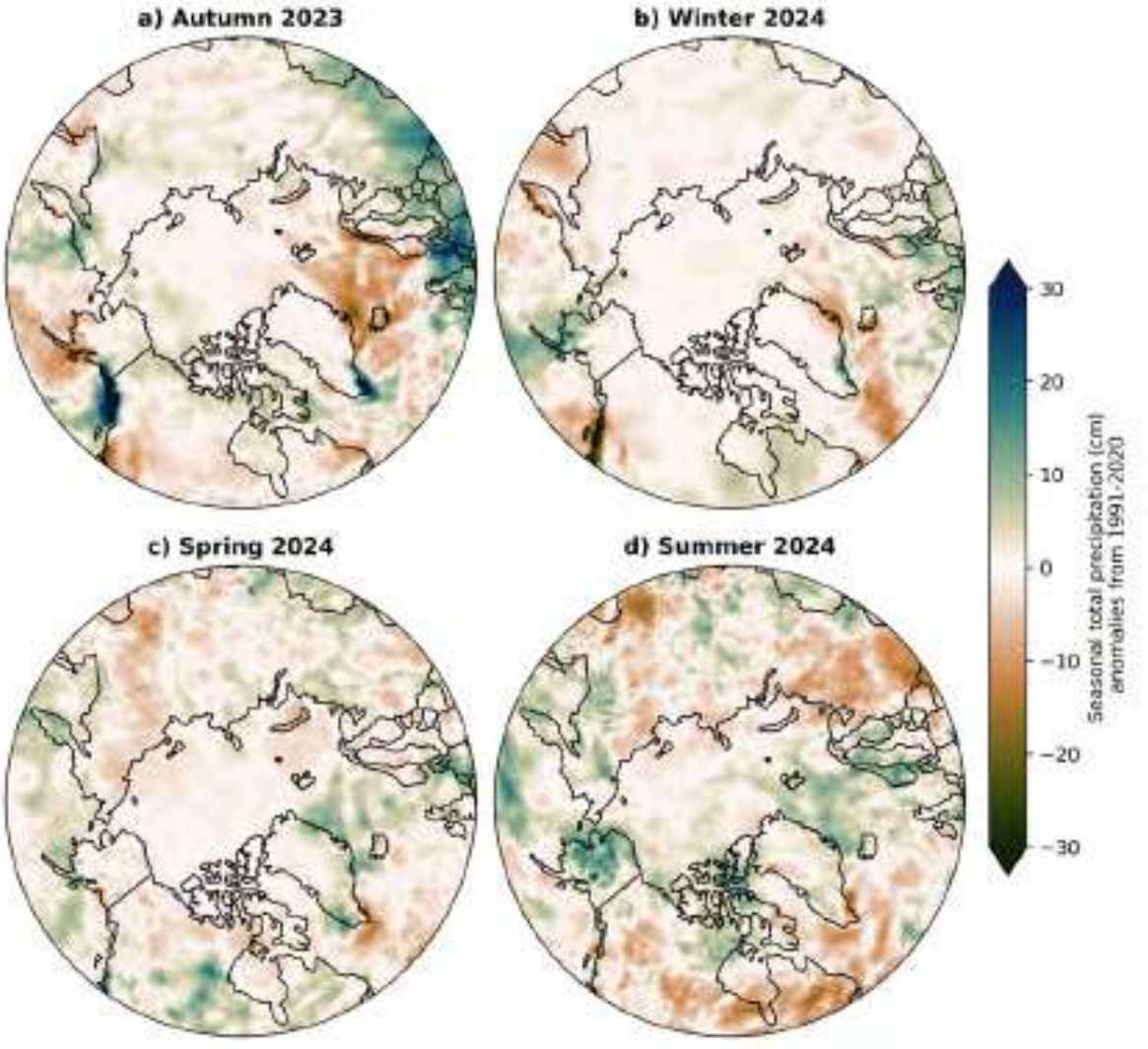

Fig. 1. Seasonal precipitation anomalies (using 1991-2020 baseline) for autumn (OND) 2023, winter (JFM) 2024, spring (AMJ) 2024, and summer 2024 (JAS). Green shades denote above-normal precipitation, brown shades denote below-normal precipitation. Data source: ERA5 reanalysis.

As was the case for the 2022/23 water year, winter precipitation anomalies were generally weak for 2023/24. One exception was sharply below average precipitation over the Alaska panhandle, a strong reversal from the situation in this area for autumn. Spring was also characterized by generally modest precipitation anomalies.

As noted above, for the region poleward of 60° N, summer (July-September) of 2024 was the wettest on record. This is largely due to above average precipitation over interior Alaska, the Canadian Arctic Archipelago, northern Scandinavia and the Barents Sea. However, precipitation was below average over northwestern Eurasia, parts of Canada south of the Archipelago, and the northern North Atlantic.

Heavy precipitation events

For any given year, there is a statistical expectation of regionally heavy precipitation events that can approach or exceed previous records, even in a stable climate. Following the approach of previous Arctic Report Cards, Fig. 2 plots heavy precipitation events during the 2023/24 water year in terms of ranks of the maximum 5-day precipitation events (Rx5) in each season (relative to the 1950-2023 baseline). Generally, heavy precipitation events are scattered across the Arctic in all four seasons with no coherent pattern. The one feature of note is the band of heavy precipitation events in winter stretching northward from south of the Aleutians across eastern Alaska into the East Siberian Sea, which is aligned with warmer-than-average conditions (see Fig. 2b in essay *Surface Air Temperature*). There were heavy precipitation events from western and northern Alaska to the Canadian Arctic Archipelago in summer, particularly during August.

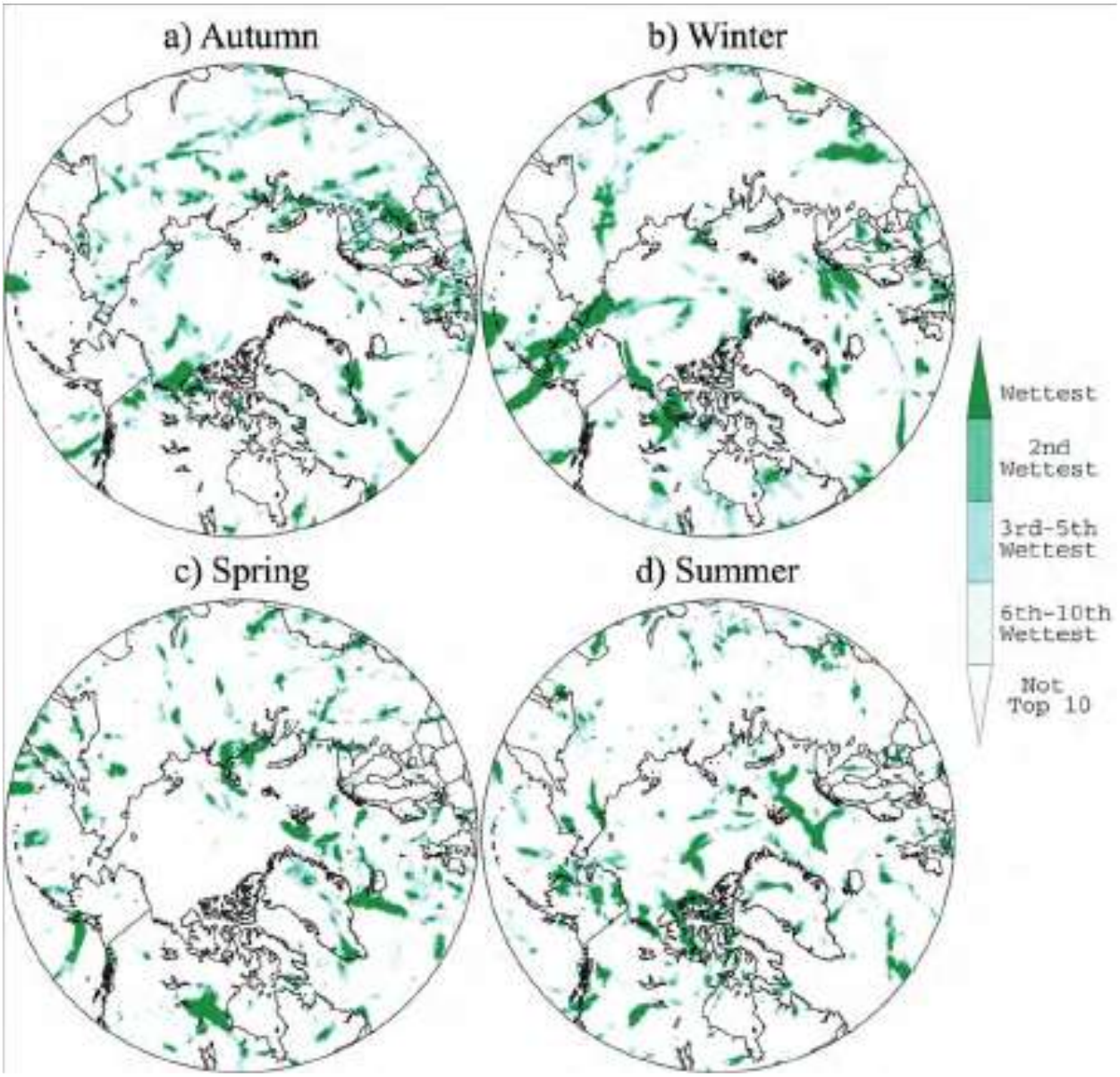

Fig. 2. Ranks of maximum 5-day precipitation for each season during the 2023/24 water year: (a) autumn (OND), (b) winter (JFM), (c) spring (AMJ), and (d) summer (JAS). Data source: ERA5 reanalysis, 1950-present.

Historical perspective

Simulations from climate models are in strong agreement that the Arctic region should see an increase in precipitation due to higher atmospheric water vapor content as the climate warms, facilitating increased moisture transport from lower latitudes. While an upward trend in annual precipitation is now detectable (Box et al. 2021; Walsh et al. 2022a), there is considerable interannual and multiyear variability and large variations in regional trends (Ye et al. 2021; Yu and Zhong 2021). There is also evidence of a transition from solid to liquid precipitation in the warmer parts of the Arctic (Box et al. 2021), although the coldest areas of the Arctic are expected to see snowfall increases in the future (McCrystall et al. 2021; Bigalke and Walsh 2022).

As is the case with previous Arctic Report Cards, the Arctic precipitation time series from ERA5 (as a percentage of 1991-2020 averages for the region poleward of 60° N) is plotted along with the corresponding time series from the station-based dataset of the Global Precipitation Climatology Center (GPCC) during 1950-2023 (Fig. 3). The GPCC dataset is for land only, while ERA5 data cover ocean areas as well as land. While the percent anomaly time series are generally similar, there are some substantial differences for individual years due to the absence of coverage over the Arctic Ocean in GPCC and inherent uncertainties in each data source. Nevertheless, the time series agree with respect to a positive long-term trend in annual precipitation and the record high precipitation for summer 2024.

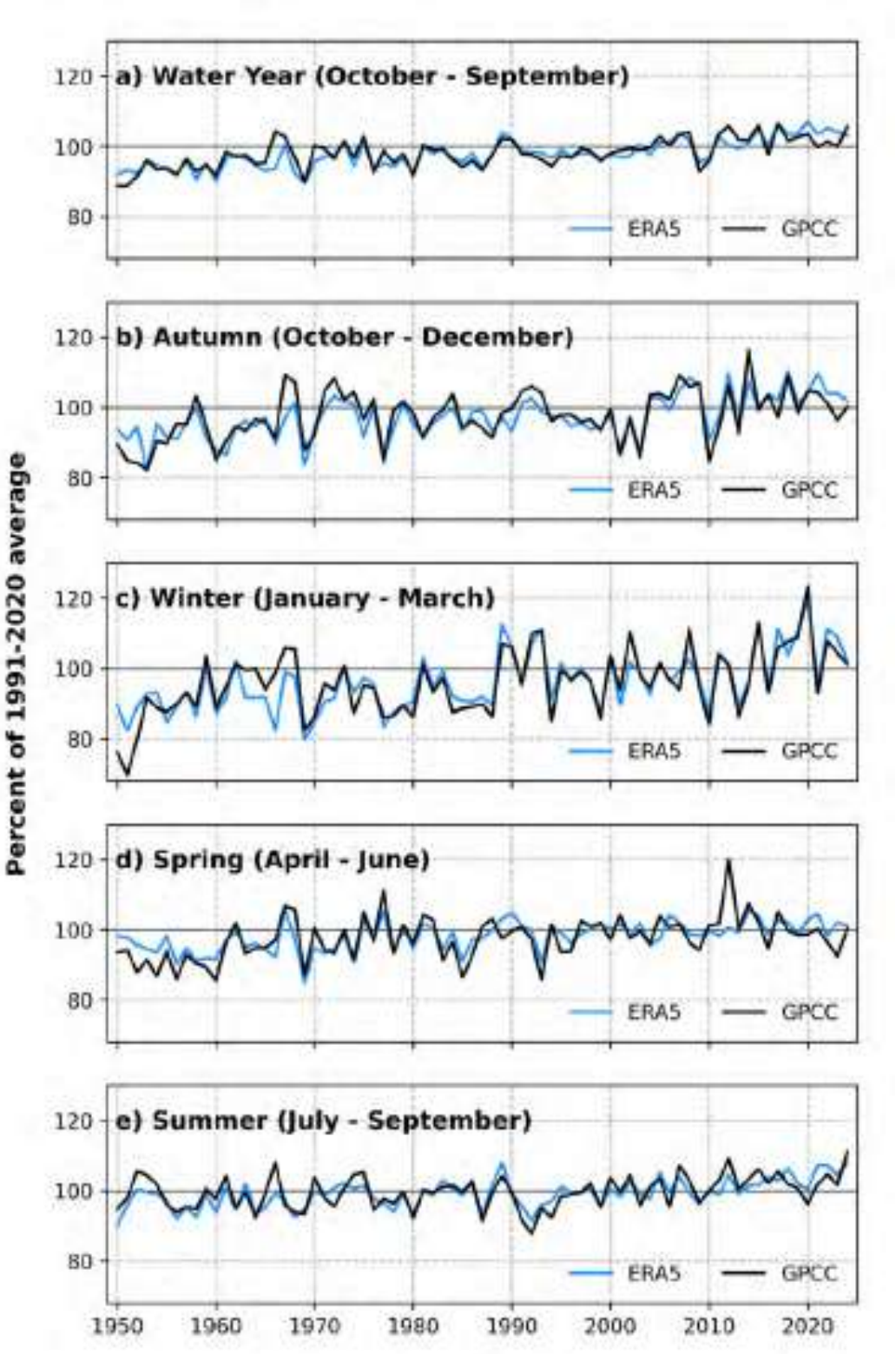

Fig. 3. Time series of Arctic (60-90° N) precipitation for water-years from 1951 through 2024 expressed as a percentage of the 1991-2020 average (shown by the horizontal black lines at 100%). Results are from ERA5 (blue lines) and GPCC 1.0° data (black lines). GPCC values are for land only; ERA5 values are for land plus ocean. The GPCC full data product is used through 2020. The ERA5 monitoring product is used for January 2021-October 2024.

Based on the ERA5 precipitation time series for the region poleward of 60° N that includes the 2023/24 water year, the trend in annual mean precipitation stands at +0.74 cm per decade, or a 10.4% percent change since 1951 (Fig. 3). Corresponding seasonal trends are +0.22 cm per decade for autumn, +0.22 cm per decade for winter, +0.12 cm per year for spring, and +0.18 cm per decade for summer. Autumn and winter hence show the strongest seasonal trends. In terms of percent change relative to the 1991-2020 average, winter is stronger (+2.17 % per decade) compared to autumn (+1.61% per decade). Summer is 0.99% per decade, spring is 1.05% per decade, and the water year as a whole is 1.41% per decade.

Methods and data

Because of the challenges of collecting in situ precipitation gauge measurements in the Arctic, we use gridded precipitation fields from both the ERA5 atmospheric reanalysis of the European Centre for Medium Range Weather Forecasts (ECMWF) (Hersbach at al. 2020) and the Global Precipitation Climatology Centre's GPCC Full Data Version Data Version 2022 (Becker et al. 2013; https://opendata.dwd.de/climate_environment/GPCC/html/fulldata-daily_v2022_doi_download.html). ERA5 data are available from January 1940 onward, but the quality of the output is more reliable starting in 1979 (Hersbach et al. 2020), after which modern satellite data are assimilated into the analysis and forecast system. ERA5 is the latest atmospheric reanalysis effort and performs slightly better than other atmospheric reanalyses at matching observed precipitation totals from Arctic extreme events (Loeb et al. 2022). Given the model-derived nature of ERA5, comparisons are made with the GPCC's Full Data Product, a monthly gridded gauge-based product available from 1891 onward (Schneider et al. 2022). Our comparisons of pan-Arctic precipitation computed from these two sources is limited to the post-1950 time period because both products were impacted by missing data during World War II.

References

Becker, A., P. Finger, A. Meyer-Christoffer, B. Rudolf , K. Schamm, U. Schneider, and M. Ziese, 2013: A description of the global land-surface precipitation data products of the Global Precipitation Climatology Centre with sample applications including centennial (trend) analysis from 1901-present. *Earth Sys. Sci. Data*, **5**, 71-99, https://doi.org/10.5194/essd-5-71-2013.

Bigalke, S., and J. E. Walsh, 2022: Future changes of snow in Alaska under stabilized global warming scenarios. *Atmosphere*, **13**, 541, https://doi.org/10.3390/atmos13040541.

Box, J. E., and Coauthors, 2021: Recent developments in Arctic climate observation indicators. *AMAP Arctic Climate Change Update 2021: Key Trends and Impacts*, Arctic Monitoring and Assessment Programme (AMAP), Tromso, Norway, 7-29, https://www.amap.no/documents/doc/amap-arctic-climate-change-update-2021-key-trends-and-impacts/3594.

Hersbach, H., and Coauthors, 2020: The ERA5 global reanalysis. *Quart. J. Roy. Meteor. Soc.*, **146**, 1999-2049, https://doi.org/10.1002/qj.3803.

Loeb, N. A., A. Crawford, J. C. Stroeve, and J. Hanesiak, 2022: Extreme precipitation in the eastern Canadian Arctic and Greenland: An evaluation of atmospheric reanalyses. *Front. Env. Sci.*, **10**, 866929, https://doi.org/10.3389/fenvs.2022.866929.

McCrystall, M. R., J. Stroeve, M. C. Serreze, B. C. Forbes, and J. A. Screen, 2021: New climate models reveal faster and larger increases in Arctic precipitation than previously projected. *Nat. Commun.*, **12**(1), 6765, https://doi.org/10.1038/s41467-021-27031-y.

Schneider, U., P. Finger, E. Rustemeier, M. Ziese, and S. Hänsel, 2022: Global precipitation analysis products of the GPCC, Global Precipitation Climatology Centre, https://opendata.dwd.de/climate_environment/GPCC/PDF/GPCC_intro_products_v2022.pdf.

Walsh, J. E., S. Bigalke, S. A. McAfee, R. Lader, M. C. Serreze, and T. J. Ballinger, 2022: Precipitation. *Arctic Report Card 2022*, M. L. Druckenmiller, R. L. Thoman, and T. A. Moon, Eds., https://doi.org/10.25923/yxs5-6c72.

Ye, H., D. Yang, A. Behrangi, S. L. Stuefer, X. Pan, E. Mekis, Y. Dibike, and J. E. Walsh, 2021: Precipitation Characteristics and Changes. *Arctic Hydrology, Permafrost and Ecosystems* (D. Yang and D. L. Kane, Eds.), Springer Nature Switzerland, https://doi.org/10.1007/978-3-030-50930-9_2.

Yu, L., and S. Zhong, 2021: Trends in Arctic seasonal and extreme precipitation in recent decades. *Theor. Appl. Climatol.*, **145**, 1541-1559, https://doi.org/10.1007/s00704-021-03717-7.

November 15, 2024

Terrestrial Snow Cover

https://doi.org/10.25923/4bb3-3f87

L. R. Mudryk[1], A. Elias Chereque[2], C. Derksen[1], K. Luojus[3], and B. Decharme[4]

[1]Climate Research Division, Environment and Climate Change Canada, Toronto, ON, Canada
[2]Department of Physics, University of Toronto, Toronto, ON, Canada
[3]Arctic Research Centre, Finnish Meteorological Institute, Helsinki, Finland
[4]Centre National de Recherches Météorologiques, Météo-France, Toulouse, France

Headlines

- Snow accumulation during the 2023/24 winter was above the 1991-2020 average across both the Eurasian and North American Arctic.
- Early snow onset and delayed spring melt resulted in a longer than average snow season over much of the Eurasian Arctic.
- Over North America late snow onset and early spring melt resulted in the shortest snow season seen in 26 years over portions of central and eastern Arctic Canada.
- Compared to historical conditions, Arctic snow melt over the past 15 years has commonly occurred 1-2 weeks earlier throughout May and June over both Eurasia and North America.

Introduction

Many Arctic land surface processes are directly influenced by snow cover from autumn through spring, including the surface energy budget, ground temperature regime, permafrost, and terrestrial and freshwater ecosystems (Brown et al. 2017; Meredith et al. 2019). Even following the snow cover season, the influence of spring snow melt timing persists through impacts on river discharge timing and magnitude, surface water, soil moisture, vegetation phenology, and fire risk (Meredith et al. 2019).

Multiple data sets derived from satellite observations and snowpack models driven by atmospheric reanalyses are used to assess Arctic seasonal snow cover (see *Methods and data*). Collectively, this approach provides a reliable picture of Arctic snow cover variability over the last five decades. We characterize snow conditions across the Arctic land surface using three quantities: how much total land area is covered by snow (snow cover extent – SCE), how much of the year snow covers the land surface (snow cover duration – SCD), and how much total water is stored in solid form by the snowpack (snow water equivalent – SWE; the product of snow depth and density and which when aggregated over a region measures the mass of snow). We examine each of these quantities in turn for the 2023/24 Arctic snow season.

Snow cover extent and duration

SCE anomalies (relative to the 1991-2020 baseline) in spring 2024 are shown separately for the North American and Eurasian sectors of the Arctic in Fig. 1. Eurasian Arctic SCE was close to normal or slightly above normal during May (20th lowest May SCE in the 58-year record) related to cold spring conditions over northern Europe and western Russia (see essay *Surface Air Temperature*). By June, however,

Eurasian Arctic SCE dropped below normal (14th lowest June SCE in the 58-year record). This change from above to below normal snow extent between May and June is clear from weekly anomalies (Fig. 2) whereby a sharp transition from above normal to below normal snow extent occurred between weeks 20 and 22 of the year (end of May). Corresponding SCD anomalies for the 2023/24 snow season (Fig. 3) indicate primarily early onset of snowfall and delayed melt during the spring across broad portions of northern Europe, western Russia, and easternmost Siberia (relative to a 25-year baseline from 1998/99 to 2022/23). The combination of early onset and delayed melt led to one of the longer snow seasons of the past 26 years across the majority of the Eurasian Arctic (Fig. 3c).

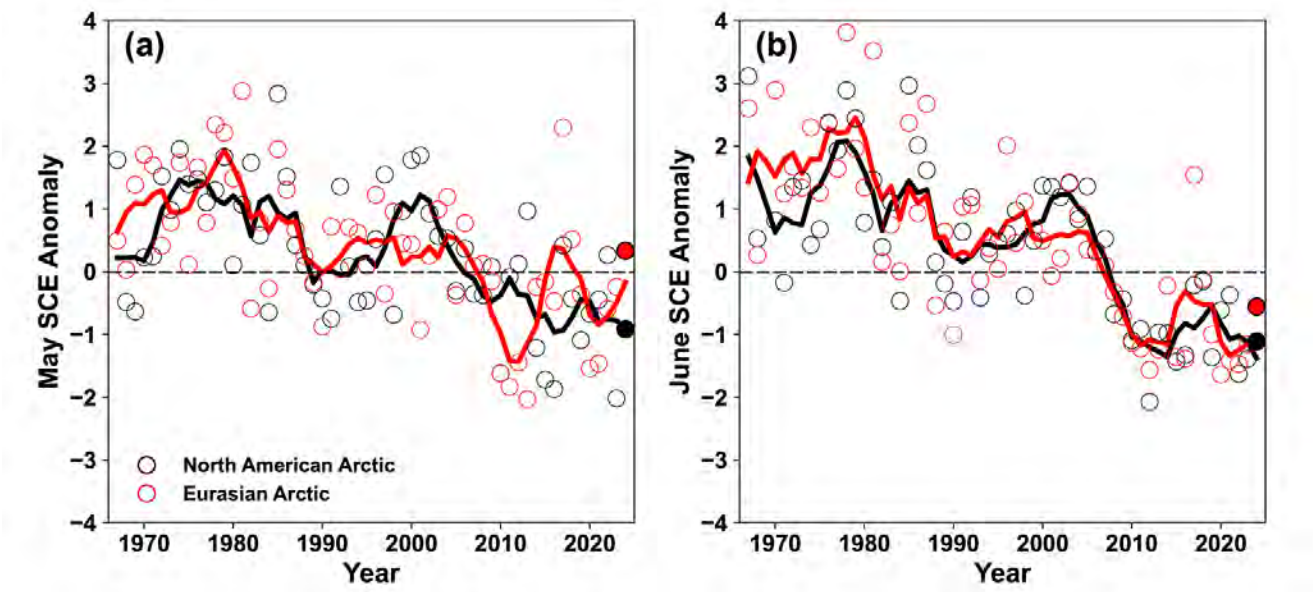

Fig. 1. Standardized monthly snow cover extent anomalies relative to the 1991-2020 baseline for Arctic land areas (>60° N) for (a) May, and (b) June from 1967 to 2024. Solid black and red lines depict 5-year running means for North America and Eurasia, respectively. Filled circles highlight 2024 anomalies. Source: NOAA snow chart Climate Data Record (CDR); available from 1967 to present.

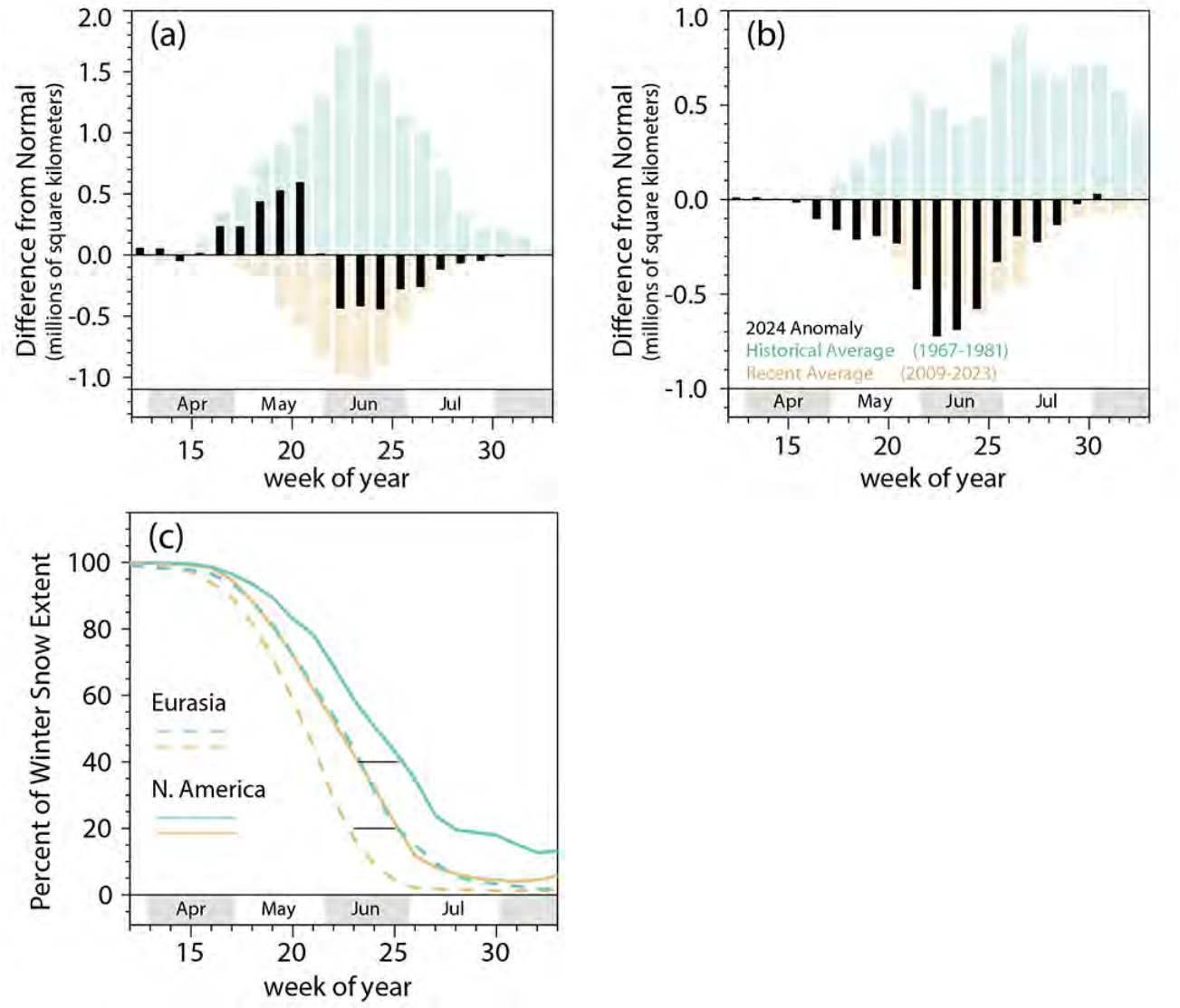

Fig. 2. Weekly snow cover extent anomalies during spring 2024 (black) relative to the 1991-2020 baseline for (a) Eurasian and (b) North American Arctic land areas (>60° N). Also depicted are the historical averages over the 1967-81 period (blue-green) and the recent averages over the 2009-23 period (tan) both relative to the 1991-2020 baseline. Difference in melt timing for each sector of the Arctic shown in (c), with colors indicating the same time periods shown in (a) and (b). Length of black bars illustrates differences of two weeks in melt timing. Source: NOAA snow chart Climate Data Record (CDR); available from 1967 to present.

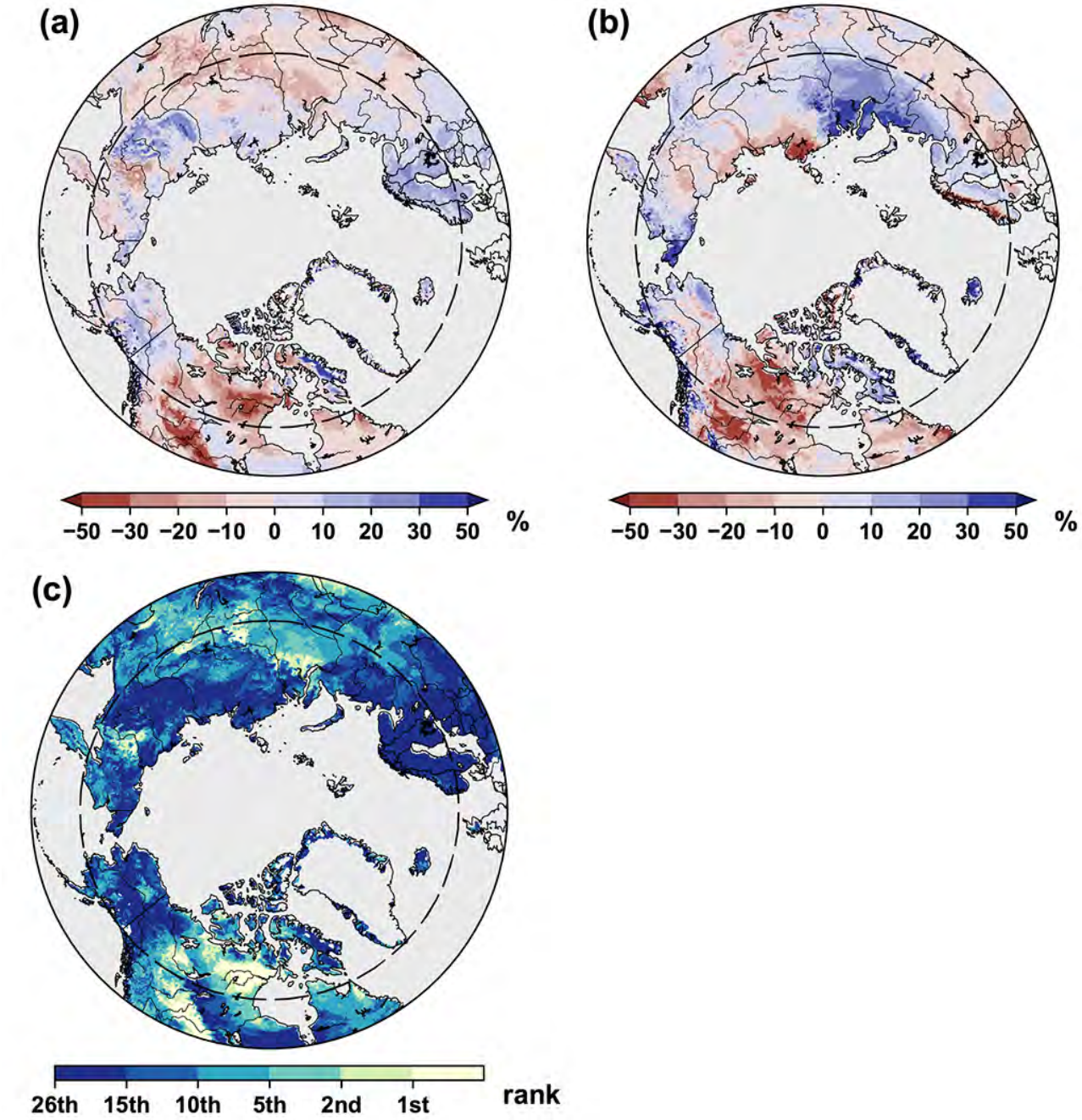

Fig. 3. Snow cover duration anomalies (% difference relative to average number of snow-free days) for the 2023/24 snow year: (a) snow onset (Aug-Jan); and (b) snow melt (Feb-Jul). Red (blue) indicates increased (decreased) snow-free days compared to the 1998/99 through 2022/23 mean, aligning with later (earlier) onset (a) or earlier (later) melt (b). Ranks of full snow season length (combined onset and melt) shown in c) where 1st rank indicates the 2023/24 season was the shortest in the available record and 26th indicates the 2023/24 season was the longest. The dashed circle marks the latitude 60° N; Arctic land areas north of this are considered in this study. Source: NOAA 4km IMS data record; available from 1998 to present.

In contrast with Eurasia, North American Arctic SCE during 2024 was below normal throughout May and June (Figs. 1 and 2), with both months ranking 7th lowest in the 58-year record. Corresponding SCD anomalies indicate a combination of late onset and early spring melt that resulted in one of the shortest

snow seasons of the last 26 years across portions of the Canadian Northwest Territories and mainland Nunavut (Fig. 3c).

Snow mass and snow water equivalent

Snow mass across the Arctic typically peaks annually during April, when snowfall has accumulated since the preceding autumn but before increasing temperatures during May and June lead to snow melt. Snow mass anomalies for April 2024 (Fig. 4) were above the 1991-2020 baseline across both the North American and Eurasian Arctic. The spatial patterns of monthly SWE (Fig. 5) illustrate how this accumulation varied regionally from just before peak (March) through to the end of the melt period (June). Positive SWE anomalies are apparent across broad portions of both continents in March and April. Strong reductions in the relative amount of SWE are apparent over the North American Arctic during May, while over Eurasia large regions of above-normal SWE still exist. By June the extent of Eurasian snow cover is much reduced, consistent with anomalies in Figs. 1 and 2b; however, the residual coverage between the Ob and Yenisei rivers and at the far eastern tip of the continent have above normal SWE consistent with the longer-than-normal melt season observed in those regions (Fig 3b). Over North America most of the Canadian Arctic Archipelago has below normal SWE during June except for Baffin Island.

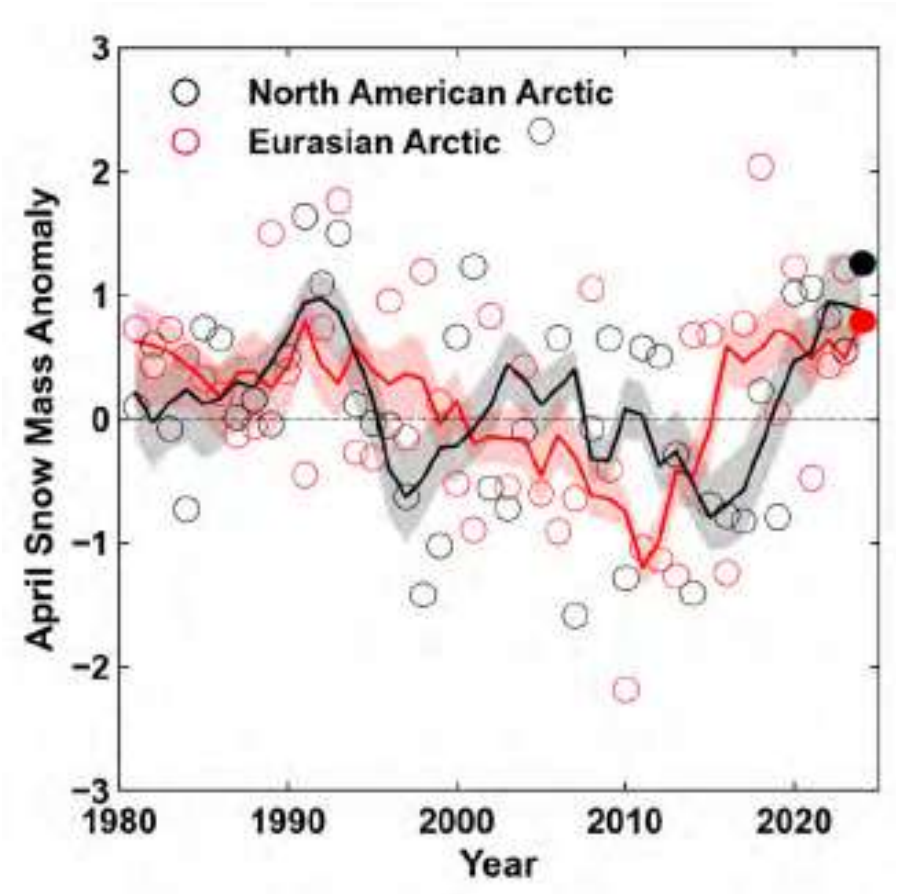

Fig. 4. Standardized April snow mass anomalies for Arctic land areas across the North American (black) and Eurasian (red) sectors. Anomalies (relative to the 1991-2020 average) represent the ensemble mean from a suite of four independent snow analyses. Filled circles highlight 2024 anomalies. Solid black and red lines depict 5-yr running means; shading depicts the spread amongst individual data set running means. Source: gridded snow products as described in *Methods and data*.

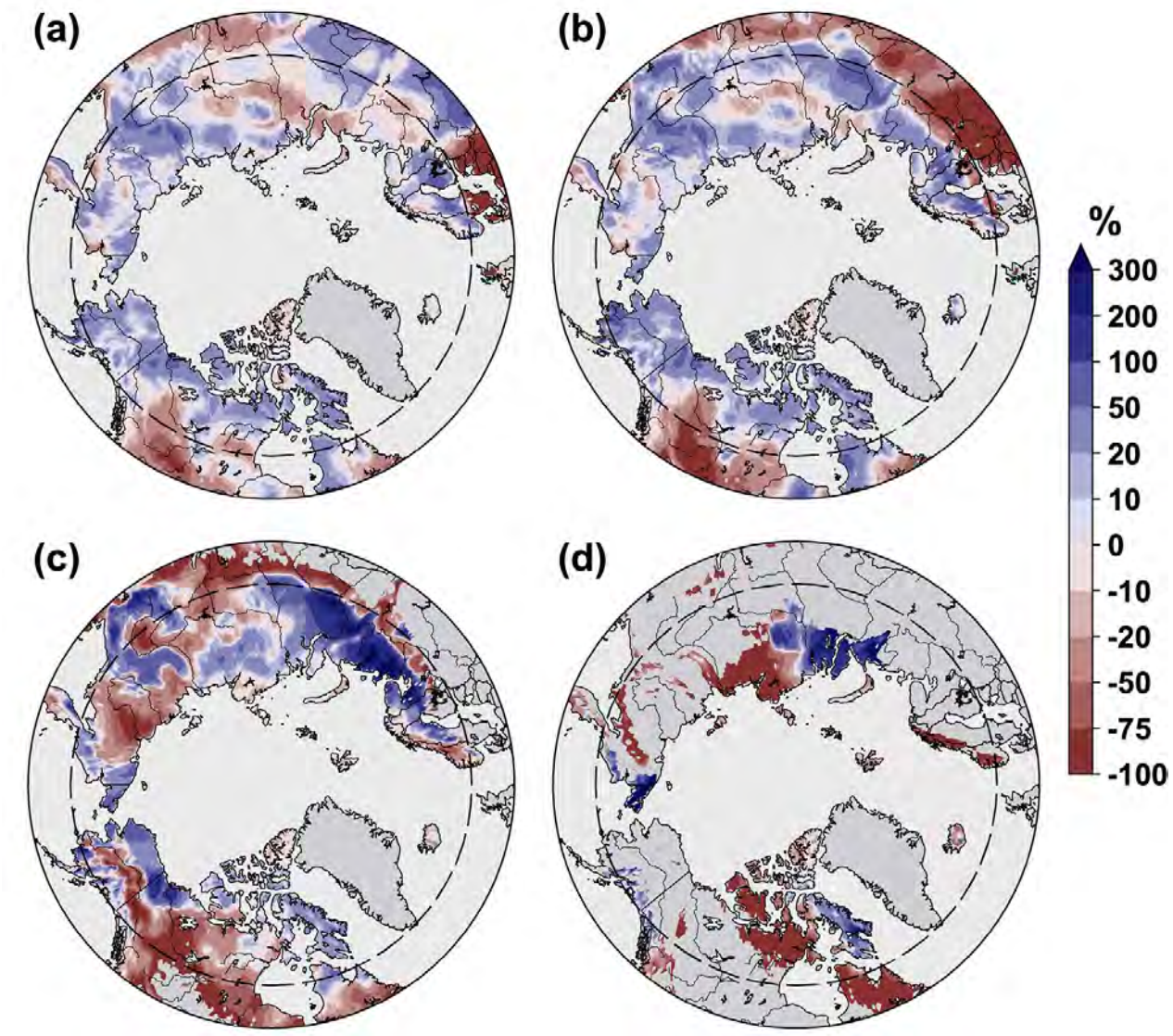

Fig.5. Snow water equivalent (SWE) anomalies (% difference from the 1991-2020 average) in 2024 for (a) March, (b) April, (c) May, and (d) June. Anomalies represent the ensemble mean from a suite of four independent gridded snow products (see *Methods and data*). The dashed circle marks the latitude 60° N.

Summary and long-term changes to snowmelt timing

Snow accumulation during the 2023/24 winter was above average across both continents; however, the duration of the snow season contrasted strongly between them. Over North America warm spring temperatures resulted in snowmelt timing consistent with or even faster than what has typically been observed over the last 15 years (Fig 2a). Over broad portions of Eurasia, the above normal SWE persisted for most of May, keeping snow cover extent above levels typically seen for the last 15 years (Fig 2b). By June, however, Eurasian snow extent returned to values consistent with those seen over the past 15 years. Compared to historical conditions (1967-81), melt timing over the past 15 years (2009-23) has occurred 1-2 weeks earlier throughout May and June over both the Eurasian and North American Arctic.

Methods and data

SCE anomalies are derived from the NOAA weekly snow chart climate data record, which extends from 1967 to present (Robinson et al. 2012). Weekly anomalies of total areal snow cover over land for a given Arctic sector (North America or Eurasia, > 60° N) are computed relative to the 1991-2020 period. The same data are grouped by month and standardized (each observation differenced from the mean and divided by the standard deviation and thus unitless) to obtain standardized monthly anomalies of total areal snow cover relative to the same 1991-2020 period.

SCD fields are derived from the NOAA daily Interactive Multisensor Snow and Ice Mapping System (IMS) snow cover product (U.S. National Ice Center 2008). Anomalies in the total number of days with snow cover were computed separately for each half of the snow season: August 2023 to January 2024, referred to as “onset period,” and February 2024 to July 2024, referred to as “melt period.” IMS availability starts in 1998, so a 1998/99 to 2022/23 climatological period (25 years) is used (including information from August-December 1998 for snow onset). Anomalies for each season are presented as percent differences from the climatological number of snow-free days. Because the Arctic is generally always snow covered between November and April, Arctic region snow onset anomalies are indicative of conditions during September and October, while Arctic region snow melt anomalies are indicative of conditions during May and June.

Four SWE data sets were used to generate multi-data set SWE fields from March-June (inclusive) for the 1981-2024 period: (1) the European Space Agency Snow Climate Change Initiative (CCI) SWE version 2 product derived through a combination of satellite passive microwave brightness temperatures and climate station snow depth observations (Luojus et al. 2022); (2) the Modern-Era Retrospective Analysis for Research and Applications version 2 (MERRA-2, GMAO 2015) daily SWE fields; (3) SWE output from the ERA5-Land analysis (Muñoz Sabater 2019); and (4) the physical snowpack model Crocus (Decharme 2024) driven by ERA5 meteorological forcing. Limited availability of climate station snow data during May and June lowers the Snow CCI SWE product accuracy during these months; therefore, we only use it during March and April. An approach using gridded products is required because in situ observations alone are too sparse to capture snow conditions across the Arctic. We consider multiple data sets because averaging multiple SWE products has been shown to be more accurate than individual data sets when validated with in situ observations (Mortimer et al 2020). The ensemble-mean SWE field is used to calculate monthly SWE anomalies relative to the 1991-2020 period, which are presented as percent differences. For April, the SWE fields for each product are also aggregated across Arctic land regions (> 60° N) for both North American and Eurasian sectors to produce multiple estimates of April snow mass. These monthly snow mass values are used to calculate standardized anomalies relative to the 1991-2020 period for each data product. The standardized anomalies are then averaged to produce an ensemble-mean time series. Greenland is primarily covered by ice rather than snow and is not represented consistently among the SWE data products. For these reasons snow cover over the land mass is not added to SCE of either Arctic sector nor included in calculations of snow mass.

Acknowledgments

ERA5-Land data (Muñoz Sabater 2019) was downloaded from the Copernicus Climate Change Service (C3S) Climate Data Store (2024). Neither the European Commission nor ECMWF is responsible for any use of the Copernicus information or data it contains.

References

Brown, R., and Coauthors, 2017: Arctic terrestrial snow cover. *Snow, Water, Ice and Permafrost in the Arctic (SWIPA) 2017*. pp. 25-64. Arctic Monitoring and Assessment Programme (AMAP), Oslo, Norway.

Decharme, B., 2024: Crocus-ERA5 daily snow product over the Northern Hemisphere at 0.25° resolution (Version 2023), Zenodo, accessed 3 September 2024, https://doi.org/10.5281/zenodo.10943718.

GMAO (Global Modeling and Assimilation Office), 2015: MERRA-2tavg1_2d_lnd_Nx:2d, 1-Hourly, Time-Averaged, Single-Level, Assimilation, Land Surface Diagnostics V5.12.4, Goddard Earth Sciences Data and Information Services Center (GESDISC), accessed: 3 August 2024, https://doi.org/10.5067/RKPHT8KC1Y1T.

Luojus, K., and Coauthors, 2022: ESA Snow Climate Change Initiative (Snow_cci): Snow Water Equivalent (SWE) level 3C daily global climate research data package (CRDP) (1979-2020), version 2.0. NERC EDS Centre for Environmental Data Analysis, accessed: 3 September 2024, https://doi.org/10.5285/4647cc9ad3c044439d6c643208d3c494.

Meredith, M., and Coauthors, 2019: Polar Regions. *IPCC Special Report on the Ocean and Cryosphere in a Changing Climate*, H.-O. Pörtner, and co-editors, Cambridge University Press, Cambridge, UK and New York, NY, USA, 203-320, https://doi.org/10.1017/9781009157964.005.

Mortimer, C., L. Mudryk, C. Derksen, K. Luojus, R. Brown, R. Kelly, and M. Tedesco, 2020: Evaluation of long-term Northern Hemisphere snow water equivalent products. *Cryosphere*, **14**, 1579-1594, https://doi.org/10.5194/tc-14-1579-2020.

Muñoz Sabater, J., 2019: ERA5-Land hourly data from 1950 to present. Copernicus Climate Change Service (C3S) Climate Data Store (CDS), accessed 3 September 2024, https://doi.org/10.24381/cds.e2161bac.

Robinson, D. A., T. W. Estilow, and NOAA CDR Program, 2012: NOAA Climate Data Record (CDR) of Northern Hemisphere (NH) Snow Cover Extent (SCE), Version 1 [r01]. NOAA National Centers for Environmental Information, accessed: 3 September 2024, https://doi.org/10.7289/V5N014G9.

U.S. National Ice Center, 2008: IMS Daily Northern Hemisphere Snow and Ice Analysis at 1 km, 4 km, and 24 km Resolutions, Version 1. Boulder, Colorado, USA. NSIDC: National Snow and Ice Data Center, accessed: 3 August 2024, https://doi.org/10.7265/N52R3PMC.

November 11, 2024

Greenland Ice Sheet

https://doi.org/10.25923/njxd-b82

K. Poinar[1], J. E. Box[2], T. L. Mote[3], B. D. Loomis[4], B. E. Smith[5], B. C. Medley[4], T. G. Askjaer[6], K. D. Mankoff[7,8], R. S. Fausto[2], and M. Tedesco[9]

[1]University at Buffalo, Buffalo, NY, USA
[2]Geological Survey of Denmark and Greenland, Copenhagen, Denmark
[3]Department of Geography, University of Georgia, Athens, GA, USA
[4]Goddard Space Flight Center, NASA, Greenbelt, MD, USA
[5]University of Washington, Seattle, WA, USA
[6]Danish Meteorological Institute, Copenhagen, Denmark
[7]Goddard Institute of Space Studies, NASA, New York, NY, USA
[8]Autonomic Integra, New York, NY, USA
[9]Lamont-Doherty Earth Observatory, Columbia Climate School, Columbia University, Palisades, NY, USA

Headlines

- The Greenland Ice Sheet lost 55 ± 35 Gt of mass in 2024, the lowest annual ice loss since 2013. This occurred due to above-average snowfall and below-average melting and despite higher glacier flow rates than the 1991-2020 average.
- Persistent summertime low pressure over southern Greenland and Iceland promoted northerly winds along western Greenland, snowfall, cloudiness, and cool conditions that limited ice melt.
- Flow rates of ice into the ocean in 2024 were substantially above the 1991-2020 average, despite moderate slowing since 2022.

Introduction

The Greenland Ice Sheet contains the equivalent of 7.4 meters of global sea level rise, currently frozen atop the world's largest island (Morlighem et al. 2017). Ice sheet mass loss affects human and natural environments worldwide through coastal erosion, saltwater intrusion, habitat loss, heightened storm surges, tidal flooding, and permanent inundation. The Greenland Ice Sheet has experienced net-annual mass loss for 27 years running, for every year since 1998 (Poinar et al. 2023). It is currently the second largest contributor to sea-level rise, after ocean water thermal expansion due to warming (Zemp et al. 2019). We summarize the mass changes for the 2024 mass balance year, 1 September 2023 through 31 August 2024, and discuss influential factors.

Ice-sheet mass balance

The Greenland Ice Sheet gains mass chiefly from snow accumulation and loses mass through meltwater runoff and discharge of solid ice into the ocean (i.e., calving icebergs). The sum of these quantities is the ice-sheet mass balance: the net gain or loss of ice, usually summarized over a mass balance year.

From 1 September 2023 to 31 August 2024, the GRACE-FO (Gravity Recovery and Climate Experiment Follow-on) satellite mission measured an ice-sheet mass balance of -55 ± 35 Gt (mean ± 1 st. dev.), the

third-lowest amount of annual ice loss in the 23-year GRACE/GRACE-FO observational record (Fig. 1a). The 2002-23 average annual mass balance (September-August) measured by GRACE/GRACE-FO was -266 ± 16 Gt (Fig. 1b). The 2024 mass balance was more than 1 st. dev. above average.

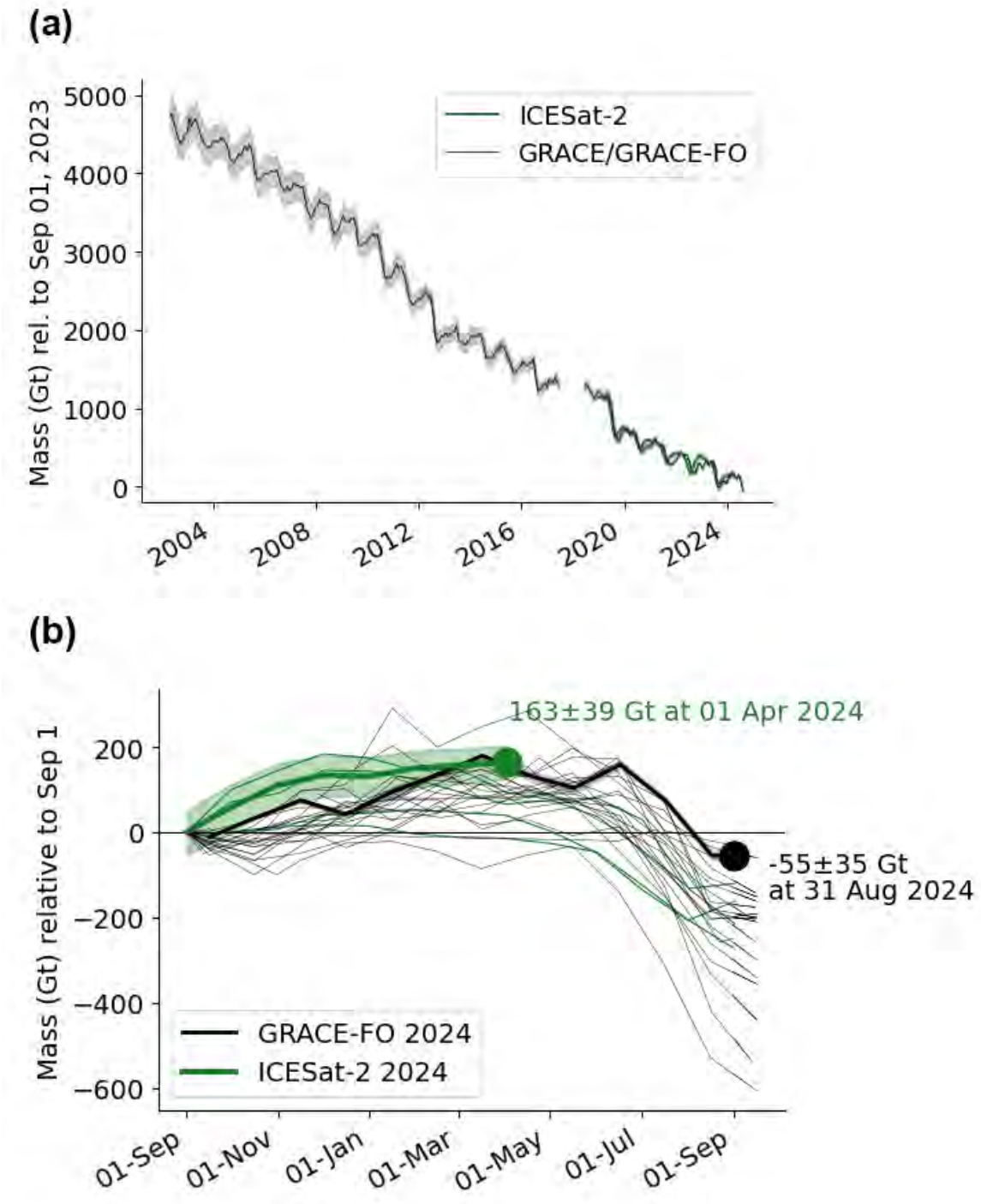

Fig. 1. (a) Observed mass balance of the Greenland Ice Sheet over 2002-24 from GRACE/GRACE-FO (black) and 2019-24 from ICESat-2 (green), with associated uncertainties (shaded). (b) Annual mass balance for 2002-23 (GRACE/GRACE-FO, thin black lines) and 2019-23 (ICESat-2, thin green lines) with the full 2024 mass balance year (GRACE-FO) and the 2024 mass balance year through 1 April (ICESat-2) in bold.

ICESat-2 measures ice-sheet surface height, from which we infer ice-sheet mass balance from 1 September 2023 through 1 April 2024, a 214-day period that ends before the onset of the melt season (Fig. 1b). The ICESat-2 and GRACE-FO mass balances through 1 April 2024 agree within 7 Gt (4%).

Surface mass balance

The sum of snow accumulation and meltwater runoff is termed surface mass balance (SMB) and is primarily responsive to snow accumulation, air temperature, albedo, snow cover, and bare-ice area. We summarize observations that influenced SMB over the 2024 mass balance year and report them relative to the 1991-2020 climatology.

Snow accumulation

Following Vandecrux et al. (2023), we integrate surface height data observed at ten inland automatic weather stations from September 2023 through June 2024 to estimate snow accumulation up to the start of the melt season (Fig. 2). Above-average pre-melt snow accumulation is evident at eight sites, with the largest positive anomalies observed across the southern ice sheet; below-average snow accumulation was observed only at two northeastern sites. These two sites contrast with coastal observations at Station Nord (location shown in Fig. 2), where the highest winter snowfall was recorded in the period of observations beginning in 1961. In Southeast Greenland, the Tasiilaq station (location shown in Fig. 2) recorded its second-highest snowfall since record-keeping began in 1898.

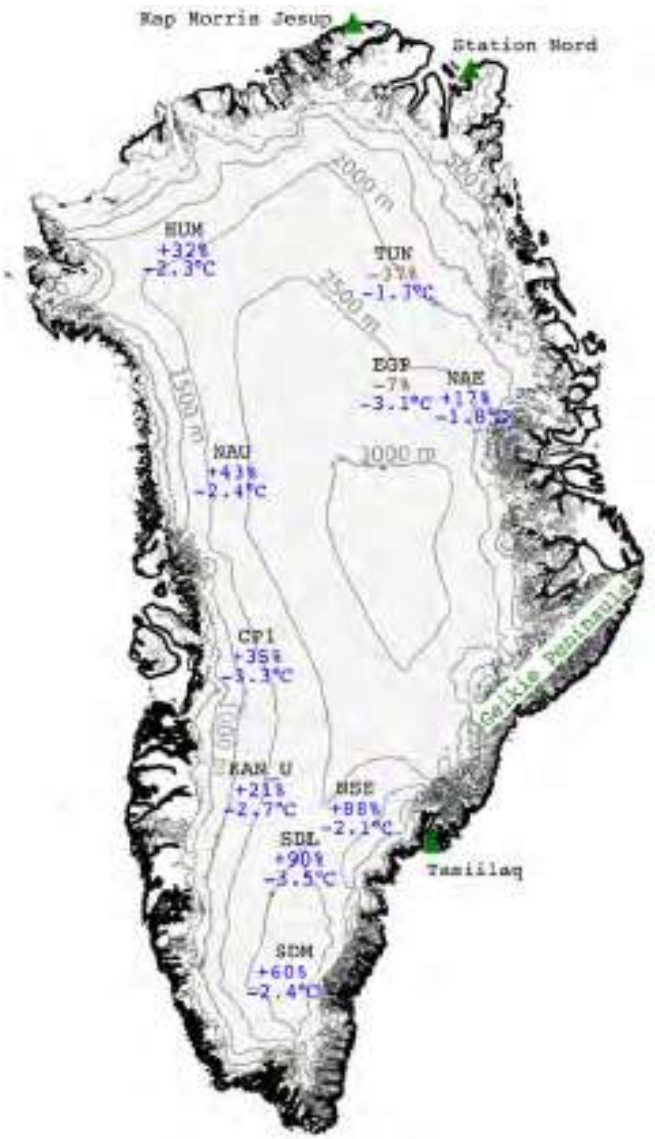

Fig. 2. Observations from 10 on-ice weather stations of snowfall accumulation anomalies from September 2023 through June 2024 compared to the 1991-2020 mean (top number, expressed as percentage), and near-surface summertime air temperature anomalies from June through August 2024 compared to 2013-23 (bottom number, expressed as anomaly). Grey shading shows ice sheet extent, with elevation contours included. Green triangles show locations of three coastal weather stations referred to in the text.

Temperature

We report monthly mean air temperatures measured at weather stations in Greenland. Air temperatures observed over the 2024 mass balance year were close to the 1991-2020 average, with seasonal and regional variation. During autumn (SON 2023), temperatures were above average; during winter (DJF 2023/24), spring (MAM 2024), and summer (JJA 2024), temperatures were close to or slightly below average at most stations. (Also see close-to-average temperatures reported across Greenland in the essay *Surface Air Temperature*.) At Kap Morris Jesup station in north Greenland (location shown in Fig. 2), average temperatures were the highest on record in September (+2.2°C anomaly) and December (+3.4°C anomaly).

Albedo and ice melt

Albedo is a measure of the sunlight reflectivity of a surface. High albedo from snow accumulation therefore helps protect the ice sheet from melting and possible mass loss. The 2024 Greenland snow and ice surface was brighter than average (Fig. 3), largely because of cloudy conditions and precipitation, including snowfall, during the melt season. These conditions occurred in western Greenland in part due to anomalously low atmospheric pressure during much of the melt season (see essay *Surface Air Temperature*) that induced northerly winds. Through May and early June, snow cover slowed the onset of melt (Fig. 4a), and surface melt extent remained largely below the 1991-2020 mean all summer, with the lowest-melt periods (e.g., late July) coinciding with periods of high albedo (Fig. 3). This corresponded to a below-average number of melt days observed across much of the western ice sheet (Fig. 4b).

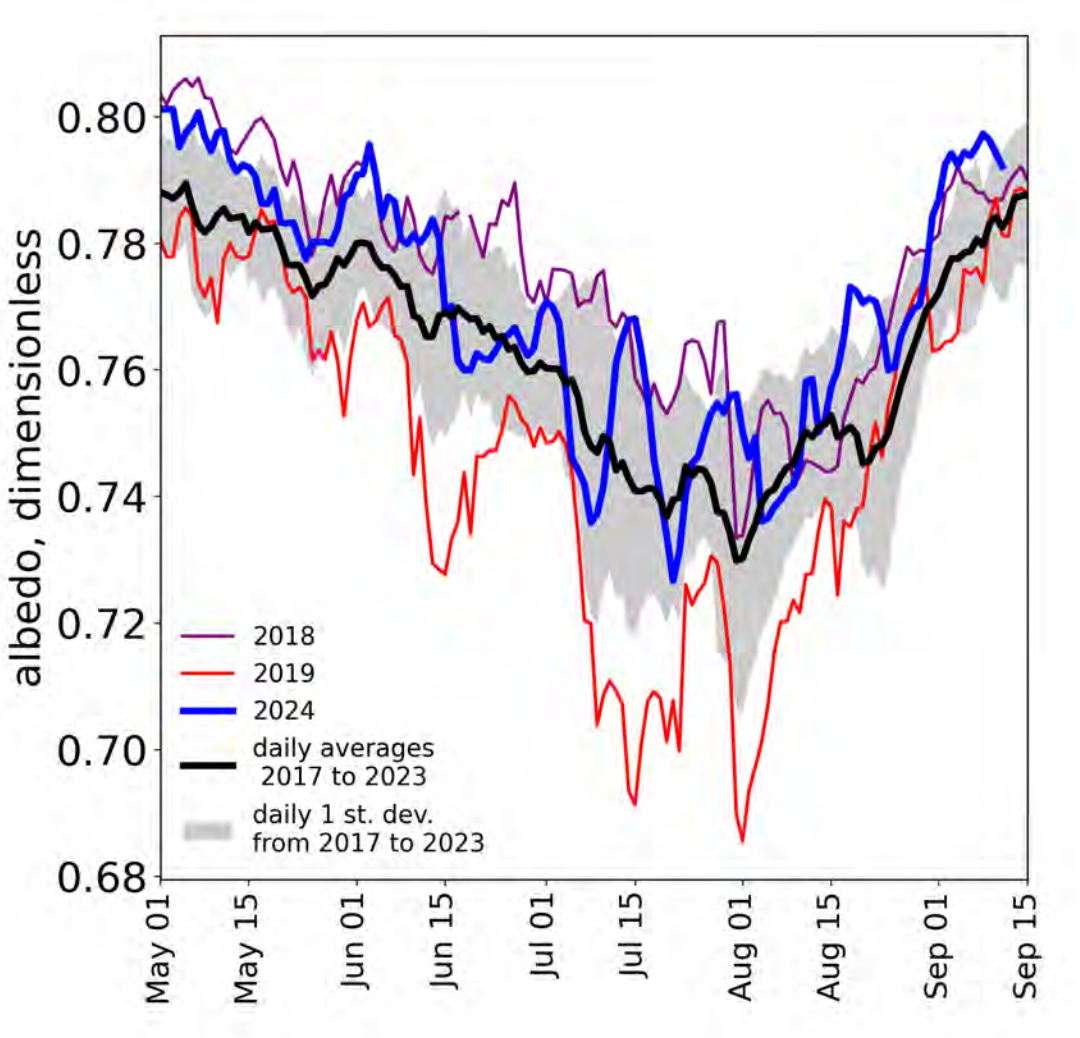

Fig. 3. Greenland daily snow and ice albedo from Sentinel-3 for the 2024 melt season through 11 September (blue) as compared to the mean and standard deviation over 2017-23 (black and gray) and recent high (bright) and low (dark) albedo years, respectively 2018 and 2019.

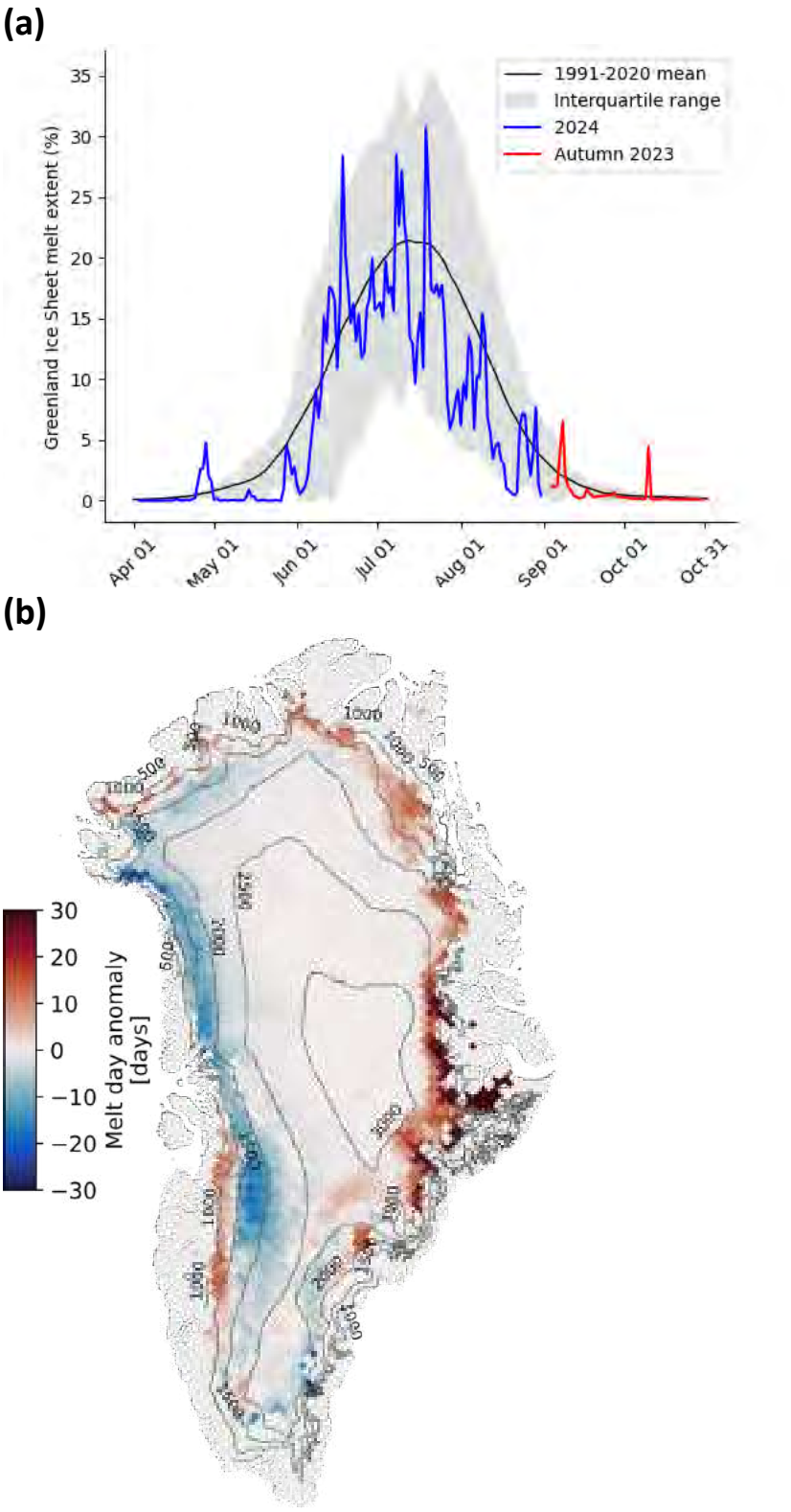

Fig. 4. (a) Surface melt extent as a percentage of ice sheet area across the 2024 mass balance year, including autumn 2023 (red) and spring/summer 2024 (blue) but omitting winter (November 2023 through March 2024), derived from SSMIS observations (Mote 2007). (b) Number of surface melt days from 1 April to 31 August 2024, expressed as an anomaly with respect to 1991-2020, also derived from SSMIS observations.

The lower-pressure conditions had a different effect in eastern Greenland, where the 2024 melt season had above-average duration. On the Geikie Peninsula (location shown in Fig. 2), melt-day anomalies as high as +46 days occurred (Fig. 4b). In Southeast Greenland, melt reached substantially farther inland than usual, with areas between 2700 and 3000 m above sea level seeing twice as many melt days as typical.

Solid ice discharge

Discharge of solid ice occurs as the hundreds of marine-terminating glaciers that ring the ice sheet export (calve) ice into the ocean; this decreases the ice sheet mass balance. We report an approximation of ice discharge: measurements of ice flux through specific locations near outlet glacier termini distributed across the ice sheet (Mankoff et al. 2020). Discharge typically peaks in July and reaches a minimum in autumn (Fig. 5). In the 2024 mass balance year through 13 August 2024, the mean discharge was 487.3 Gt/yr, approximately 1 st. dev. above the 1991-2020 mean of 458 ± 27 Gt/yr (mean ± 1 st. dev.). Total solid ice discharge at all observation times during the 2024 mass balance year exceeded the 1991-2020 mean. The above-average discharge in 2024 continues an ongoing high-discharge period that began in 2005 and peaked over 2020-21.

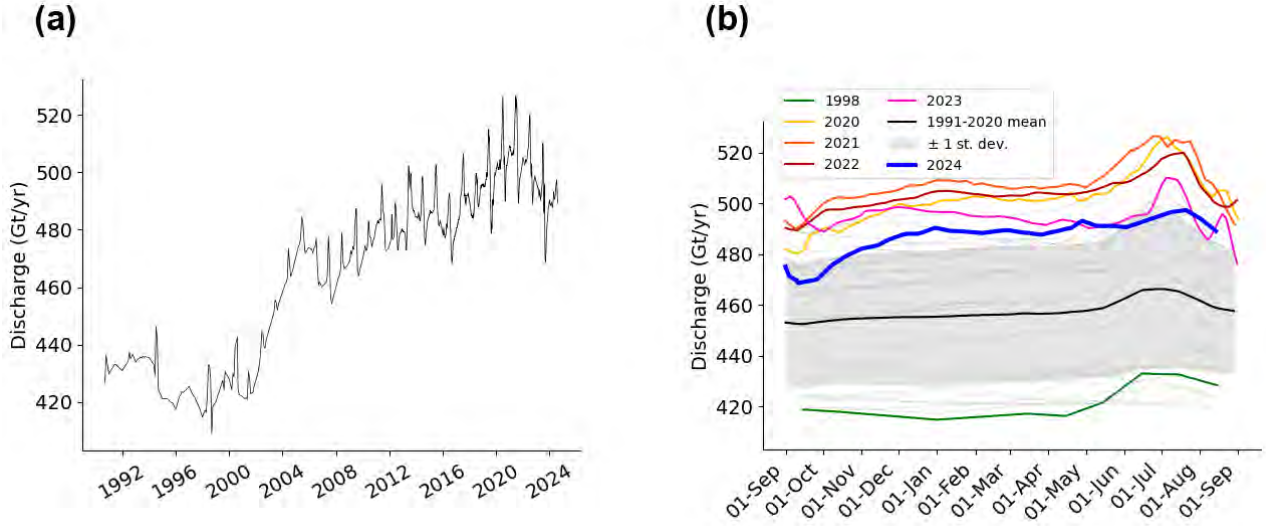

Fig. 5. (a) Solid ice discharge across the Greenland Ice Sheet observed over 1991-2024. (b) Discharge over the mass balance years 1991 through 2020 (thin gray lines) and 2024 (blue line), atop the 1991-2020 mean ± 1 st. dev. range (black line and gray shading). Notable years of high and low discharge are also shown.

Methods and data

The GRACE (Gravity Recovery and Climate Experiment, 2002-17) and GRACE-FO (Follow On, 2018-present) satellite missions detect gravity anomalies to measure changes in total ice mass (GRACE/GRACE-FO Level-2: JPL RL06.1 doi:10.5067/GFL20-MJ061; Technical Notes 13 & 14: https://podaac.jpl.nasa.gov/gravity/gracefo-documentation). We apply a regional averaging kernel (Wahr et al. 1998) to the GRACE/GRACE-FO Level-2 products that is consistent with the JPL and GSFC mascon solutions (Watkins et al. 2015; Loomis et al. 2019). The GRACE/GRACE-FO source data include peripheral glaciers and ice masses that are not part of the Greenland Ice Sheet. We scale these numbers by 0.84 to approximate changes on the ice sheet only (Colgan et al. 2015).

Weather data are obtained from 20 Danish Meteorological Institute (DMI) land-based weather stations with records starting from 1784 (Nuuk), 11 Mittarfeqarfiit stations, and Summit Station (from DMI over 1991-2019 and provided by NOAA GEOSummit since 2019). Temperature and surface ablation measurements come from ten automatic weather station transects from the Programme for Monitoring of the Greenland Ice Sheet (PROMICE) at the Geological Survey of Greenland and Denmark (GEUS), following Van As et al. (2016).

Surface melt duration and extent are derived from daily Special Sensor Microwave Imager/Sounder (SSMIS) 37 GHz horizontally polarized passive microwave radiometer satellite data (Mote 2007). This detects the presence of melt, but not the magnitude of it.

PROMICE combines ice thickness estimates with ice velocity measurements to approximate solid-ice discharge over Greenland (Mankoff et al. 2020). The approximation arises in the areas between the measurement sites and the downstream calving fronts, as the product does not measure accumulation or ablation in these areas, nor does it account for short-term ice front advance or retreat.

Changes in ice surface elevation measured by ICESat-2 reflect ice mass gain or loss as well as changes in density, snow accumulation, and melt. ICESat-2 mass-difference estimates were calculated by correcting ICESat-2 elevation measurements (Smith et al. 2023) for these anomalies (Medley et al. 2022) following the processing strategy for ICESat-2 level-3B products (Smith 2023). The largest error comes from the density, snow accumulation, and melt anomalies, together estimated at 14% of the value (Medley et al. 2022).

Acknowledgments

Sentinel-3 data processing was supported by the European Space Agency (ESA) EO Science for Society contract CCN 4000125043/18/I-NB and the ESA Network of Resources via Polar View and Polar TEP.

References

Colgan, W., and Coauthors, 2015: Hybrid glacier Inventory, Gravimetry and Altimetry (HIGA) mass balance product for Greenland and the Canadian Arctic. Remote Sens. Environ., **168**, 24-39, https://doi.org/10.1016/j.rse.2015.06.016.

Loomis, B. D., S. B. Luthcke, and T. J. Sabaka, 2019: Regularization and error characterization of GRACE mascons. *J. Geodesy*, **93**, 1381-1398, https://doi.org/10.1007/s00190-019-01252-y.

Mankoff, K. D., A. Solgaard, W. Colgan, A. P. Ahlstrøm, S. A. Khan, and R. S. Fausto, 2020: Greenland ice sheet solid ice discharge from 1986 through March 2020. *Earth Syst. Sci. Data*, **12**, 1367-1383, https://doi.org/10.5194/essd-12-1367-2020.

Medley, B., T. A. Neumann, H. J. Zwally, B. E. Smith, and C. M. Stevens, 2022: Simulations of firn processes over the Greenland and Antarctic ice sheets: 1980-2021. *Cryosphere*, **16**, 3971-4011, https://doi.org/10.5194/tc-16-3971-2022.

Morlighem, M., and Coauthors, 2017: BedMachine v3: Complete bed topography and ocean bathymetry mapping of Greenland from multibeam echo sounding combined with mass conservation. *Geophys. Res. Lett.*, **44**(21), 11051-11061, https://doi.org/10.1002/2017GL074954.

Mote, T. L., 2007: Greenland surface melt trends 1973-2007: Evidence of a large increase in 2007. *Geophys. Res. Lett.*, **34**(22), L22507, https://doi.org/10.1029/2007GL031976.

Poinar, K., and Coauthors, 2023: Greenland Ice Sheet. *Arctic Report Card 2023*, R. L. Thoman, T. A. Moon, and M. L. Druckenmiller, Eds., https://doi.org/10.25923/yetx-rs76.

Smith, B., 2023: Algorithm Theoretical Basis Document (ATBD) for Land-ice DEM (ATL14) and Land-ice height change (ATL15). NASA Goddard Space Flight Center, https://nsidc.org/sites/default/files/documents/technical-reference/icesat2_atl14_atl15_atbd_v003.pdf.

Smith, B., S. Dickinson, B. P. Jelley, T. A. Neumann, D. Hancock, J. Lee, and K. Harbeck, 2023: ATLAS/ICESat-2 L3B Slope-Corrected Land Ice Height Time Series, Version 6 [Data Set]. NASA National Snow and Ice Data Center Distributed Active Archive Center, Boulder, CO, USA, accessed: 25 August 2024, https://doi.org/10.5067/ATLAS/ATL11.006.

van As, D., R. S. Fausto, J. Cappelen, R. S. W. van de Wal, R. J. Braithwaite, H. Machguth, and PROMICE project team, 2016: Placing Greenland ice sheet ablation measurements in a multi-decadal context. *GEUS Bull.*, **35**, 71-74, https://doi.org/10.34194/geusb.v35.4942.

Vandecrux, B., and Coauthors, 2023: The historical Greenland Climate Network (GC-Net) curated and augmented level-1 dataset. *Earth Syst. Sci. Data*, **15**, 5467-5489, https://doi.org/10.5194/essd-15-5467-2023.

Wahr, J., M. Molenaar, and F. Bryan, 1998: Time variability of the Earth's gravity field: Hydrological and oceanic effects and their possible detection using GRACE. *J. Geophys. Res.*, **103**(B12), 30205-30229, https://doi.org/10.1029/98JB02844.

Watkins, M. M., D. N. Wiese, D. N. Yuan, C. Boening, and F. W. Landerer, 2015: Improved methods for observing Earth's time variable mass distribution with GRACE using spherical cap mascons. *J. Geophys. Res.-Sol. Ea.*, **120**(4), 2648–2671, https://doi.org/10.1002/2014JB011547.

Zemp, M., and Coauthors, 2019: Global glacier mass changes and their contributions to sea-level rise from 1961 to 2016. *Nature*, **568**, 382-386, https://doi.org/10.1038/s41586-019-1071-0.

November 15, 2024

Sea Ice

https://doi.org/10.25923/aksk-7p66

W. N. Meier[1], A. Petty[2], S. Hendricks[3], A. Bliss[4], L. Kaleschke[3], D. Divine[5], S. Farrell[6], S. Gerland[5], D. Perovich[7], R. Ricker[8], X. Tian-Kunze[3], and M. Webster[9]

[1]National Snow and Ice Data Center, Cooperative Institute for Research in Environmental Sciences, University of Colorado Boulder, Boulder, CO, USA
[2]Earth System Science Interdisciplinary Center, University of Maryland, College Park, MD, USA
[3]Alfred Wegener Institute, Helmholtz Centre for Polar and Marine Research, Bremerhaven, Germany
[4]Goddard Space Flight Center, NASA, Greenbelt, MD, USA
[5]Norwegian Polar Institute, Fram Centre, Tromsø, Norway
[6]Department of Geographical Sciences, University of Maryland, College Park, MD, USA
[7]Thayer School of Engineering, Dartmouth College, Hanover, NH, USA
[8]NORCE Norwegian Research Centre, Tromsø, Norway
[9]Polar Science Center, Applied Physics Laboratory, University of Washington, Seattle, WA, USA

Headlines

- Sea ice extent in September 2024 was the 6th lowest in the satellite record (1979 to present); the last 18 September extents (2007-24) are the 18 lowest in the record.
- The long-term negative trends in total extent and the amount of older, thicker ice continued. The more recent period since 2007 has been characterized by low extent, but without a significant trend.
- Average sea ice thickness for winter 2023/24 winter was lower than the previous winter, and close to the 2011-23 average thickness; volume at the end of the 2022/23 winter was nearly the same as the previous year.

Introduction

Arctic sea ice is the frozen interface between the ocean and the atmosphere. It reduces the absorption of solar energy because of its high albedo relative to the darker open ocean surface. As a physical barrier, it modifies the heat and moisture transfer between the atmosphere and ocean. Sea ice plays a key role in polar ecosystems, providing an essential habitat for marine life and modulating the biogeochemical balance of the Arctic. The sea ice cover has long played a practical and cultural role in Indigenous communities of the North. Historically, the presence of sea ice limited national and corporate activities in the Arctic, but sea ice decline is allowing an increase in maritime traffic and drives reevaluation of resource extraction and national security activities in the Arctic.

Ice freeze-up in winter 2023/24 was relatively rapid compared to recent years, particularly in the East Siberian and Laptev Seas. The autumn and winter sea ice growth rates brought the ice cover nearer to, but below, average in those months. The extent remained below average through spring, before starting a rapid decline in June.

Near-surface air temperatures during the 2023/24 winter were higher than the 1991-2020 average for most of the Arctic Ocean, particularly north of Greenland and the Canadian Archipelago (see essay *Surface Air Temperature*). Summer temperatures were also largely above average, particularly in the Barents Sea region; cooler than average summer temperatures were found over the Chukchi Sea.

Sea ice extent

Sea ice extent, defined as the total area covered by ice of at least 15% concentration, is one of the most commonly used indicators of long-term Arctic sea ice conditions. The primary source of extent observations is the 46-year record (starting in 1979) derived from satellite-borne passive microwave sensors.

This satellite record tracks long-term trends, variability, and seasonal changes from the annual extent maximum in late February or March to the annual extent minimum in September. In recent years, minimum extents are ~50% of the values in the 1980s. In 2024, March and September extents were similar to other recent years (Fig. 1), but much lower than the 1991-2020 average, and the long-term negative trends continue (Table 1). March 2024 was marked by near-average sea ice extent around most of the perimeter of the sea ice edge, with low ice cover in the Barents Sea and the Gulf of St. Lawrence (Fig. 2). At the beginning of the melt season, ice retreat was initially fairly slow through May. A notable exception was the extremely early opening of eastern Hudson Bay where substantial open water began appearing by mid-May 2024 due to strong easterly winds. This was unusual, since typically Hudson Bay's western sector opens up first and the eastern part of the bay remains largely ice-covered well into June.

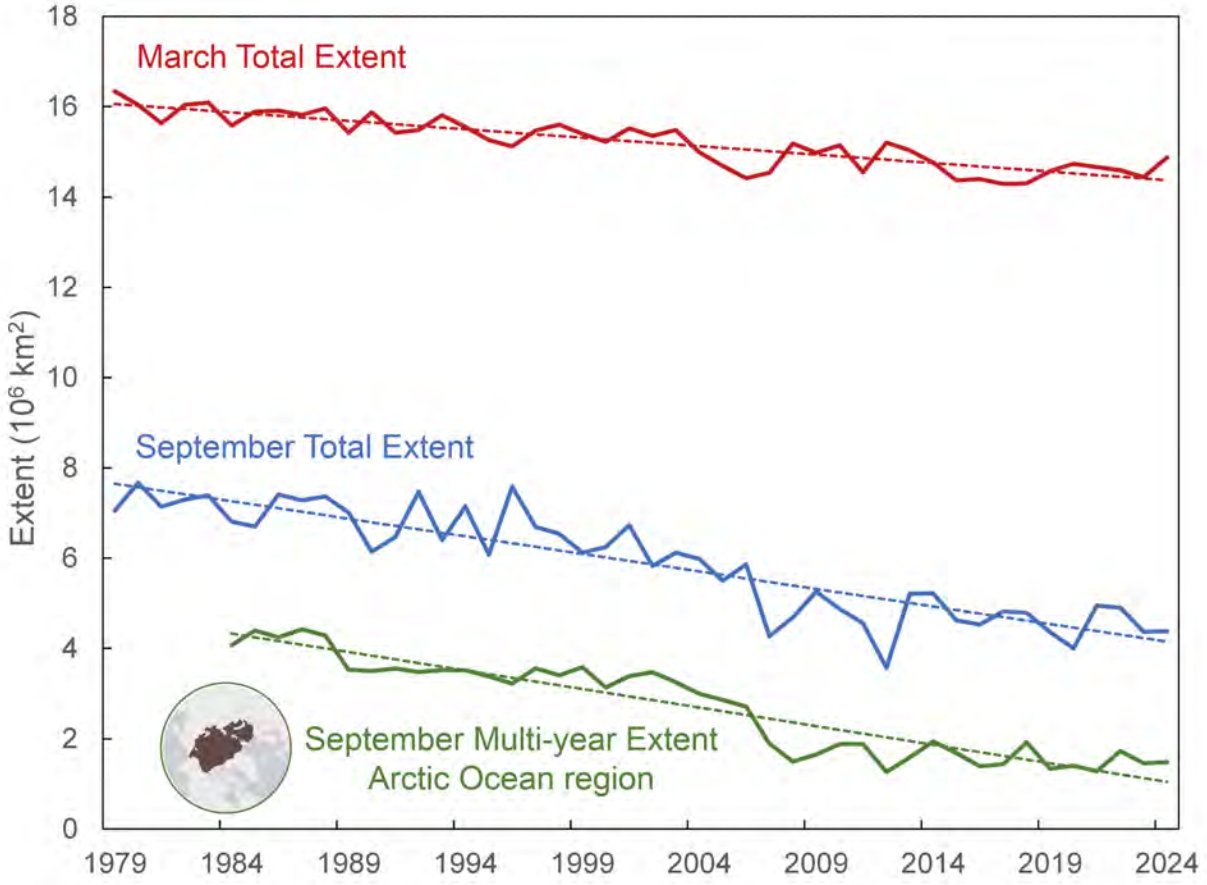

Fig. 1. March (red) and September (blue) total extent for 1979-2024, multi-year September extent (green) for 1984-2024 and linear trend lines (dashed lines). The Arctic Ocean region map is inset in the bottom left.

Table 1. March and September monthly averages and annual daily maximum and minimum extents for 2024 and related statistics. The rank is from least sea ice to most sea ice of the 46 years (1 = least, 46 = most).

Values	**March** Monthly Average	**March** Daily Maximum	**September** Monthly Average	**September** Daily Minimum
Extent (10^6 km^2)	14.87	15.01	4.38	4.28
Rank (out of 46 years)	15	15	6	7
1991-2020 average (10^6 km^2)	15.03	15.26	5.58	5.37
Anomaly rel. **1991-2020** average (10^6 km^2)	-0.16	-0.25	-1.20	-1.09
Trend, 1979-2024 (km^2/yr)	-37,400	-40,800	-77,800	-76,900
% change from 1979 linear trend value	-7.6	-8.3	-42.7	-42.5

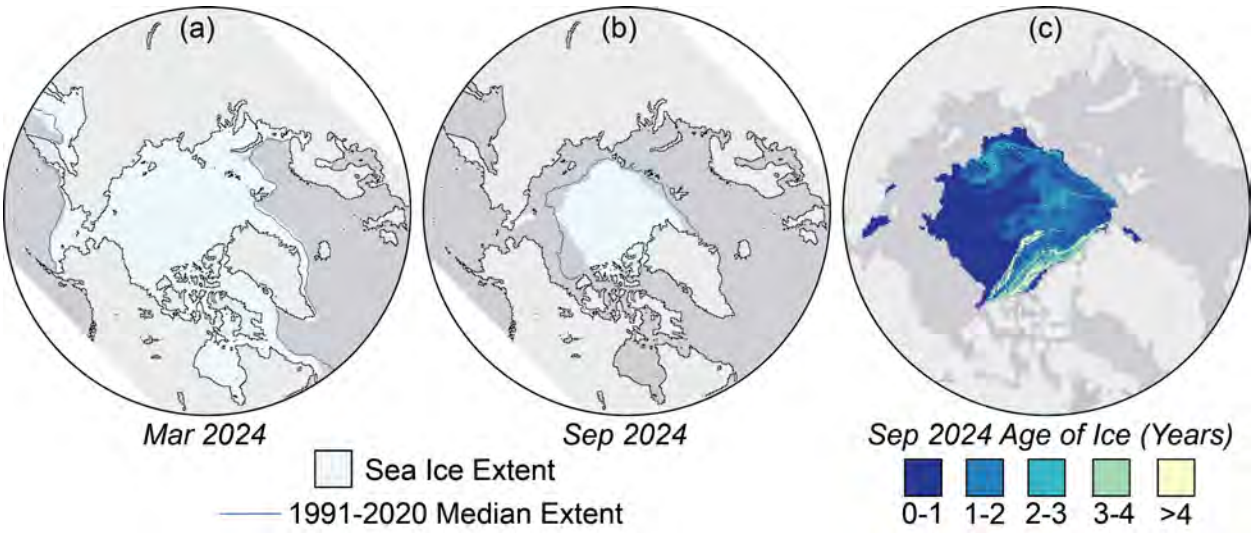

Fig. 2. Monthly average sea ice extent (light blue) for (a) March 2024, and (b) September 2024; the median extent for 1991-2020 is shown by the dark blue contour. (c) September sea ice age extent.

In June, the overall rate of retreat in ice extent was near-average, but then accelerated in July and August. Nonetheless, substantial ice remained in the Chukchi and East Siberian Seas into late August, delaying the opening of the Northern Sea Route. One factor was an unusually persistent area of ice between Wrangell Island and the northeastern Siberian coast that remained throughout the summer. This ice formed from strong convergence and deformation during the spring, which caused substantial ridging, enabling the ice to resist thermodynamic melt. The ice was brownish-gray, suggesting entrapment of shelf bottom sediment within the ice. A rapid and early sea ice retreat was observed in Fram Strait in the northern Greenland Sea, which was nearly ice free by mid-August, with the only traces of sea ice being landfast ice east of northeast Greenland.

By late August, sea ice finally retreated from the Siberian coast, opening up the Northern Sea Route, while the deformed Wrangell Island ice persisted. Summer extent remained closer to average for most regions on the Atlantic side in the Laptev, Kara, and Barents Seas (Fig. 2). The Northwest Passage through the Canadian Archipelago became clear of ice along the southern route in late August. The northern route was blocked at the western end of through most of the summer by ice in M'Clure Strait, but even here ice cleared in late September. The summer 2024 extent in the Passage reached the lowest observed in the satellite record, based on Canadian Ice Service ice charts (Sea Ice Today 2024).

The extent of older ice (here defined as >4 years old), observed by tracking the motion of ice with satellite imagery and buoys, was similar to recent years. Age is a proxy for ice thickness because multiyear ice generally grows thicker through successive winter periods. Multiyear ice was largely constrained near the north coast of Greenland and the Canadian Archipelago, with some drifting into the Beaufort and Chukchi Seas (Fig. 2c). Multiyear ice extent has shown interannual oscillations but no clear trend since 2007, reflecting variability in the summer sea ice melt and export out of the Arctic. After a year when substantial multiyear ice is lost, a much larger area of first-year ice generally takes its place. Some of this first-year ice can persist through the following summer, contributing to the replenishment of the multiyear ice extent. However, since 2012, old ice has remained consistently low, less than 5% of the levels in the 1980s. Thus, multiyear ice remains in the Arctic for fewer years than in earlier decades. At the end of summer 2024, multiyear ice extent was similar to 2022 and 2023 values (Fig. 1), 40% of the multiyear extents in the 1980s and 1990s.

Melt onset of sea ice

In spring, the snow cover on top of the sea ice begins to melt, which lowers the albedo and increases the potential absorption of solar radiation within the snow and sea ice cover. Sea ice melt typically begins in early March in the southern fringes of the ice cover and on average proceeds latitudinally, with melt in the high Arctic around the North Pole beginning in August, if it occurs at all (Fig 3a). The 2024 melt onset was mixed, with earlier melt in eastern Hudson Bay, Baffin Bay, northeast of Greenland and much of the Beaufort Sea (Fig. 3b). Melt was later than average along the Siberian coast, corresponding to the late decline of sea ice extent in that region. Overall, the average date of the melt onset has trended earlier since 1979, but with large year-to-year variability (Fig 3c). On average, melt starts about 15 days earlier today than in the 1980s.

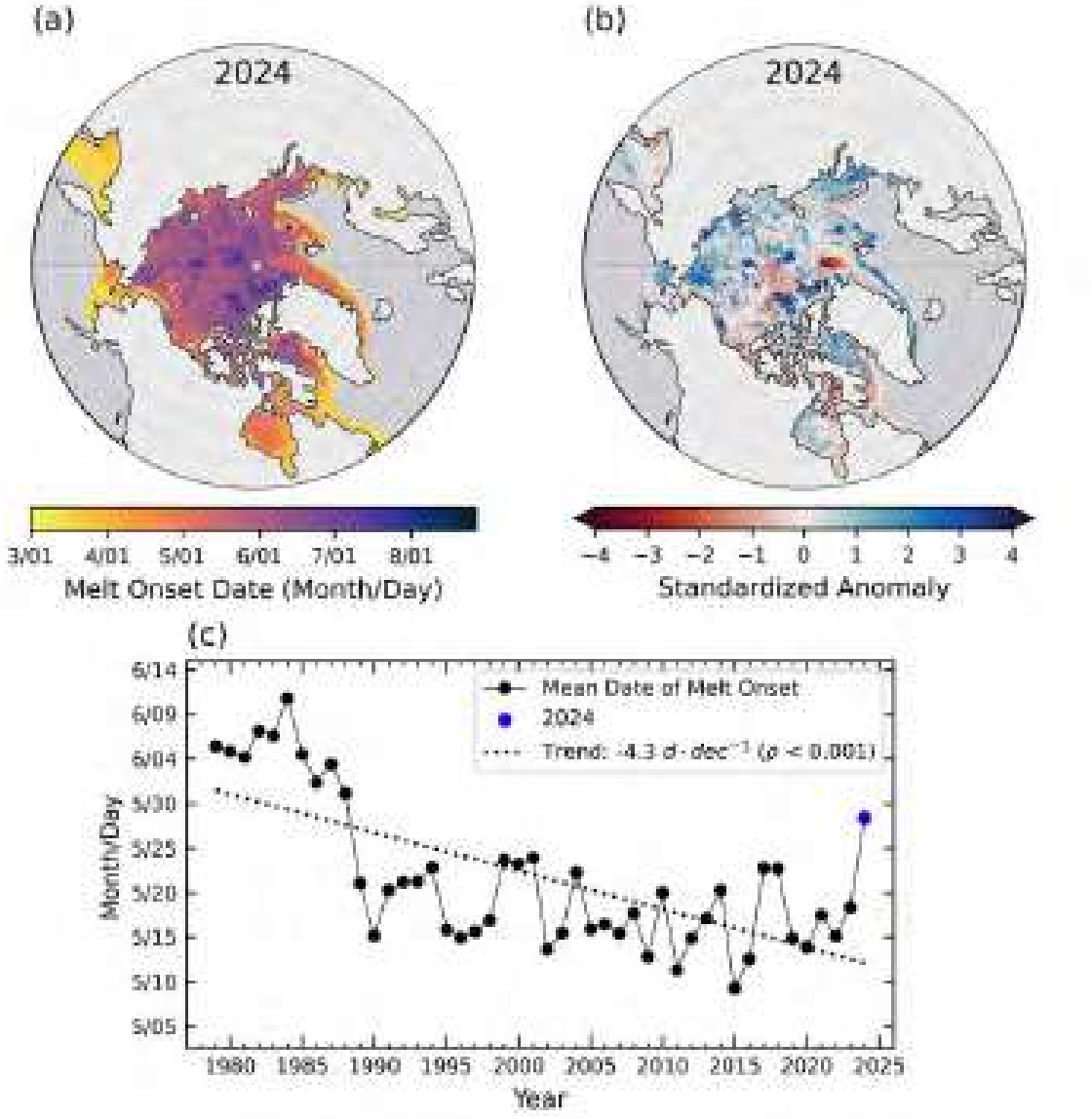

Fig. 3. (a) 2024 sea ice melt onset date; (b) 2024 melt standardized anomaly (anomaly divided by standard deviation) relative to the 1991-2020 average; (c) Arctic mean melt onset date for 1979-2024 and linear trend line for the Arctic Ocean Region, which includes the Arctic Ocean and the Kara and Barents Seas.

Sea ice thickness and volume

Estimates of sea ice thickness from satellite altimetry are used to more directly track this important metric of sea ice conditions, although the satellite altimeter record is shorter than that for extent, ice age, and melt onset. ICESat-2 and CryoSat-2/SMOS satellite data are used to track seasonal ice growth in winter between October and April (Fig. 4a). The timeseries since 2010 shows a slightly thinner ice cover during 2023-24, particularly during October 2023. The ice thickness anomaly map for April 2024 (Fig. 4b), derived from CryoSat-2/SMOS observations relative to the 2010-23 April mean, shows that ice in the Canada Basin between the Beaufort Sea and the pole was thinner than average, as was ice in the Laptev Sea, while for the Siberian side of the Arctic, ice was thicker than average. Although the 14-year time series is relatively short, there is a trend toward thinner ice across most of the thicker multi-year ice of the North American Arctic, offset to some degree by a thickening trend in the Siberian Arctic, particularly in the Kara Sea (Fig. 4c).

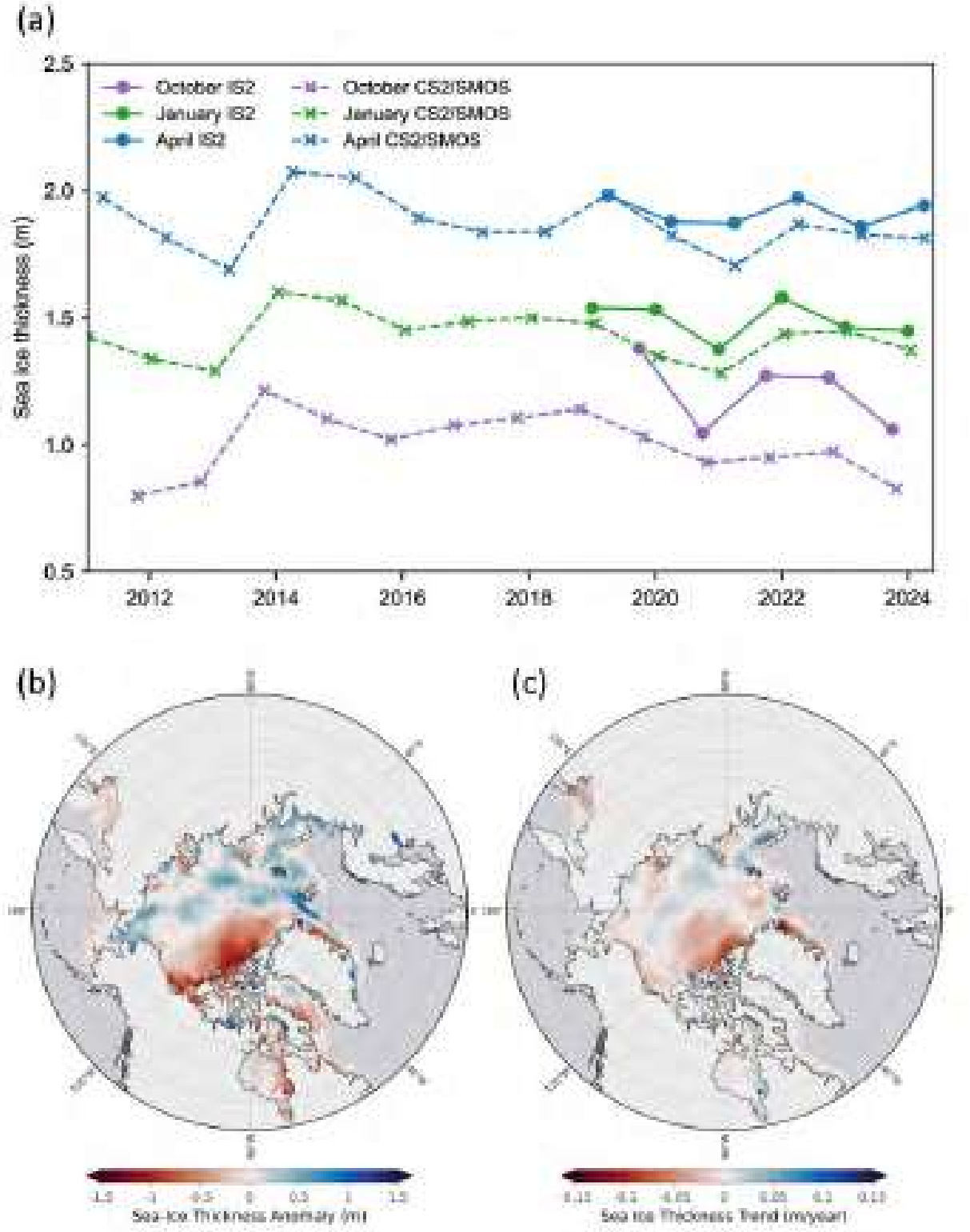

Fig. 4. (a) 2011-24 October (purple), January (green), and April (blue) monthly average sea ice thickness, calculated over an Inner Arctic Ocean Domain (Central Arctic, Beaufort, Chukchi, Laptev, East Siberian Seas), from ICESat-2 (circles) and CryoSat-2/SMOS (crosses); (b) April 2024 sea ice thickness anomaly map from CryoSat-2/SMOS (relative to the 2011-23 average); (c) CryoSat-2/SMOS March thickness trend map over the period of 2011-24.

Sea ice thickness is integrated with ice concentration to provide winter volume estimates for the CryoSat-2/SMOS measurement time period. Seasonal change, from winter maximum to summer minimum and back, shows the strong seasonal cycle and interannual variability (Fig. 5). There is little indication of a trend through the relatively short 13-year time series.

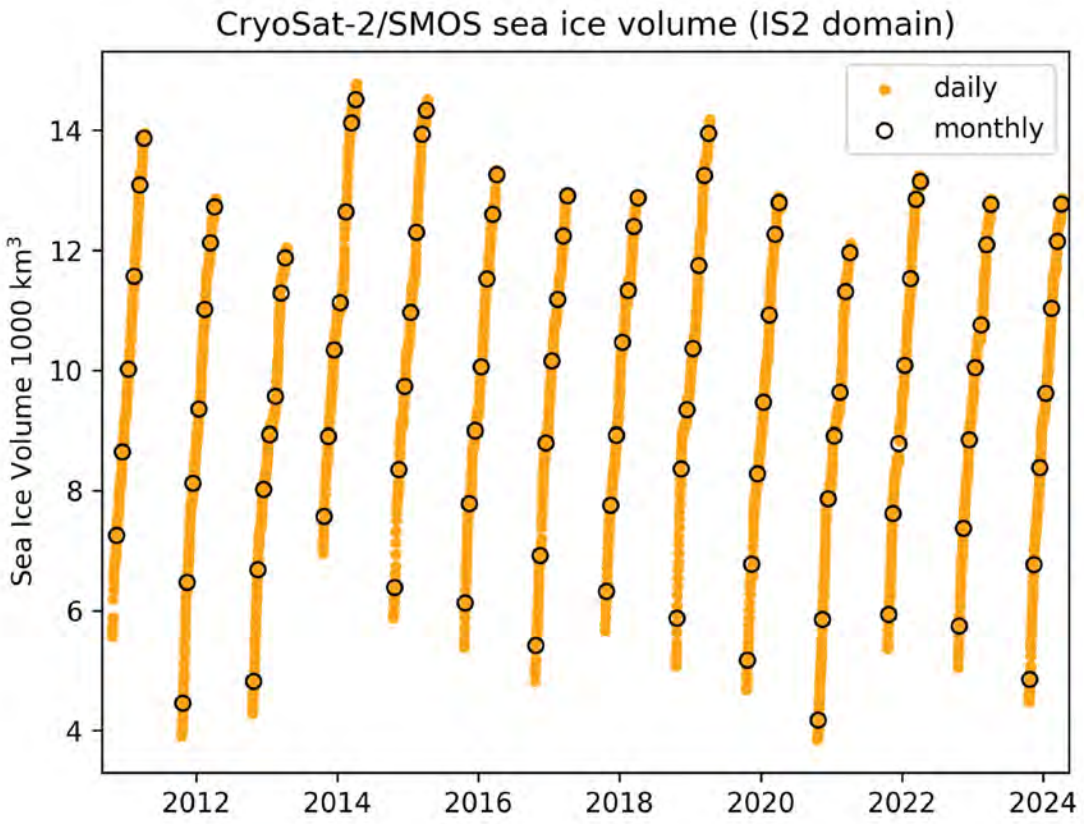

Fig. 5. Winter (October-April) sea ice volume for October 2010 to April 2024 from CrySat-2/SMOS. Each year volume increases from October (bottom of orange points) through April (top of orange points), with no data during the summer (May-September) melt season.

Methods and data

Sea ice extent values are from the NSIDC Sea Ice Index (Fetterer et al. 2017), based on passive microwave derived sea ice concentrations from the NASA Team algorithm (Cavalieri et al. 1996; Maslanik and Stroeve 1999), though other high quality products exist (e.g., Lavergne et al. 2019).

Sea ice age data are from the EASE-Grid Sea Ice Age, Version 4 (Tschudi et al. 2019a) and Quicklook Arctic Weekly EASE-Grid Sea Ice Age, Version 1 (Tschudi et al. 2019b) archived at the NASA Snow and Ice Distributed Active Archive Center (DAAC) at NSIDC. Age is calculated via Lagrangian tracking of ice parcels using weekly sea ice motion vectors. Only the oldest age category is preserved for each grid cell.

Melt onset is estimated from passive microwave brightness temperatures, which change significantly when liquid water develops on snow and ice surfaces (Bliss 2023).

Satellite altimetry has enabled the continuous retrieval of sea ice freeboard for ice thickness and volume estimates over the entire Arctic basin during the freezing season (October-April). A consistent record

began in 2010 with the launch of the European Space Agency (ESA) CryoSat-2 radar altimeter. This was followed in September 2018 by the launch of the NASA Ice, Cloud, and land Elevation 2 (ICESat-2) laser altimeter. Thus, there are now two independent altimetry sources for deriving sea ice thickness and volume estimates.

Weekly CryoSat-2 estimates have been combined with thin ice (<1 m) estimates from the ESA Soil Moisture Ocean Salinity (SMOS) instrument, launched in 2009, to obtain an optimal estimate across thin and thick ice regimes (Ricker et al. 2017) on a 25 km resolution EASE2 grid. Optimal interpolation is used to fill data gaps in the weekly CryoSat-2 fields and to merge the CryoSat-2 and SMOS estimates. The results here are from Version 206 (European Space Agency 2023). When combined with sea ice concentration, the CryoSat-2/SMOS record of ice thickness is used to compute sea ice volume; data are available at ftp://ftp.awi.de/sea_ice/product/cryosat2_smos/.

The ICESat-2 thickness data (Petty et al. 2023a) used here are the gridded 25 km x 25 km monthly data using Version 6 ATL10 freeboards from the three strong beams of ICESat-2 and v1.1 NESOSIM snow loading (depth and density) as described in Petty et al. (2023b).

Acknowledgments

W. Meier thanks the NSIDC DAAC and the NASA ESDIS projects for support.

References

Bliss, A. C., 2023: Passive microwave Arctic ice melt onset dates from the advanced horizontal range algorithm 1979-2022. *Sci. Data*, **10**, 857, https://doi.org/10.1038/s41597-023-02760-5.

Cavalieri, D. J., C. L. Parkinson, P. Gloersen, and H. J. Zwally, 1996 (updated yearly): Sea Ice Concentrations from Nimbus-7 SMMR and DMSP SSM/I-SSMIS Passive Microwave Data, Version 1. NASA National Snow and Ice Data Center Distributed Active Archive Center, Boulder, CO, USA, accessed 12 September 2023, https://doi.org/10.5067/8GQ8LZQVL0VL.

European Space Agency, 2023: SMOS-CryoSat L4 Sea Ice Thickness, Version 206. https://doi.org/10.57780/sm1-4f787c3.

Fetterer, F., K. Knowles, W. N. Meier, M. Savoie, and A. K. Windnagel, 2017 (updated daily): Sea Ice Index, Version 3. NSIDC: National Snow and Ice Data Center, Boulder, CO, USA, accessed 12 September 2023, https://doi.org/10.7265/N5K072F8.

Lavergne, T., and Coauthors, 2019: Version 2 of the EUMETSAT OSI SAF and ESA CCI sea-ice concentration climate data records. *Cryosphere*, **13**, 49-78, https://doi.org/10.5194/tc-13-49-2019.

Maslanik, J., and J. Stroeve, 1999: Near-Real-Time DMSP SSMIS Daily Polar Gridded Sea Ice Concentrations, Version 1. NASA National Snow and Ice Data Center Distributed Active Archive Center, Boulder, CO, USA, accessed 12 September 2023, https://doi.org/10.5067/U8C09DWVX9LM.

Petty, A. A., N. Kurtz, R. Kwok, T. Markus, T. A. Neumann, and N. Keeney, 2023a: ICESat-2 L4 Monthly Gridded Sea Ice Thickness, Version 3 [Data Set]. NASA National Snow and Ice Data Center Distributed

Active Archive Center, Boulder, CO, USA, accessed 13 August 2023, https://doi.org/10.5067/ZCSU8Y5U1BQW.

Petty A. A., N. Keeney, A. Cabaj, P. Kushner, and M. Bagnardi, 2023b: Winter Arctic sea ice thickness from ICESat-2: upgrades to freeboard and snow loading estimates and an assessment of the first three winters of data collection.. *Cryosphere*, **17**, 127-156, https://doi.org/10.5194/tc-17-127-2023.

Ricker, R., S. Hendricks, L. Kaleschke, X. Tian-Kunze, J. King, and C. Haas, 2017. A weekly Arctic sea-ice thickness data record from merged CryoSat-2 and SMOS satellite data. *Cryosphere*, **11**, 1607-1623, https://doi.org/10.5194/tc-11-1607-2017.

Sea Ice Today, 2024: The waning of Arctic summer. National Snow and Ice Data Center, Northwest Passage image and analysis from Stephen Howell, Environment and Climate Change Canada, accessed 19 August 2024, https://nsidc.org/sea-ice-today/analyses/waning-arctic-summer.

Tschudi, M., W. N. Meier, J. S. Stewart, C. Fowler, and J. Maslanik, 2019a: EASE-Grid Sea Ice Age, Version 4. [March, 1984-2020]. NASA National Snow and Ice Data Center Distributed Active Archive Center, Boulder, CO, USA, accessed 5 September 2023, https://doi.org/10.5067/UTAV7490FEPB.

Tschudi, M., W. N. Meier, and J. S. Stewart, 2019b: Quicklook Arctic Weekly EASE-Grid Sea Ice Age, Version 1. [March, 2021]. NASA National Snow and Ice Data Center Distributed Active Archive Center, Boulder, CO, USA, accessed 5 September 2023, https://doi.org/10.5067/2XXGZY3DUGNQ.

November 11, 2024

Sea Surface Temperature

https://doi.org/10.25923/9z96-aq19

M. -L. Timmermans[1] and Z. M. Labe[2]

[1]Department of Earth and Planetary Sciences, Yale University, New Haven, CT, USA
[2]Geophysical Fluid Dynamics Laboratory, NOAA, Princeton, NJ, USA

Headlines

- August 2024 mean sea surface temperatures (SSTs) were ~2-4°C warmer than 1991-2020 August mean values in most Arctic Ocean marginal seas.
- Anomalously cool August 2024 SSTs (~1-4°C cooler) were observed in the Chukchi Sea.
- August mean SSTs show warming trends for 1982-2024 in almost all Arctic Ocean regions that are ice-free in August, with mean SST increases of ~0.3°C per decade in the region north of 65° N.

Arctic Ocean sea-surface temperatures (SSTs) in the summer are primarily influenced by the amount of incoming solar radiation absorbed by the sea surface and by the flow of warm waters into the Arctic from the North Atlantic and North Pacific Oceans. Solar warming of the Arctic Ocean surface is influenced by the sea-ice distribution (with greater warming occurring in ice-free regions), cloud cover, and upper-ocean stratification. Inflows of relatively warm Arctic river waters can provide an additional heat source in coastal regions.

Arctic SST is an essential indicator of the strength of the ice-albedo feedback cycle in any given summer sea-ice melt season. As the brighter sea-ice cover decreases, more incoming solar radiation is absorbed by the darker ocean surface and, in turn, the warmer ocean melts more sea ice. Marine ecosystems are also influenced by SSTs, which affect the timing and development of primary production cycles, as well as available habitat. In addition, higher SSTs are associated with delayed autumn sea ice freeze-up and increased ocean heat storage throughout the year. An essential point for consideration, however, is that the total heat content contained in the ocean surface layer (i.e., the mixed layer) depends on the mixed-layer depth; a shallower mixed layer with higher SSTs could contain the same amount of heat as a deeper mixed layer with lower SSTs. We focus only on SSTs here and do not quantify ocean heat content (in the mixed layer and in deeper warm layers) due to a lack of in situ observations. While pan-Arctic assessments are limited by a lack of observations, particularly in the boundary regions of the Arctic basin, global climate model studies suggest an increasing role for ocean heat content in accelerating Arctic sea-ice loss (e.g., Oldenburg et al. 2024).

The SST data analyzed span June 1982 through August 2024, with 1991-2020 used as the climatological reference period (i.e., “normal”; see *Methods and data*). Here, we focus most closely on August 2024 mean SSTs in context with the climatological record. August mean SSTs provide the most appropriate representation of Arctic Ocean summer SSTs because sea-ice extent is near a seasonal low at this time of year, and there is not yet the influence of surface cooling and subsequent sea-ice growth that typically takes place in the latter half of September. For this reason, there is more temporal variability in SST (quantified by the standard deviation) in September compared to August. As an example, the mean of each year’s standard deviation of weekly Arctic Ocean (north of 65° N) average SST over the 1991-2020

reference period is approximately 0.1°C in August but increases to 0.3°C in September. This variance in September is even higher if considering the individual marginal seas separately.

August 2024 mean SSTs were as high as ~12°C in the southern Barents Sea and reached values as high as ~7°C in other Arctic basin marginal regions (Fig. 1a,b). August 2024 mean SSTs were anomalously warm compared to the 1991-2020 August mean in the Barents, Kara, Laptev, and southern Beaufort Seas (around 1°C-4°C higher), and anomalously cold in the East Siberian, Chukchi, and northern Beaufort Seas (around 0.5°C-4.0°C lower than the 1991-2020 mean; Fig. 1c). The cold SSTs in the Arctic Pacific sector also extend through the Bering Sea. This general pattern of August 2024 SSTs is consistent with regional patterns of anomalously warm and cold surface-air temperatures in July-August 2024 (see essay *Surface Air Temperature*). Regional SST variations differ significantly from year to year. For example, there were considerably higher SSTs in the northern Barents Sea in August 2024 compared to August 2023, with differences of up to 2°C, and mostly lower 2024 SSTs in the Kara and southern Beaufort Seas (Fig. 1d).

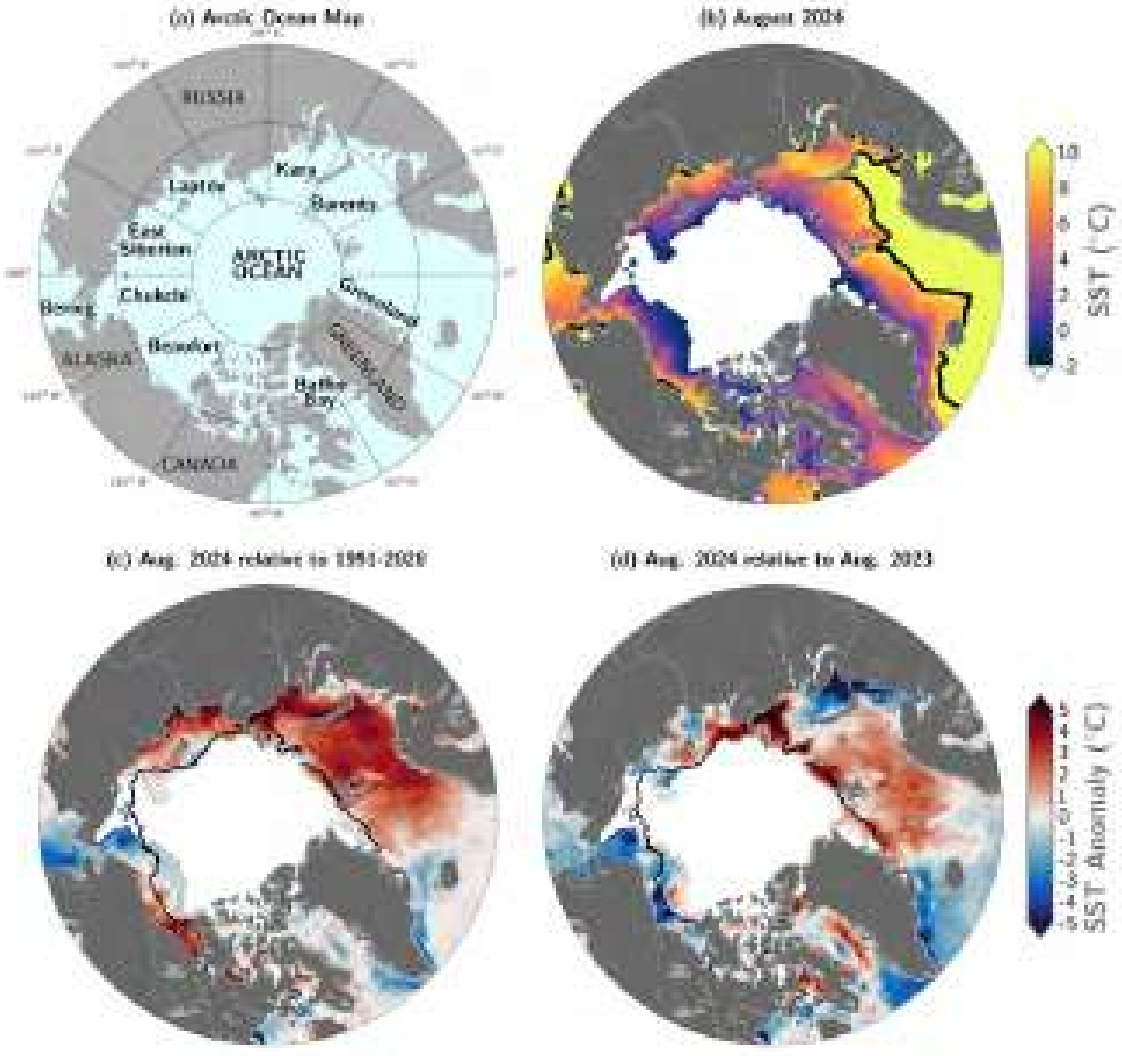

Fig. 1. (a) Arctic Ocean map showing relevant marginal sea locations and geographic features. (b) Mean sea-surface temperature (SST; °C) in August 2024. Black contours indicate the 10°C-SST isotherm. (c) SST anomalies (°C) in August 2024 relative to the August 1991-2020 mean. (d) Difference between August 2024 SSTs and August 2023 SSTs (negative values indicate where 2024 was cooler). White shading in all panels is the August 2024 mean sea-ice extent. Black lines in (c) and (d) indicate the August 1991-2020 median ice edge.

Below-normal August 2024 SSTs in the Chukchi Sea were also observed in June and July, as well as in the eastern sector of the Bering Sea (Fig. 2). This is consistent with relatively cold July/August 2024 surface-air temperatures in the region (see essay *Surface Air Temperature*) and persistent areas of higher sea-ice concentration (see essay *Sea Ice*). Above-normal August 2024 SSTs in the Kara and Laptev Seas were also observed in July (Fig. 2b,c) as sea ice began to retreat from those regions, suggesting the ice-albedo feedback was playing a role in ice retreat and SST warming. The transition from below-normal to above-normal August SSTs from June to August in the Barents Sea corresponded with the transition from anomalously cool surface air temperatures in June to warm in July/August (see essay *Surface Air Temperature*).

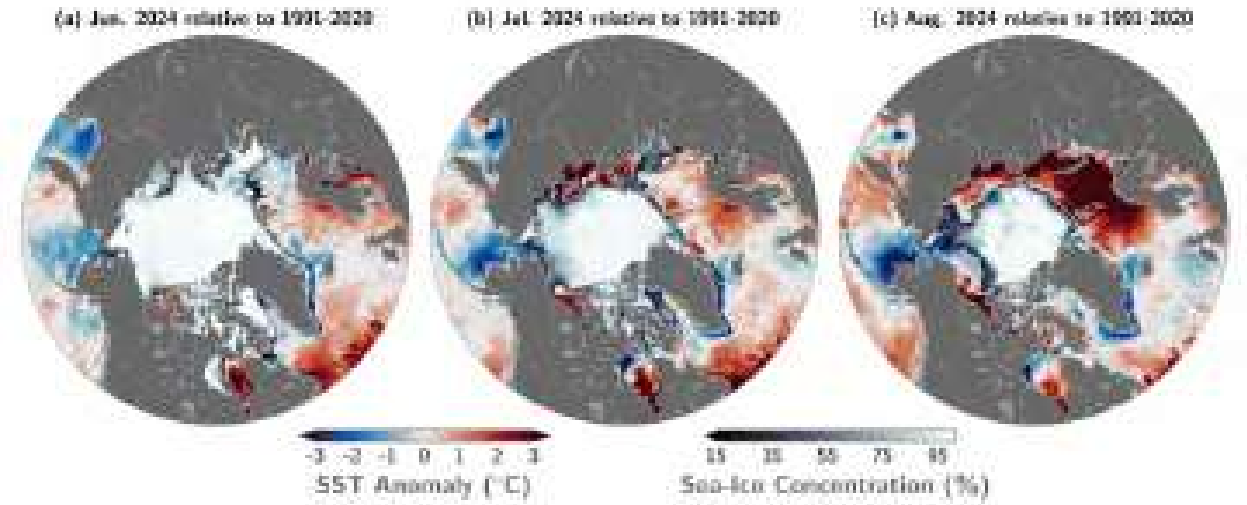

Fig. 2. Sea-surface temperature (SST) anomalies (°C) for (a) June 2024, (b) July 2024, and (c) August 2024 relative to the 1991-2020 mean for the respective months. Note a difference in the color bar scale compared to Fig. 1c,d. The mean sea-ice concentration for the corresponding month is also shown.

The Arctic Ocean has experienced mean August SST warming trends from 1982 to 2024, with statistically significant (at the 95% confidence interval) linear warming trends in almost all regions (Fig. 3). Mean August SSTs for the entire region of the Arctic Ocean north of 65° N exhibit a linear warming trend of 0.03±0.01°C/yr (Fig. 4a). For context, both the North Pacific and North Atlantic (between 50° N and 65° N) show linear warming trends over this same period of 0.04±0.01°C/yr.

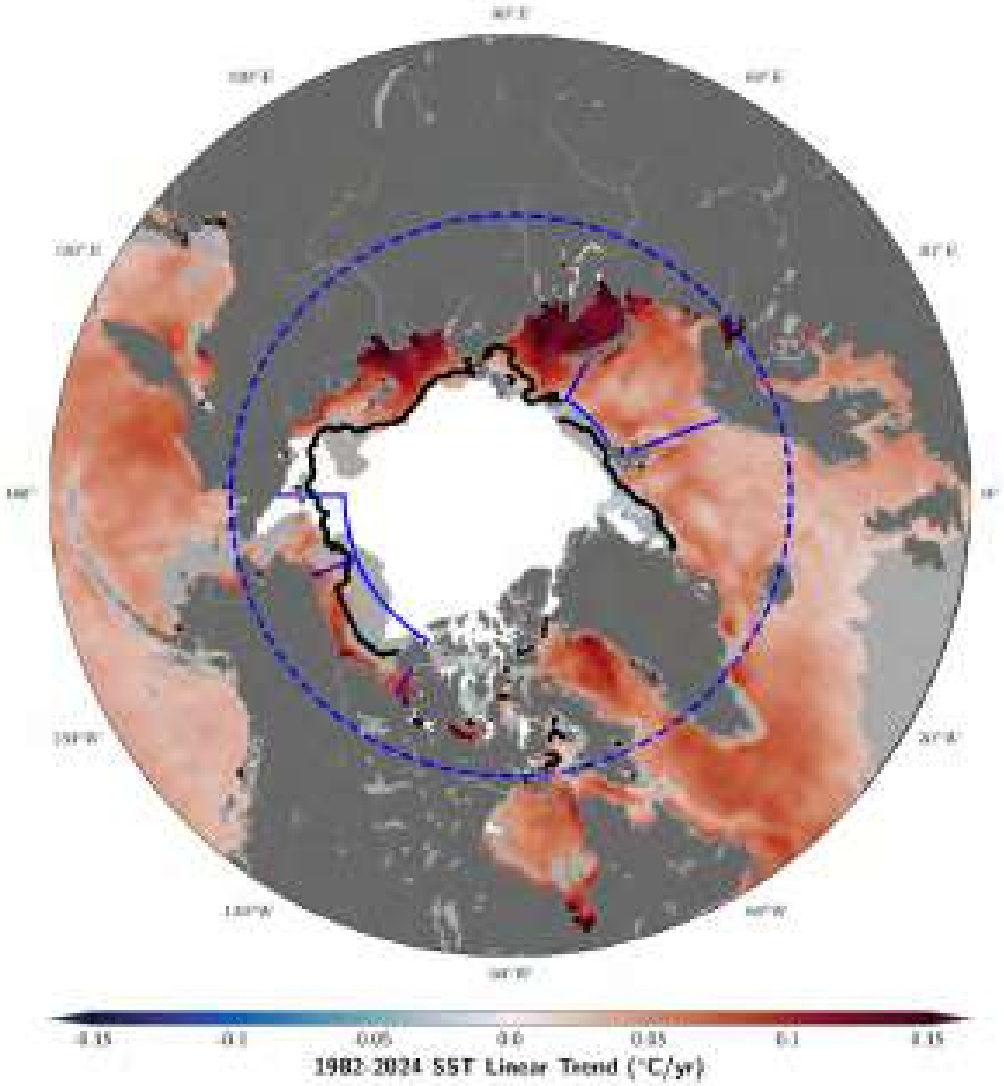

Fig. 3. Linear sea-surface temperature (SST) trend (°C/yr) for August of each year from 1982 through 2024. The trend is only shown for values that are statistically significant at the 95% confidence interval; the region is shaded light gray otherwise. White shading is the August 2024 mean sea-ice extent, and the black line indicates the August 1991-2020 median ice edge. The dashed blue circle marks 65° N (the Arctic Ocean region), and other solid blue line boundaries delineate the Barents, Beaufort, and Chukchi Seas.

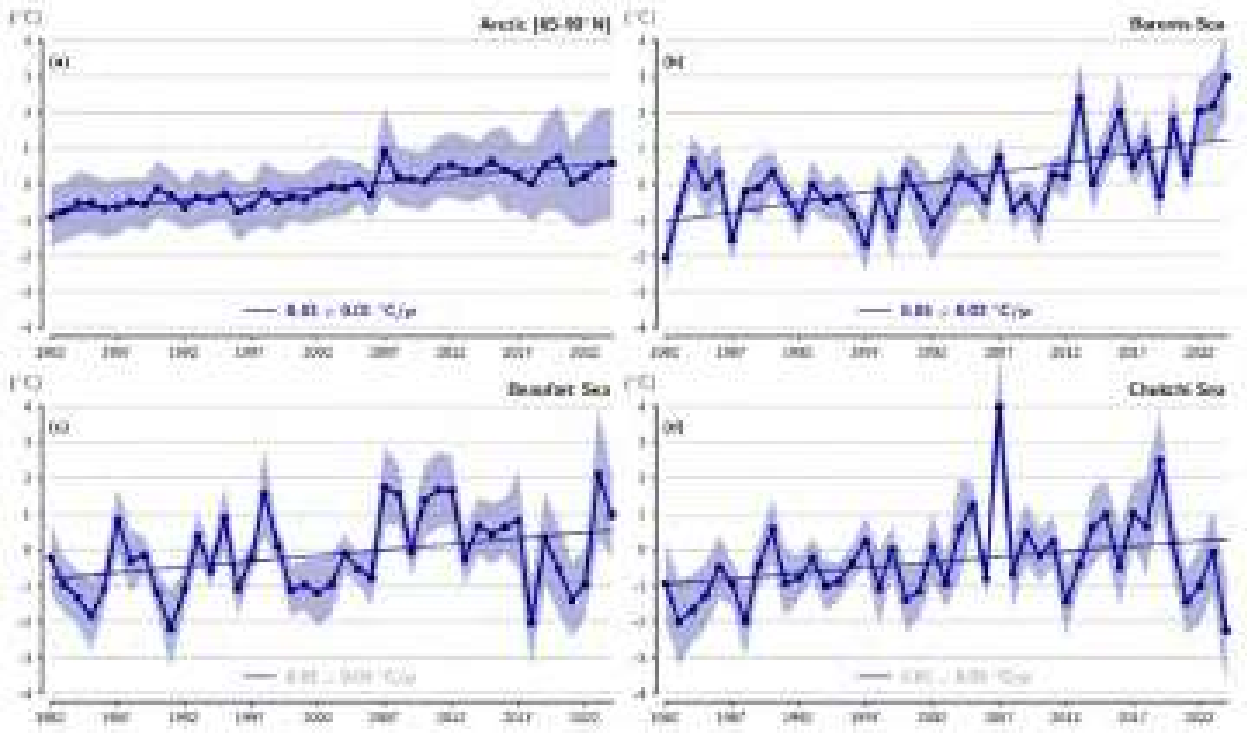

Fig. 4. Area-averaged SST anomalies (°C) for August of each year (1982-2024) relative to the 1991-2020 August mean for (a) the Arctic Ocean north of 65° N (indicated by the dashed blue circle in Fig. 3), (b) the Barents Sea, (c) the Beaufort Sea, and (d) the Chukchi Sea regions shown by blue boundaries in Fig. 3. The dotted lines show the linear SST anomaly trends over 1982-2024, and numbers in the legends indicate the trends in °C/year (with 95% confidence intervals; trends that are not statistically significant are labeled in grey). Blue shading indicates ±1 standard deviation of the regional mean SST anomaly fields.

Regionally, the Kara and Laptev Seas show the strongest warming trends in the Arctic Ocean, with August SST linear trends in these seas of around 0.12°C/yr (Fig. 3). This is consistent with large declines in August sea-ice extent in these regions (Timmermans and Labe 2020). Statistically significant linear trends in August SST are also observed in the Barents Sea (0.06±0.02°C/yr), where August 2024 mean SSTs were the warmest on record (Fig. 4b). On the other hand, there is no statistically significant trend in August SSTs in the Beaufort and Chukchi Seas (Fig. 4c,d), although the southernmost portion of the Beaufort Sea does show a statistically significant warming trend (Fig. 3). The Beaufort Sea shows considerable interannual variability in mean August SST values (Fig. 4c), while Chukchi Sea trends are notably influenced by anomalously cool SSTs in the region in recent years with record low August 2024 mean SSTs (Fig. 4d).

Methods and data

The SST data presented here are from the 0.25° × 0.25° NOAA Optimum Interpolation Sea Surface Temperature (OISST) Version 2.1 product, a blend of in situ and satellite measurements (Reynolds et al. 2002, 2007; Huang et al. 2021); https://psl.noaa.gov/data/gridded/data.noaa.oisst.v2.highres.html. The datafile “sst.mon.mean.nc” (comprising monthly means from the daily data) was retrieved from https://downloads.psl.noaa.gov/Datasets/noaa.oisst.v2.highres/ (accessed 3 September 2024). Note that in January 2023, OISST Version 2.1 replaced the 1° × 1° NOAA OISST Version 2, which was analyzed in *Arctic Report Cards* before 2023; while overall SST trends and patterns are similar between versions,

the difference merits caution when comparing *Arctic Report Cards* across years (for further details, see Timmermans and Labe 2023).

For setting a proxy SST in sea-ice covered regions, OISST Version 2.1 sets SST equal to the freezing temperature (computed using a climatological sea-surface salinity) where ice concentrations are greater than 35% (see Banzon et al. 2020). Therefore, uncertainty in inferring SSTs (and SST trends) may be significant in the vicinity of the sea-ice edge, which varies in location each year, and when sea ice covers a significant portion of the region of interest.

Note that Timmermans and Labe (2023) excluded the region north of 80° N in their calculation of the Arctic Ocean SST trend. For the same calculation in this essay (Fig. 4a), we consider the entire region to 90° N. Considering the larger region yields a somewhat smaller trend (although statistically indistinguishable) because the extra area considered mostly remains perennially ice covered. Given the rapid pace of sea-ice loss and poleward expansion of ice-free areas, we choose to include even the northernmost regions of the Arctic Ocean in the calculation. Recent work has produced a combined SST and sea-ice temperature dataset (Nielsen-Englyst et al. 2023); given the rate of sea-ice area change, in future work it may be sensible to additionally examine trends in this combined field.

Sea-ice concentration data are the Near-Real-Time NOAA/NSIDC Climate Data Record of Passive Microwave Sea Ice Concentration, Version 2 (https://nsidc.org/data/g10016) (Peng et al. 2013; Meier et al. 2021a,b). The 1991-2020 median ice edge is from the NOAA/NSIDC Climate Data Record of Passive Microwave Sea Ice Concentration, Version 4 (https://nsidc.org/data/g02202) with a threshold of 15% concentration defined as the ice edge.

Acknowledgments

M. -L. Timmermans acknowledges support from the National Science Foundation Office of Polar Programs and the Office of Naval Research. Z. Labe acknowledges support through base funding from the National Oceanic and Atmospheric Administration to the Geophysical Fluid Dynamics Laboratory (GFDL). We also thank Drs. Xia Li and William Gregory for their insightful comments and suggestions on the GFDL internal review of the essay. NOAA OI SST V2 High Resolution Dataset data provided by the NOAA PSL, Boulder, Colorado, USA, from their website at https://psl.noaa.gov.

References

Banzon, V., T. M. Smith, M. Steele, B. Huang, and H. -M. Zhang, 2020: Improved estimation of proxy sea surface temperature in the Arctic. *J. Atmos. Ocean. Tech.*, **37**, 341-349, https://doi.org/10.1175/JTECH-D-19-0177.1.

Huang, B., C. Liu, V. Banzon, E. Freeman, G. Graham, B. Hankins, T. Smith, and H. Zhang, 2021: Improvements of the Daily Optimum Interpolation Sea Surface Temperature (DOISST) Version 2.1. *J. Climate*, **34**(8), 2923-2939, https://doi.org/10.1175/JCLI-D-20-0166.1.

Meier, W. N., F. Fetterer, A. K. Windnagel, and J. S. Stewart, 2021a: NOAA/NSIDC Climate Data Record of Passive Microwave Sea Ice Concentration, Version 4. [1982-2021]. NSIDC: National Snow and Ice Data Center, Boulder, CO, USA, accessed 3 September 2024, https://doi.org/10.7265/efmz-2t65.

Meier, W. N., F. Fetterer, A. K. Windnagel, and J. S. Stewart, 2021b: Near-Real-Time NOAA/NSIDC Climate Data Record of Passive Microwave Sea Ice Concentration, Version 2. [1982-2021], accessed 3 September 2024, https://doi.org/10.7265/tgam-yv28.

Nielsen-Englyst, P., J. L. Høyer, W. M. Kolbe, G. Dybkjær, T. Lavergne, R. T. Tonboe, S. Skarpalezos, and I. Karagali, 2023: A combined sea and sea-ice surface temperature climate dataset of the Arctic, 1982-2021. *Remote Sens. Environ.*, **284**, 113331, https://doi.org/10.1016/j.rse.2022.113331.

NOAA, 2024: Optimum Interpolation Sea Surface Temperature (OISST) high resolution dataset, version 2.1. NOAA/PSL, accessed 3 September 2024, https://psl.noaa.gov/data/gridded/data.noaa.oisst.v2.highres.html.

Oldenburg, D., Y. Kwon, C. Frankignoul, G. Danabasoglu, S. Yeager, and W. M. Kim, 2024: The respective roles of ocean heat transport and surface heat fluxes in driving Arctic Ocean warming and sea ice decline. *J. Climate*, **37**, 1431-1448, https://doi.org/10.1175/JCLI-D-23-0399.1.

Peng, G., W. N. Meier, D. J. Scott, and M. H. Savoie, 2013: A long-term and reproducible passive microwave sea ice concentration data record for climate studies and monitoring. *Earth Syst. Sci. Data*, **5**, 311-318, https://doi.org/10.5194/essd-5-311-2013.

Reynolds, R. W., N. A. Rayner, T. M. Smith, D. C. Stokes, and W. Wang, 2002: An improved in situ and satellite SST analysis for climate. *J. Climate*, **15**, 1609-1625, https://doi.org/10.1175/1520-0442(2002)015<1609:AIISAS>2.0.CO;2.

Reynolds, R. W., T. M. Smith, C. Liu, D. B. Chelton, K. S. Casey, and M. G. Schlax, 2007: Daily high-resolution-blended analyses for sea surface temperature. *J. Climate*, **20**, 5473-5496, https://doi.org/10.1175/2007JCLI1824.1.

Timmermans, M. -L., and Z. M. Labe, 2020: Sea surface temperature. *Arctic Report Card 2020*, R. L. Thoman, J. Richter-Menge, and M. L. Druckenmiller, Eds., https://doi.org/10.25923/v0fs-m920.

Timmermans, M. -L., and Z. M. Labe, 2023: Sea surface temperature. *Arctic Report Card 2023*, M. L. Druckenmiller, R. L. Thoman, and T. A. Moon, Eds., https://doi.org/10.25923/e8jc-f342.

November 13, 2024

Arctic Ocean Primary Productivity: The Response of Marine Algae to Climate Warming and Sea Ice Decline

https://doi.org/10.25923/9ex0-t425

K. E. Frey[1], L. V. Stock[2], C. Garcia[3], L. W. Cooper[4], and J. M. Grebmeier[4]

[1]Graduate School of Geography, Clark University, Worcester, MA, USA
[2]Cryospheric Sciences Laboratory, Goddard Space Flight Center, NASA, Greenbelt, MD, USA
[3]Arctic Research Program, Global Ocean Monitoring and Observing Program, NOAA, Silver Spring, MD, USA
[4]Chesapeake Biological Laboratory, University of Maryland Center for Environmental Science, University of Maryland, Solomons, MD, USA

Headlines

- Satellite estimates of ocean primary productivity (i.e., the rate at which marine algae transform dissolved inorganic carbon into organic material) show lower values for 2024 (relative to the 2003-22 mean) for six of nine regions assessed across the Arctic.
- All regions, except for the Amerasian Arctic (namely the Chukchi Sea, Beaufort Sea, and Canadian Archipelago), continue to exhibit positive trends in ocean primary productivity during 2003-24, with the largest percent change in the Eurasian Arctic (+57.3%), Barents Sea (+20.5%), and Sea of Okhotsk (+13.5%).
- While lower-than-average values of annual ocean primary productivity were dominant across much of the Arctic for 2024, higher-than-average values were observed in eastern Hudson Bay, the Canadian Archipelago, and subareas of the Kara and Laptev Seas.

Introduction

Arctic marine primary productivity (the conversion of dissolved inorganic carbon into organic material by photosynthetic organisms) forms the foundation of the marine food web and plays a critical role in global carbon cycling. It is highly sensitive to changes in sea ice cover (see essay *Sea Ice*), ocean temperature (see essay *Sea Surface Temperature*), and nutrient availability, all of which are altered by ongoing climate change. Marine primary productivity in the Arctic varies significantly across different regions, influenced by local oceanographic conditions and the timing of sea ice retreat.

Recent in-situ observations reveal a complex picture: Although primary productivity has been boosted in many regions by thinner and more transparent sea ice, expanded ice-free areas, and enhanced nutrient upwelling (Fujiwara et al. 2018; Ardyna et al. 2020), the highest localized productivity is still associated with the retreating ice edge (Castagno et al. 2023; Amargant-Arumí et al. 2024) and lipid biomarker studies indicate that sea ice derived organic material is still critical on a year-round basis in Arctic ecosystems (Koch et al. 2023). Another complexity is that increased stratification and changing species compositions (Li et al. 2009) do not necessarily lead to long-term increases in primary production (Castro de la Guardia et al. 2023). The diverse sectors of the Arctic, from the Atlantic-influenced Barents

Sea to the Pacific-dominated Chukchi Sea, each respond uniquely to these changes, underscoring the need for region-specific analyses (e.g., Lalande et al. 2020).

Because of these complexities, synoptic observations using satellite-derived primary production data can be helpful in identifying localized productivity hotspots and phenological shifts that may not be apparent from traditional shipboard observations (Frey et al. 2023a). In this year's assessment, we continue to utilize Moderate Resolution Imaging Spectroradiometer (MODIS)-Aqua satellite data across the Arctic Ocean region, now spanning a 22-year record (2003-24). Monitoring these shifts remains vital given their profound implications for marine ecosystems, global climate feedback mechanisms, and marine resource management in a changing Arctic. The ongoing transformations in sea ice cover and ocean temperatures continue to reshape the patterns of primary productivity, highlighting the dynamic nature of the Arctic marine environment and the importance of sustained, accurate observations (Terhaar et al. 2021; Rantanen et al. 2022).

Chlorophyll-*a*

We present satellite-based estimates of algal chlorophyll-*a* (occurring in all species of phytoplankton), based on ocean color, and subsequently provide calculated primary production estimates (below). Observed patterns in chlorophyll-*a* (Fig. 1), which are spatially and temporally heterogeneous across the Arctic Ocean, are often associated with the timing of the seasonal break-up and retreat of the sea ice cover (Fig. 2) (see essay *Sea Ice*): high chlorophyll-*a* percentages (i.e., relative to the 2003-22 average) tend to occur in regions where the break-up is relatively early, while low percentages tend to occur in regions where the break-up is delayed. May 2024 (Fig. 1a) showed more geographically widespread higher-than-average chlorophyll-*a* concentrations than any other month of 2024, particularly in the Norwegian Sea, eastern Greenland Sea, Davis Strait, southeast Bering Sea, and eastern Hudson Bay (associated with early sea ice breakup in eastern Hudson Bay; Fig. 2a). During June 2024 (Fig. 1b), small areas of higher-than-average chlorophyll-*a* concentrations occurred in the Norwegian Sea, southeast Bering Sea, and northern Laptev Sea, but otherwise lower-than-average values were pervasive across the Arctic. During July 2024 (Fig. 1c), lower-than-average values were widespread across most of the Arctic, with areas of higher-than-average values in the Sea of Okhotsk, Bering Sea, East Siberian Sea, and southern Chukchi Sea. Lastly, during August 2024 (Fig. 1d), lower-than-average values were again observed across most of the Arctic, with noteworthy higher-than-average values clustered in the Bering Sea and southern Chukchi Sea.

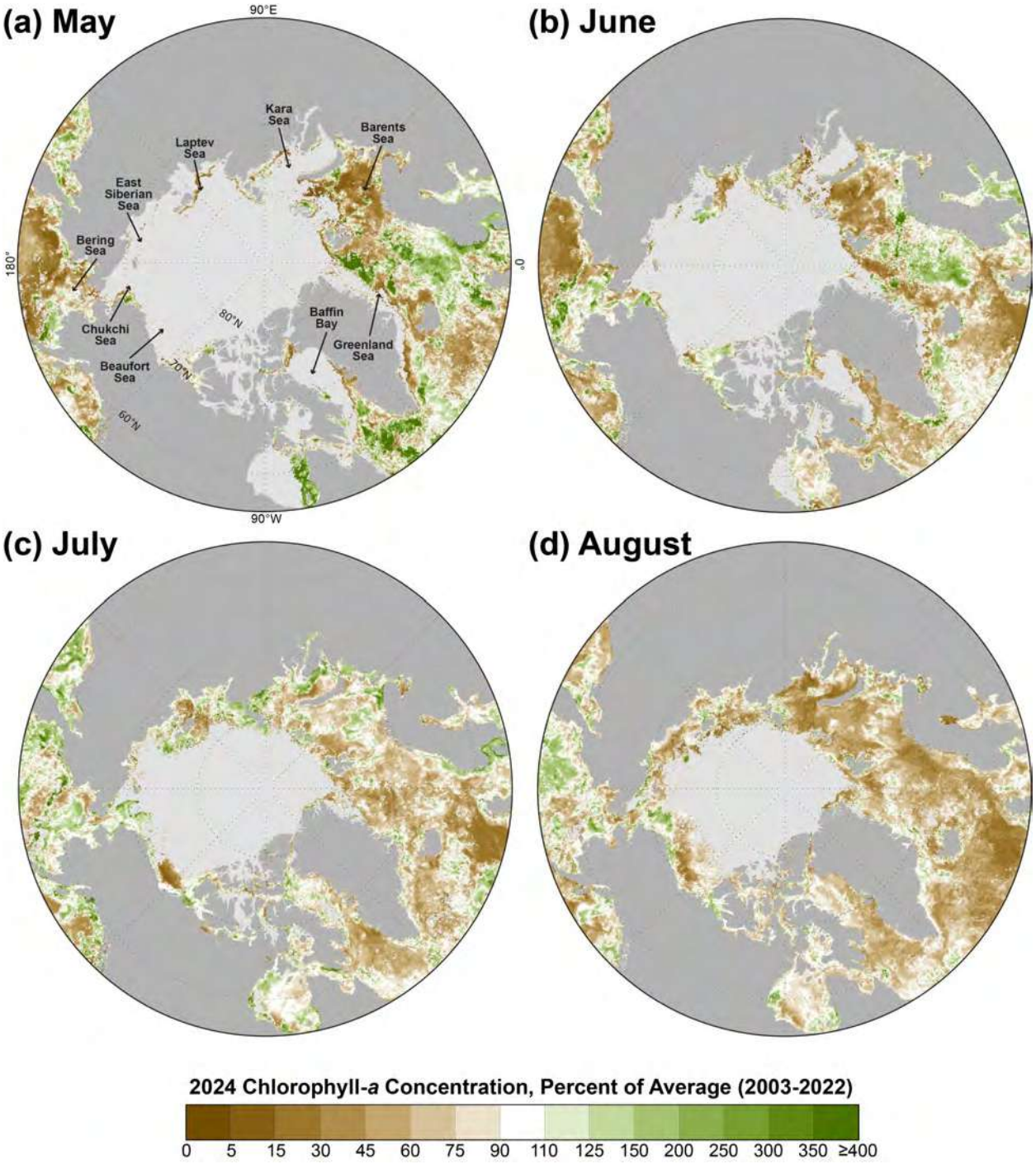

Fig. 1. Mean monthly chlorophyll-*a* concentrations during 2024, shown as a percent of the 2003-22 average for (a) May, (b) June, (c) July, and (d) August. August 2024 data were only available as Near Real Time (not final) data at the timing of this publication. The light gray regions represent areas where no data are available (owing to either the presence of sea ice or cloud cover). The color scale bar uses unequal intervals ranging from 5 to 50 percentage units, including the largest intervals for values greater than 125%. Data source: MODIS-Aqua Reprocessing 2022.0.1, chlor_a algorithm: http://oceancolor.gsfc.nasa.gov/.

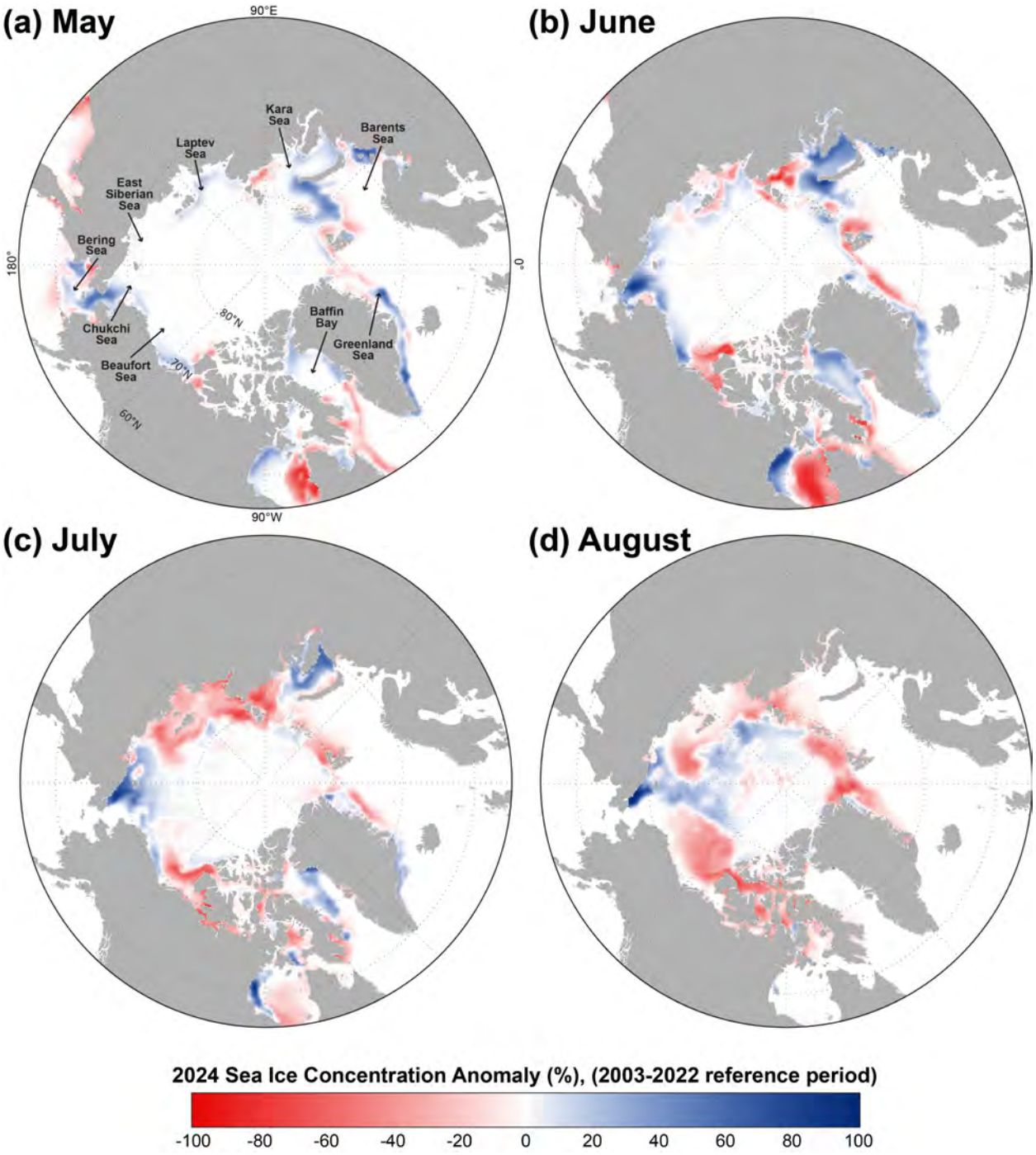

Fig. 2. Sea ice concentration anomalies (%) in 2024 (compared to a 2003-22 mean reference period) for (a) May, (b) June, (c) July, and (d) August. Data source: SSM/I and SSMIS passive microwave data, calculated using the Goddard Bootstrap (SB2) algorithm (Comiso et al. 2017).

Primary production

While chlorophyll-*a* concentrations give an estimate of the total standing stock of algal biomass, rates of primary production (i.e., the production of organic carbon via photosynthesis) provide a different perspective since not all algae in the water column are necessarily actively producing. The mean annual

(March through September) primary productivity across the Arctic shows important spatial patterns, most notably that productivity rates decrease northward as sea ice becomes more prevalent and nutrients become less available (Fig. 3a). Spatial trends in annual primary productivity (Fig. 3b) are a particularly useful tool for understanding hotspots of change. Statistically significant positive trends in primary productivity appear clustered in the Norwegian Sea, Barents Sea, Kara Sea, Laptev Sea, southeastern Chukchi Sea, and Canadian Archipelago (Fig. 3b). Positive trends adjacent to the Eurasian coastline may also be associated with variability in river-derived chromophoric (light absorbing) dissolved organic matter (CDOM) (e.g., Lewis and Arrigo 2020). There is almost no evidence of clustered significant negative trends in primary productivity across the Arctic (Fig. 3b). Investigations of 2024 annual primary productivity (Fig. 3c), as well as 2024 compared to the 2003-22 average (Fig. 3d), show higher-than-average annual productivity in eastern Hudson Bay, subareas of the Kara and Laptev Seas, and the Canadian Archipelago. Lower-than-average annual productivity occurred across much of the Arctic Ocean region for 2024, with the lowest values clustering in the East Siberian Sea, Chukchi Sea, and Beaufort Sea (Fig. 3d). Although sea ice cover was lower-than-average in large portions of the Beaufort Sea during July (Fig. 2c) and August (Fig. 2d), sea ice was either near-average or higher-than-average here during May (Fig. 2a) and June (Fig. 2b). For the East Siberian Sea and Chukchi Sea, sea ice was either near-average or higher-than-average during May through August (Fig. 2a-d). The overall higher sea ice cover or delayed sea ice breakup in these regions could have contributed to the widespread lower-than-average annual primary productivity rates also observed in these regions (Fig. 3d).

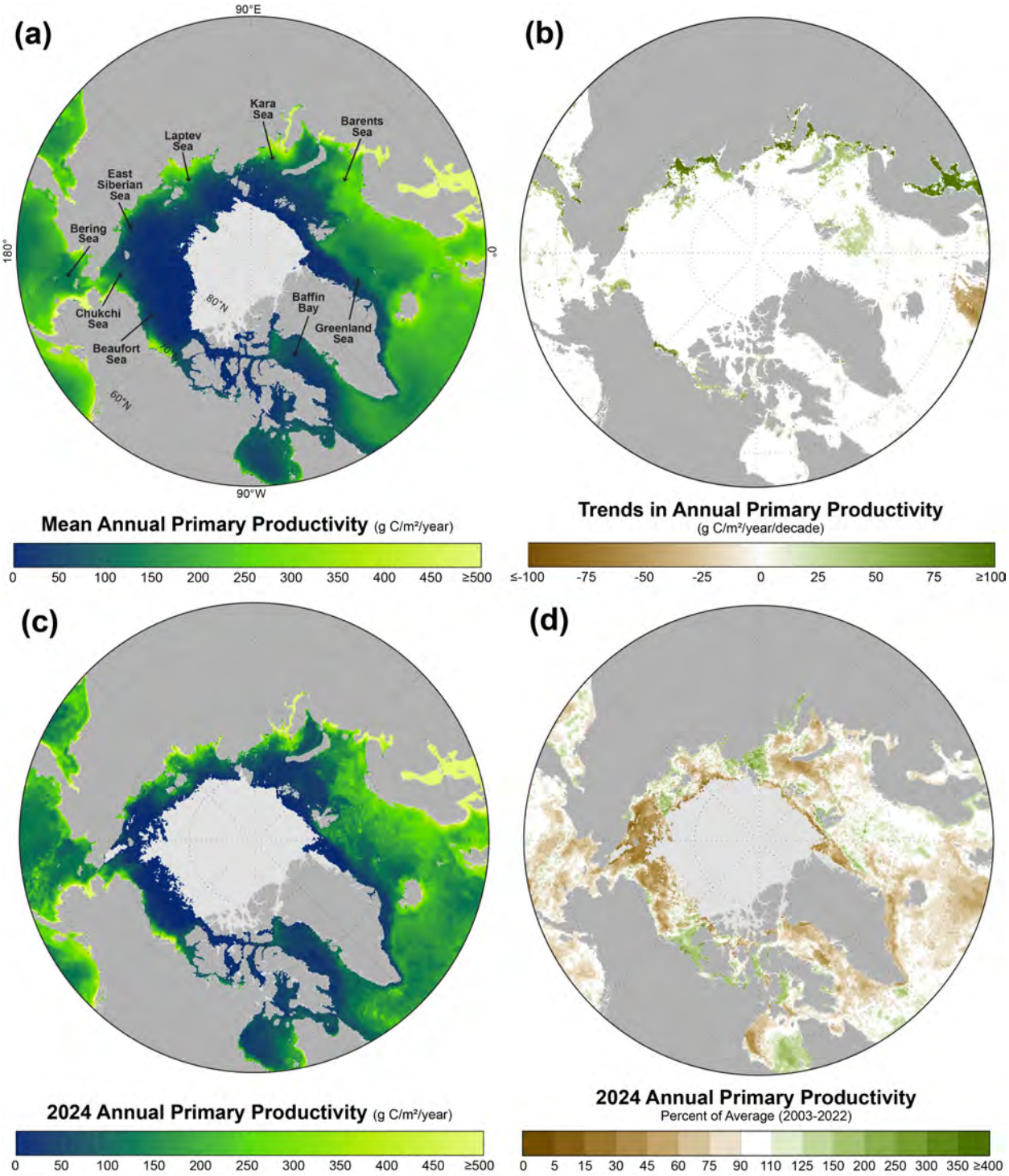

Fig. 3. For the pan-Arctic region: (a) mean annual (March-September only) primary productivity (2003-24); (b) trends in annual productivity (over 2003-24) where only those trends that are statistically significant (p<0.05) are shown; (c) annual primary productivity for 2024 only; and (d) 2024 annual primary productivity anomalies (shown as a percent of the 2003-22 average). In a, c, and d, light gray indicates no data owing to the presence of sea ice. Additional information regarding these data can be found in Table 1. August and September 2024 chlorophyll-*a* data (inputs into the primary productivity algorithm) were only available as Near Real Time (not final) data at the timing of this publication. See *Methods and data* section for details of how primary productivity was calculated.

Overall estimates of ocean primary productivity in 2024 for nine regions and across the Northern Hemisphere (relative to the 2003-22 reference period) were assessed (Fig. 4, Table 1). The Eurasian Arctic region includes the Kara, Laptev, and East Siberian Seas. The Amerasian Arctic region includes the Chukchi Sea, Beaufort Sea, and Canadian Archipelago. The North Atlantic is categorized as south of 60° N and east of 45° W, which excludes the Labrador and Greenland Seas. Our results show below-average primary productivity for 2024 in six of the nine regions assessed, while the Eurasian Arctic, Sea of Okhotsk, and Hudson Bay exhibited higher-than-average values (Fig. 4, Table 1). Positive trends in primary productivity continued in all regions (except for the Amerasian Arctic) during the 2003-24 period. Those trends that are statistically significant (p<0.05) occurred in the Eurasian Arctic (27.11 g C/m^2/yr/decade; a 57.3% increase), Barents Sea (15.07 g C/m^2/yr/decade; a 20.5% increase), and the Sea of Okhotsk (13.31 g C/m^2/yr/decade; a 13.5% increase). Annual net primary production was also calculated for the Arctic region, defined as 60-90° N (Fig. 5), which shows a trend over the 2003-24 time period of 14.7 Tg C/yr (Mann-Kendall significance p<0.001). The percent increase over the 22-year time series is estimated to be 19.2%. In summary, while observations of primary productivity show complex interannual and spatial patterns over the 2003-24 period, we continue to observe overall positive trends across most Arctic regions.

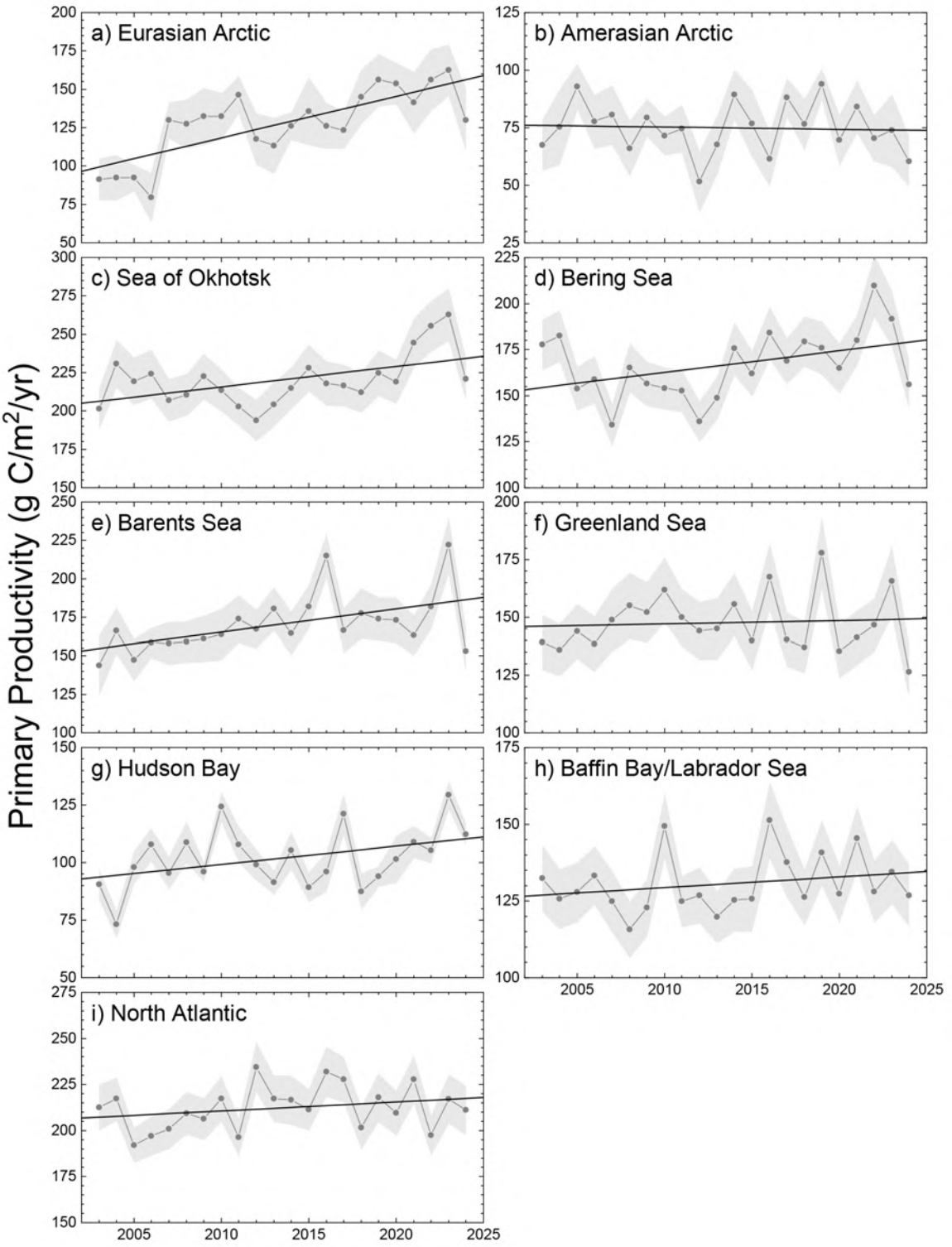

Fig. 4. Primary productivity (2003-24, March-September only) in nine different regions of the Northern Hemisphere (for a definition of the regions see Comiso 2015). The statistical significance of the trends (based on the Mann-Kendall test), *p*-values, and additional information regarding these data can be found in Table 1. August and September 2024 chlorophyll-*a* data (inputs into the primary productivity algorithm) were only available as Near Real Time (not final) data at the timing of this publication. See *Methods and data* section for primary productivity calculation details.

Table 1. Linear trends, statistical significance, and percent change in primary productivity (2003-24) and primary productivity anomalies for 2024 (March-September) in the nine regions as shown in Fig. 4. Values in bold are statistically significant (p<0.05) using the Mann-Kendall test for trend. The percent change was estimated from the linear regression of the 22-year time series.

Region	**2003-24** Trend (g C/m^2/yr/ decade)	**2003-24** Mann-Kendall p-value	**2003-24** % Change	**2024** Anomaly (g C/m^2/yr) from the 2003-22 reference period	**2024** Primary Productivity (% of the 2003-22 average)
Eurasian Arctic	**27.11**	<0.001	57.3	4.12	103.3
Amerasian Arctic	-0.99	0.697	-2.7	-15.36	79.7
Sea of Okhotsk	**13.31**	0.036	13.5	2.65	101.2
Bering Sea	11.75	0.081	16.0	-9.97	94.0
Barents Sea	**15.07**	0.002	20.5	-15.76	90.7
Greenland Sea	1.47	0.781	2.1	-21.40	85.5
Hudson Bay	7.94	0.116	17.8	12.20	112.2
Baffin Bay/Labrador Sea	3.52	0.161	5.8	-3.78	97.1
North Atlantic	4.87	0.289	4.9	-1.09	99.5

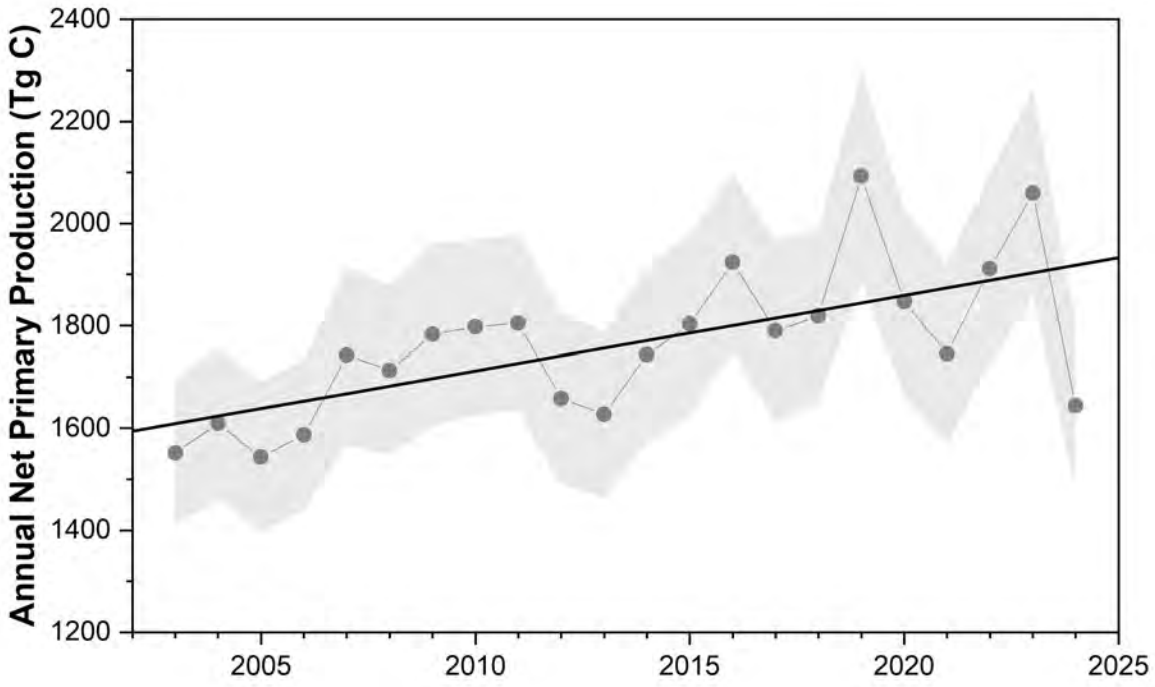

Fig. 5. Annual net primary production (2003-24, March-September only) for the Arctic region defined as 60-90° N. The trend over the 2003-24 time period is 14.7 Tg C/yr (Mann-Kendall significance p<0.001). The percent change estimated from the linear regression over the 22-year time series is 19.2%. August and September 2024 chlorophyll-*a* data (inputs into the primary productivity algorithm) were only available as Near Real Time (not final) data at the timing of this publication. See *Methods and data* section for primary productivity calculation details.

Methods and data

Measurements of the algal pigment chlorophyll (specifically, chlorophyll-*a*) serve as a proxy for algal biomass present in the ocean as well as overall plant health. The complete, updated MODIS-Aqua satellite record of chlorophyll-*a* concentrations within northern polar waters for the years 2003-24 serves as a time-series against which individual years can be compared. Satellite-based chlorophyll-*a* data across the pan-Arctic region were derived using the MODIS-Aqua Reprocessing 2022.0.1 (July 2024), chlor_a algorithm: http://oceancolor.gsfc.nasa.gov/. For this report, we show mean monthly chlorophyll-*a* concentrations calculated as a percentage of the 2003-22 average. This is the first time the same reference period (2003-22) has been utilized in two consecutive Arctic Ocean Primary Productivity Arctic Report Card essays (i.e., Frey et al. 2023b; *this essay*) now that the MODIS-Aqua satellite record has accrued at least 20 years of data. Satellite-based sea ice concentrations were derived from the Special Sensor Microwave/Imager (SSM/I) and Special Sensor Microwave Imager/Sounder (SSMIS) passive microwave instruments, calculated using the Goddard Bootstrap (SB2) algorithm (Comiso et al. 2017). Monthly sea ice concentration anomalies were additionally calculated for 2024 (compared to the 2003-22 average) to streamline comparisons with the variability in monthly chlorophyll-*a* satellite data. Primary productivity data were derived using chlorophyll-*a* concentrations from MODIS-Aqua data (Reprocessing 2022.0.1, chlor_a algorithm), the NOAA 1/4° daily Optimum Interpolation Sea Surface Temperature dataset (or daily OISST) that uses satellite sea surface temperatures from AVHRR, incident solar irradiance, mixed layer depths, and additional parameters. Primary productivity values were calculated based on the Vertically Generalized Production Model (VGPM) algorithm described by Behrenfeld and Falkowski (1997) as applied by Frey et al. (2023a). Chlorophyll-*a* and primary

productivity data only incorporate pixels where sea ice is less than 10%, which is a compromise between potential pixel contamination with sea ice and an attempt to incorporate open water near the ice edge that typically exhibits high rates of primary production. We define annual productivity as productivity over the March-September time period. The 2024 annual primary productivity percent of average (compared to 2003-22) was calculated the same way as for chlorophyll-*a*, as described above. Lastly, spatial trends of primary productivity (Fig. 3b) were calculated using a Theil-Sen median trend estimator, and regional (and total Arctic) linear trends/percent change (Table 1, Figs. 4 and 5) were calculated through ordinary least squares regression. The statistical significance of all trends (p<0.05) was determined using the Mann-Kendall trend test. The MODIS-Aqua Reprocessing 2022.0.1 (https://oceancolor.gsfc.nasa.gov/data/reprocessing/r2022.0.1/aqua/) that took place in July 2024 includes revised data from 2021-present in response to satellite orbital shifts and resulting declines in data accuracy. As such, values and trends shown in our time series analyses this year (e.g., Table 1, Figs. 1, 3, 4, and 5) are updated from previous Arctic Report Card essays based on these newly revised data for 2021 onwards.

Importantly, the chlorophyll-*a* and primary productivity data are shown for ocean areas with less than 10% sea ice concentration and, therefore, do not include production by sea ice algae or under-ice phytoplankton blooms, which can be significant (Ardyna et al. 2013). Furthermore, it is known that satellite observations can underestimate production under stratified conditions when a deep chlorophyll maximum is present. The variable distribution of sediments and CDOM (owing to riverine delivery, coastal erosion, and sea ice dynamics) can also affect the accuracy of satellite-based estimations of chlorophyll-*a* and primary productivity in Arctic waters (Lewis and Arrigo 2020). As such, in-situ observations continue to provide important overall context for changes to and drivers of primary productivity across Arctic marine ecosystems.

Acknowledgments

K. Frey acknowledges financial support from the National Science Foundation (NSF) Arctic Observing Network (AON) Program (Grant 1917434). Support for J. Grebmeier and L. Cooper was provided through NSF AON (Grant 1917469) and the NOAA Global Ocean Monitoring and Observing, Arctic Research Program (CINAR 22309.07_UMCES_Grebmeier).

References

Amargant-Arumí, M., and Coauthors, 2024: Interannual differences in sea ice regime in the north-western Barents Sea cause major changes in summer pelagic production and export mechanisms. *Prog. Oceanogr.*, **220**, 103178, https://doi.org/10.1016/j.pocean.2023.103178.

Ardyna, M., M. Babin, M. Gosselin, E. Devred, S. Bélanger, A. Matsuoka, and J. -É. Tremblay, 2013: Parameterization of vertical chlorophyll *a* in the Arctic Ocean: impact of the subsurface chlorophyll maximum on regional, seasonal, and annual primary production estimates. *Biogeosciences*, **10**(6), 4383-4404, https://doi.org/10.5194/bg-10-4383-2013.

Ardyna, M., and Coauthors, 2020: Under-ice phytoplankton blooms: Shedding light on the “invisible” part of Arctic primary production. *Front. Mar. Sci.*, **7**, 608032, https://doi.org/10.3389/fmars.2020.608032.

Behrenfeld, M. J., and P. G. Falkowski, 1997: Photosynthetic rates derived from satellite-based chlorophyll concentration. *Limnol. Oceanogr.*, **42**(1), 1-20, https://doi.org/10.4319/lo.1997.42.1.0001.

Castagno, A. P., T. J. W. Wagner, M. R. Cape, C. W. Lester, E. Bailey, C. Alves-de-Souza, R.A. York, and A. H. Fleming, 2023: Increased sea ice melt as a driver of enhanced Arctic phytoplankton blooming. *Glob. Change Biol.*, **29**(17), 5087-5098, https://doi.org/10.1111/gcb.16815.

Castro de la Guardia, L., and Coauthors, 2023: Assessing net primary production in the northwestern Barents Sea using in situ, remote sensing and modelling approaches. *Prog. Oceanogr.*, **219**, 103160, https://doi.org/10.1016/j.pocean.2023.103160.

Comiso, J. C., 2015: Variability and trends of the global sea ice cover and sea level: Effects on physicochemical parameters. *Climate Change and Marine and Freshwater Toxins*, L. M. Botana, M. C. Lauzao, and N. Vilarino, Eds., De Gruyter, Berlin, Germany, https://doi.org/10.1515/9783110333596-003.

Comiso, J. C., W. N. Meier, and R. Gersten, 2017: Variability and trends in the Arctic Sea ice cover: Results from different techniques. *J. Geophys. Res.-Oceans*, **122**, 6883-6900, https://doi.org/10.1002/2017JC012768.

Frey, K. E., J. C. Comiso, L. V. Stock, L. N. C. Young, L. W. Cooper, and J. M. Grebmeier, 2023a: A comprehensive satellite-based assessment across the Pacific Arctic Distributed Biological Observatory shows widespread late-season sea surface warming and sea ice declines with significant influences on primary productivity. *PLoS ONE*, **18**(7), e0287960, https://doi.org/10.1371/journal.pone.0287960.

Frey, K. E., J. C. Comiso, L. W. Cooper, C. Garcia, J. M. Grebmeier, and L. V. Stock, 2023b: Arctic ocean primary productivity: The response of marine algae to climate warming and sea ice decline. *Arctic Report Card 2023*, R. L. Thoman, T. A. Moon, and M. L. Druckenmiller, Eds., https://doi.org/10.25923/nb05-8w13.

Fujiwara, A., and Coauthors, 2018: Changes in phytoplankton community structure during wind-induced fall bloom on the central Chukchi shelf. *Polar Biol.*, **41**, 1279-1295, https://doi.org/10.1007/s00300-018-2284-7.

Koch, C. W., and Coauthors, 2023: Year-round utilization of sea ice-associated carbon in Arctic ecosystems. *Nat. Commun.*, **14**, 1964, https://doi.org/10.1038/s41467-023-37612-8.

Lalande, C., J. M. Grebmeier, R. R. Hopcroft, and S. L. Danielson, 2020: Annual cycle of export fluxes of biogenic matter near Hanna Shoal in the northeast Chukchi Sea. *Deep-Sea Res. Pt. II*, **177**, 104730, https://doi.org/10.1016/j.dsr2.2020.104730.

Lewis, K. M., and K. R. Arrigo, 2020: Ocean color algorithms for estimating chlorophyll *a*, CDOM absorption, and particle backscattering in the Arctic Ocean. *J. Geophys. Res.- Ocean*s, **125**, e2019JC015706, https://doi.org/10.1029/2019JC015706.

Li, W. K., F. A. McLaughlin, C. Lovejoy, and E. C. Carmack, 2009: Smallest algae thrive as the Arctic Ocean freshens. *Science*, **326**, 539-539, https://doi.org/10.1126/science.1179798.

Rantanen, M., A. Y. Karpechko, A. Lipponen, K. Nordling, O. Hyvärinen, K. Ruosteenoja, T. Vihma, and A. Laaksonen, 2022: The Arctic has warmed nearly four times faster than the globe since 1979. *Commun. Earth Environ.*, **3**, 168, https://doi.org/10.1038/s43247-022-00498-3.

Terhaar, J., R. Lauerwald, P. Regnier, N. Gruber, and L. Bopp, 2021: Around one third of current Arctic Ocean primary production sustained by rivers and coastal erosion. *Nat. Commun.*, **12**, 169, https://doi.org/10.1038/s41467-020-20470-z.

November 15, 2024

Tundra Greenness

https://doi.org/10.25923/5t2g-fm41

G. V. Frost[1], M. J. Macander[1], U. S. Bhatt[2], L. T. Berner[3], J. J. Assmann[4], H. E. Epstein[5], B. C. Forbes[6], S. J. Goetz[3], S. R. Karlsen[7], M. J. Lara[8,9], E. López-Blanco[10], R. Í. Magnússon[11], P. M. Montesano[12,13], C. S. R. Neigh[12], G. K. Phoenix[14], H. Tømmervik[15], C. Waigl[16], D. A. Walker[17], and D. Yang[18]

[1]Alaska Biological Research, Inc., Fairbanks, AK, USA
[2]Geophysical Institute, University of Alaska Fairbanks, Fairbanks, AK, USA
[3]School of Informatics, Computing and Cyber Systems, Northern Arizona University, Flagstaff, AZ, USA
[4]Department of Evolutionary Biology and Environmental Studies, University of Zurich, Zurich, Switzerland
[5]Department of Environmental Sciences, University of Virginia, Charlottesville, VA, USA
[6]Arctic Centre, University of Lapland, Rovaniemi, Finland
[7]NORCE Norwegian Research Centre AS, Tromsø, Norway
[8]Department of Plant Biology, University of Illinois, Urbana, IL, USA
[9]Department of Geography, University of Illinois, Urbana, IL, USA
[10]Department of Ecoscience and Arctic Research Centre, Aarhus University, Roskilde, Denmark
[11]Plant Ecology and Nature Conservation Group, Wageningen University & Research, Wageningen, Netherlands
[12]Goddard Space Flight Center, NASA, Greenbelt, MD, USA
[13]ADNET Systems, Inc., Bethesda, MD, USA
[14]School of Biosciences, University of Sheffield, Sheffield, UK
[15]Norwegian Institute for Nature Research, FRAM – High North Research Centre for Climate and the Environment, Tromsø, Norway
[16]University of Alaska Fairbanks, Fairbanks, AK, USA
[17]Institute of Arctic Biology, University of Alaska Fairbanks, Fairbanks, AK, USA
[18]Environmental Sciences Division and Climate Change Science Institute, Oak Ridge National Laboratory, Oak Ridge, TN, USA

Headlines

- In 2024, the circumpolar mean maximum tundra greenness value was the second highest in the high-resolution 25-year MODIS satellite record, continuing a sequence of record or near-record high values since 2020.
- Tundra greenness reached a record high value over the North American Arctic, while the value in the Eurasian Arctic was sixth highest in the MODIS record.
- The “greening of the Arctic,” first reported in the late 1990s as an increase in the productivity and abundance of tundra vegetation due to rapid warming and sea-ice decline, is an ongoing phenomenon evident in all available long-term satellite records.

Introduction

The Arctic tundra biome occupies Earth's northernmost lands, covering a 5.1 million km^2 area that encircles the Arctic Ocean and is bound to the south by the boreal forest biome (Raynolds et al. 2019). Arctic tundra ecosystems are experiencing profound changes as vegetation and underlying permafrost soils are strongly influenced by rising air temperatures and the rapid decline of sea ice (see essays *Surface Air Temperature* and *Sea Ice*). By the late 1990s, an increase in the productivity of tundra vegetation became evident in global satellite observations, a phenomenon that continued and soon became known as "the greening of the Arctic." Arctic greening is dynamically linked with Earth's changing climate, seasonal snow, permafrost, and sea-ice cover, and remains a focus of multi-disciplinary scientific research.

Spaceborne monitoring of Arctic tundra greenness

Global vegetation has been monitored from space since late 1981 with the launch of the Advanced Very High Resolution Radiometer (AVHRR) sensor. In 2000, the Moderate Resolution Imaging Spectroradiometer (MODIS) and the Landsat series of satellites began providing complementary circumpolar greenness records with higher spatial resolution and improved calibration. All of these instruments monitor vegetation greenness using the Normalized Difference Vegetation Index (NDVI), a spectral metric that exploits the unique way in which vegetation absorbs and reflects visible and infrared light.

Both AVHRR and MODIS have recorded increasing annual maximum tundra greenness (MaxNDVI) across most of the circumpolar Arctic during 1982-2023 and 2000-24, respectively (Figs. 1a,b). Both records display widespread greening trends in Low Arctic Eurasia and North America, except for portions of southwestern Alaska, and central and northeastern Siberia where flat or negative ("browning") trends are evident. Trends in the High Arctic—particularly the Canadian Arctic Archipelago—are mixed between the two satellite records, which may be partly due to their different observational periods, as well as observational challenges posed by the very short growing season, persistent cloudiness, and high interannual variability in snowmelt and surface water in these environments (Karlsen et al. 2024). Regional contrasts in greening highlight the complexity of Arctic change and the rich web of interactions that exist between tundra ecosystems and the local properties of sea ice, permafrost, seasonal snow (see essay *Terrestrial Snow Cover*), soil composition and moisture, microtopography, disturbance processes, wildlife, and human activities (Heijmans et al. 2022; Tassone et al. 2024). Understanding the underlying drivers of complex Arctic trends is important for improved monitoring and prediction of tundra ecosystem functions and the consequences of Arctic change on the global carbon cycle (see essay *Carbon Cycling*).

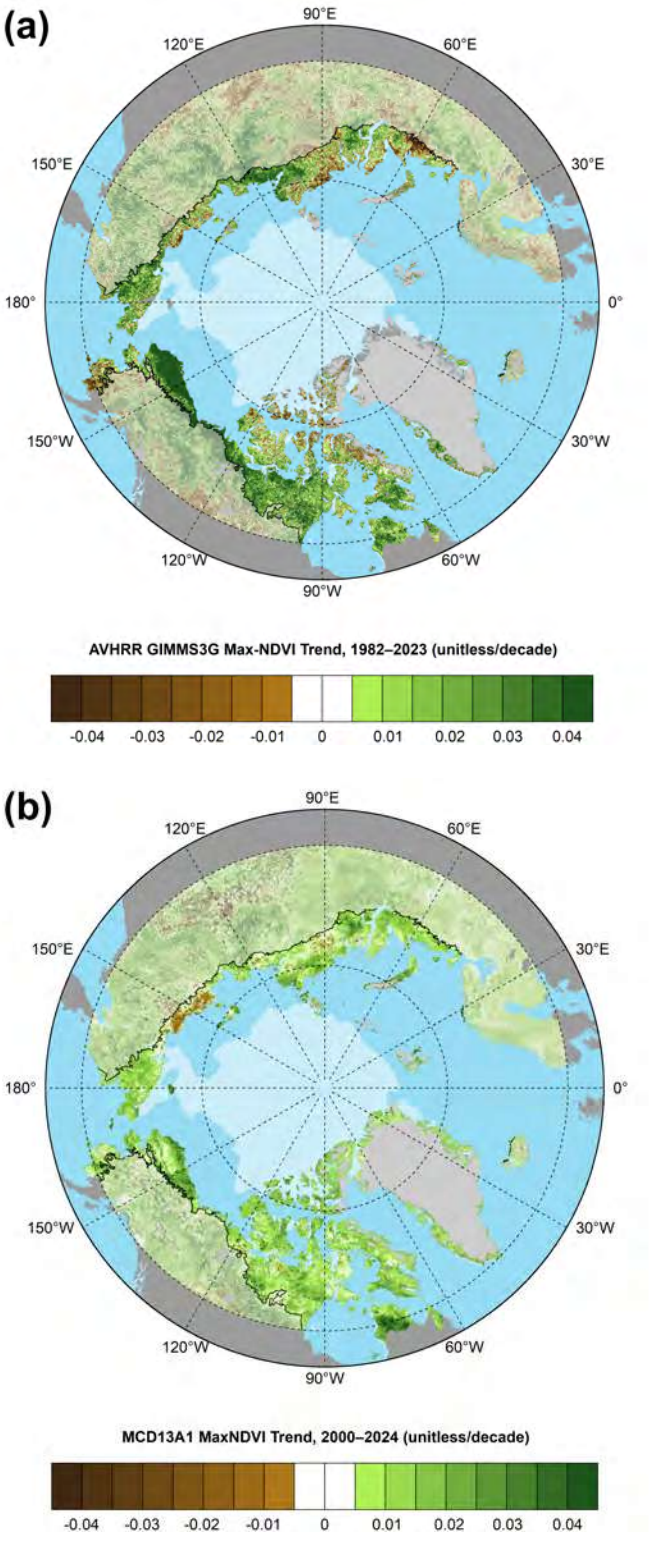

Fig. 1. Magnitude of the MaxNDVI trend calculated as the change per decade using ordinary least squares regression for Arctic tundra (solid colors), and boreal forest north of 60° latitude (muted colors) during (a) 1982-2023 based on the AVHRR GIMMS 3-g+ dataset, and (b) 2000-24 based on the MODIS MCD13A1 v6.1 dataset. In each panel, the circumpolar treeline is indicated by a black line, and the 2024 mean August sea-ice extent is indicated by light shading.

The neighboring boreal forest biome (see Fig. 1a,b) occupies large swaths of northern Eurasia and North America, and has also emerged as a focal point of global environmental change. Patches of positive and negative greenness trends are widely interspersed, reflecting complex interactions among the biome's active wildfire regime, climate change, permafrost thaw, extreme events, pathogens, and other factors (Kim et al. 2024). Browning has generally prevailed in the warmer southern boreal zone (Berner and Goetz 2022), but greening has been widespread along the forest-tundra ecotone in the north, often in association with tall shrub and tree expansion (Wong et al. 2024).

At the time of writing, MaxNDVI data for 2024 were only available for MODIS. In 2024, the MODIS observed circumpolar average MaxNDVI value was slightly higher (0.9%) compared to 2023 and represents the second highest in the 25-year record for that sensor. This continued a sequence of record or near-record high values that began in 2020, with the four highest MaxNDVI values in the 25-year MODIS record being observed since that year. Tundra greenness reached a new record high value in the North American Arctic, and was much higher than normal in northern Alaska, central and eastern Canada, and Greenland (Fig. 2). Localized areas of lower-than-normal greenness in Canada's Northwest Territories were likely the result of intense wildfire activity in 2023 and 2024. The Eurasian Arctic, however, featured a mixture of positive and negative departures from normal, a pattern that was also evident in summer 2023. Interestingly, while some of the Eurasian regions with below normal MaxNDVI also experienced cooler than normal summer temperatures (e.g., easternmost Chukchi Peninsula), others experienced very warm conditions (e.g., north-central Siberia), complicating the degree to which greening can be attributed simply to warmer summer temperatures (see essay *Surface Air Temperature*). Negative anomalies in northeastern Siberia could partly reflect the highly active fire season in that region. Nonetheless, the long-term trend in MODIS-observed tundra greenness is strongly positive (greening) for most of the circumpolar region. Although 2024 data are not yet available for AVHRR, this dataset also corroborates the MODIS record, with the three highest MaxNDVI values in the 42-year AVHRR record all observed since 2020 (Fig. 3).

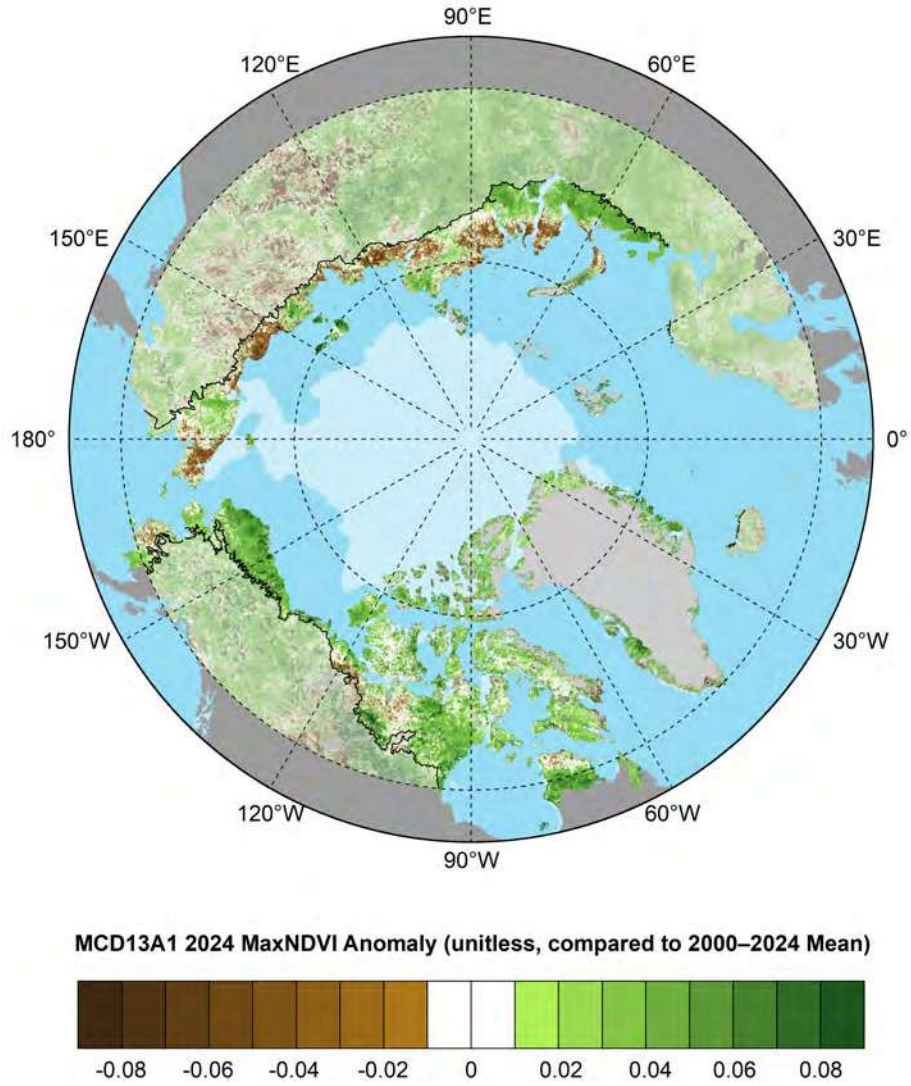

Fig. 2. Circumpolar MaxNDVI anomalies for the 2024 growing season relative to mean values (2000-24) from the MODIS MCD13A1 v6.1 dataset. The 2024 mean August sea-ice extent is indicated by light shading.

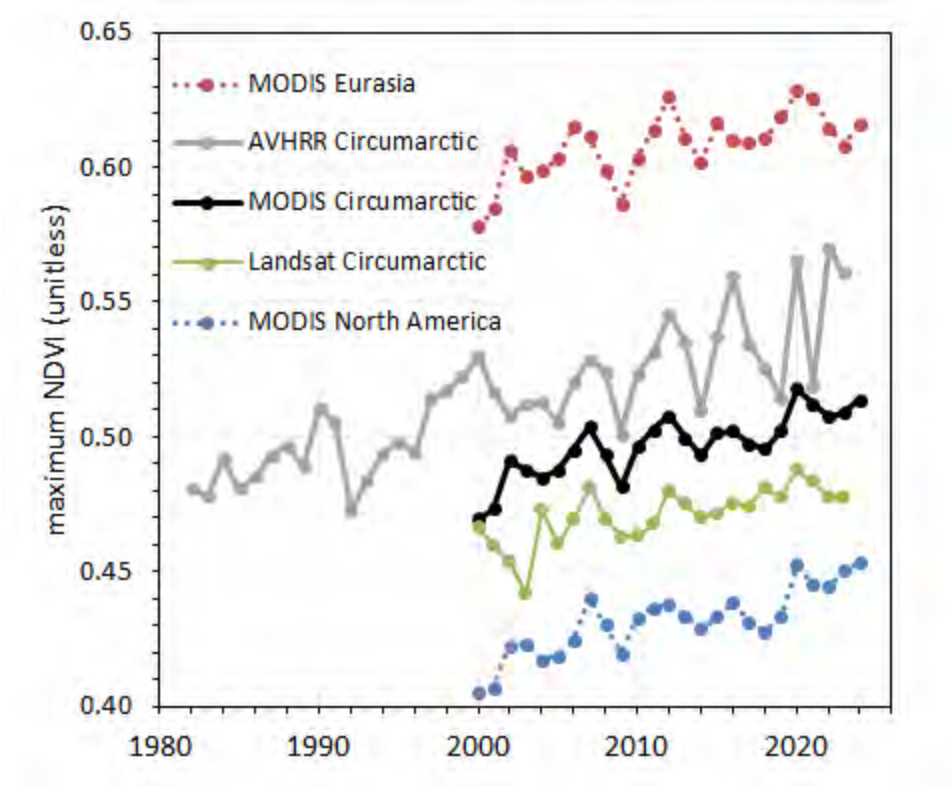

Fig. 3. Time-series of mean MaxNDVI for Arctic tundra from the MODIS MCD13A1 v6.1 (2000-24) dataset for the Eurasian Arctic (red), North American Arctic (blue), and the circumpolar Arctic (black), and from the AVHRR GIMMS-3g+ (1982-2023; gray) and Landsat Collection 2 (2000-23; green) datasets.

Drivers and consequences of Arctic greening

A widely recognized manifestation of Arctic greening is *shrubification*—an increase in the cover, height, and biomass of tundra shrubs such as willows, birches, and alders (Fig. 4), which have higher NDVI than low-growing tundra plants. Newly developed tall shrubs create complex vertical structure and foraging opportunities that have supported the northward expansion of boreal mammals and birds in recent decades (Tape et al. 2022). On the other hand, shrubs tend to crowd out low-growing tundra plants, particularly lichens, which are an important part of the diet of caribou (Ramirez et al. 2024; see essay *Western Arctic Caribou Herd*).

Fig. 4. A major driver of circumpolar greening trends is the expansion of tall, canopy-forming shrubs, such as alder (upper left and upper right). Increases in the cover and height of shrubs have far-reaching effects on Arctic ecosystems and can reduce the abundance of other tundra plants, particularly of lichens (lower left) which provide important forage for caribou and reindeer. Field-based efforts to monitor Arctic ecosystems (lower right) are critical to understanding the drivers and consequences of Arctic greenness trends. Photos are from the Seward Peninsula, western Alaska, July 2024 (credit G. V. Frost).

Arctic greenness trends are influenced by a complex set of interacting climatic and environmental drivers and the dynamics evident in satellite time-series reflect many sources of interannual and decadal variability. Interannual variability in snow cover and subsequent impacts on plant phenology, productivity, and soil hydrology further complicate the greening and browning signals (Bennett et al. 2022). Persistent summer cloudiness can also lead to the underestimation of MaxNDVI in certain years and locations, potentially masking the greening trend. Ground-based monitoring is therefore essential to understand the causes and consequences of Arctic greening and browning (Fig. 4), something that is challenging to standardize across multiple observers and areas of the Arctic, but for which standard protocols are now being made (CAFF 2024). Nonetheless, the sequence of record or near-record MaxNDVI values observed in multiple satellite datasets since 2020 provides strong evidence that the overall cover and biomass of vegetation in the Arctic tundra biome are without historic precedent, and likely exceeds that of any period since at least the “Little Ice Age,” a period of cool global temperatures that ended in the late 19th century.

Methods and data

The satellite record of Arctic tundra greenness began in 1982 using AVHRR, a sensor that collects daily observations and continues to operate onboard polar-orbiting satellites. We also report observations from the Moderate Resolution Imaging Spectroradiometer (MODIS) and the Landsat series of satellites, which are modern systems that provide circumpolar greenness observations since 2000. MODIS is nearing the end of its service life, but continuity of this important record will be maintained by its successor, the Visible Infrared Imaging Radiometer Suite (VIIRS). At the time of writing, data for the 2024 growing season were not fully processed for AVHRR and Landsat, so we report on 2024 conditions using MODIS only. The long-term AVHRR dataset analyzed here for 1982-2023 is the Global Inventory Modeling and Mapping Studies 3g V1.2 dataset (GIMMS-3g+), which is based on corrected and calibrated AVHRR data with a spatial resolution of about 8 km (Pinzon et al. 2023). For MODIS, we computed tundra greenness trends for 2000-24 with a higher spatial resolution of 500 m, combining 16-day Vegetation Index products from Terra (MOD13A1, version 6.1) and Aqua (MYD13A1, version 6.1) (Didan 2021a,b), referred to here as MCD13A1. Landsat provides tundra greenness data at a much higher spatial resolution of 30 m; we computed time-series of greenness from Landsat Collection 2 (Crawford et al. 2023) using the methods of Berner and Goetz (2022). Circumpolar maps depicting greenness trends (AVHRR and MODIS only) cover the Arctic tundra biome, as well as boreal forest and non-Arctic tundra above 60° N latitude. For time-series plots, data were masked to include only ice-free land within the extent of the Circumpolar Arctic Vegetation Map (Raynolds et al. 2019). MODIS and Landsat data were further masked to exclude permanent water based on the 2015 MODIS Terra Land Water Mask (MOD44W, version 6). We summarize the GIMMS-3g+, MODIS, and Landsat records for Maximum NDVI (MaxNDVI), the peak yearly value that is typically observed during the months of July and August.

Acknowledgments

We thank J. Pinzon at the Biospheric Sciences Laboratory, NASA Goddard Space Flight Center for providing updates for the GIMMS-3g+ dataset. This work was funded in part by the NASA Arctic Boreal Vulnerability Experiment, grant 80NSSC22K1256.

References

Bennett, K. E., and Coauthors, 2022: Spatial patterns of snow distribution in the sub-Arctic. *Cryosphere*, **16**, 3269-3293, https://doi.org/10.5194/tc-16-3269-2022.

Berner, L. T., and S. J. Goetz, 2022: Satellite observations document trends consistent with a boreal forest biome shift. *Global Change Biol.*, **28**(10), 3275-3292, https://doi.org/10.1111/gcb.16121.

Conservation of Arctic Flora and Fauna (CAFF), 2024: Extreme events monitoring tool, accessed 10 September 2024, https://www.caff.is/work/approach/extreme-events/.

Crawford, C. J., and Coauthors, 2023: The 50-year Landsat collection 2 archive. *Sci. Remote Sens.*, **8**, 100103, https://doi.org/10.1016/j.srs.2023.100103.

Didan, K., 2021a: MODIS/Terra Vegetation Indices 16-Day L3 Global 500m SIN Grid V061 [Data set]. NASA EOSDIS Land Processes Distributed Active Archive Center, https://doi.org/10.5067/MODIS/MOD13A1.061.

Didan, K., 2021b: MODIS/Aqua Vegetation Indices 16-Day L3 Global 500m SIN Grid V061 [Data set]. NASA EOSDIS Land Processes Distributed Active Archive Center, https://doi.org/10.5067/MODIS/MYD13A1.061.

Heijmans, M. M. P. D., and Coauthors, 2022: Tundra vegetation change and impacts on permafrost. *Nat. Rev. Earth Environ.*, **3**, 68-84, https://doi.org/10.1038/s43017-021-00233-0.

Karlsen, S. R., A. Elvebakk, L. Stendardi, K. A. Høgda, and M. Macias-Fauria, 2024: Greening of Svalbard. *Sci. Total Environ.*, **945**, 174130, https://doi.org/10.1016/j.scitotenv.2024.174130.

Kim, J. E., J. A. Wang, Y. Li, C. I. Czimczik, and J. T. Randerson, 2024: Wildfire-induced increases in photosynthesis in boreal forest ecosystems of North America. *Glob. Change Biol.*, **30**(1), e17151, https://doi.org/10.1111/gcb.17151.

Pinzon, J. E., E. W. Pak, C. J. Tucker, U. S. Bhatt, G. V. Frost, and M. J. Macander, 2023: Global Vegetation Greenness (NDVI) from AVHRR GIMMS-3G+, 1981-2022 [Data set]. ORNL DAAC, Oak Ridge, TN, USA, https://doi.org/10.3334/ORNLDAAC/2187.

Ramirez, J. I., and Coauthors, 2024: Reindeer grazing reduces climate-driven vegetation changes and shifts trophic interactions in the Fennoscandian tundra. *Oikos*, **2024**(11), e10595, https://doi.org/10.1111/oik.10595.

Raynolds, M. K., and Coauthors, 2019: A raster version of the Circumpolar Arctic Vegetation Map (CAVM). *Remote Sens. Environ.*, **232**, 111297, https://doi.org/10.1016/j.rse.2019.111297.

Tape, K. D., J. A. Clark, B. M. Jones, S. Kantner, B. V. Gaglioti, G. Grosse, and I. Nitze, 2022: Expanding beaver pond distribution in Arctic Alaska, 1949 to 2019. *Sci. Rep.*, **12**, 7123, https://doi.org/10.1038/s41598-022-09330-6.

Tassone, M. S., H. E. Epstein, A. H. Armstrong, U. S. Bhatt, G. V. Frost, B. Heim, M. K. Raynolds, and D. A. Walker, 2024: Drivers of heterogeneity in tundra vegetation productivity on the Yamal Peninsula, Siberia, Russia. *Environ. Res.: Ecology*, **3**, 015003, https://doi.org/10.1088/2752-664X/ad220f.

Wong, R. E., L. T. Berner, P. F. Sullivan, C. S. Potter, and R. J. Dial, 2024: Pixel walking along the boreal forest-Arctic tundra ecotone: Large scale ground-truthing of satellite-derived greenness (NDVI). *Glob. Change Biol.*, **30**(6), e17374, https://doi.org/10.1111/gcb.17374.

January 7, 2025

Migratory Tundra Caribou in a Warmer Climate

https://doi.org/10.25923/qn4a-td90

A. Gunn[1], D. Russell[1], K. Joly[2], L. Manzo[3], J. Pellissey[4], J. Tulagak[3], and A. V. Whiting[5]

[1]CircumArctic Rangifer Monitoring and Assessment (CARMA), Whitehorse, YT, Canada
[2]National Park Service, Fairbanks, AK, USA
[3]Kivalliq Inuit Association, Rankin Inlet, NU, Canada
[4]Wek'èezhìi Renewable Resources Board, Yellowknife, NT, Canada
[5]Native Village of Kotzebue, AK, USA

Headlines

- Arctic migratory tundra caribou populations have declined by 65% overall over the last 2-3 decades. More recently, the relatively smaller coastal herds in the western Arctic are showing signs of recovery while the larger inland herds are either stable or continuing to decline.
- Warmer summer and fall temperatures, changes in winter snowfall, and an increasing human footprint collectively stress Arctic caribou, altering their distribution, movements, survival, and productivity.
- The extent of recent herd declines and onsets of recoveries varies regionally, consistent with regional climate trends. Arctic regions of greatest projected summer warming are projected to see the largest continued population declines.
- Sharing knowledge is essential, as those charged with managing caribou endeavor to more fully understand climate impacts on herd health and implement strategies that encourage herd growth, while accommodating the cultural, nutritional, and spiritual relationships northern people have with caribou.

Introduction

Climate influences almost every aspect of caribou ecology, which means the Arctic's rapid warming will have far-reaching, cascading, and complex impacts. The Arctic climate is strongly regional, such as differences between coastal and interior climates. Besides climate, geological influences on vegetation add to the regional differences which, in turn, complicate predicting how cold-adapted caribou (and their Eurasian counterpart, wild reindeer) can balance beneficial and adverse impacts of a warmer climate. Caribou spend about 3/4 of their day foraging and digesting, so how climate interacts with forage quality and quantity is key. However, climate impacts on arctic vegetation are complex; grasses, sedges and shrubs are likely to increase while many plant groups are relatively resilient to climate change (Callaghan et al. 2022).

Historically, the caribou's cyclic abundance (Gunn 2003) anchored their central role in arctic tundra food webs and Arctic Indigenous cultures through spiritual and nutritional sustenance. Migratory tundra caribou numbers increased to peak values in the 1990s and early 2000s (Table 1) but have since declined 65%, from 5.5 million to 1.88 million with timing varying regionally (Gunn 2016; Russell et al. 2018; CARMA unpubl. data). In the western Arctic, the coastal herds (Table 1) are, in general, smaller and

recovery has been underway for 6-16 years for 4 of the 5 herds. The five largest herds are inland (Taimyr, Bathurst, George River, Qamanirjuaq and Western Arctic), with peak herd sizes of close to or above 500,000 caribou. These herds have not yet started to recover and are either stable at low numbers or continuing to decline (Table 1, Fig. 1). Concerns are heightened for those herds as Indigenous Elders state that numbers have never been so low. Why caribou have declined is complicated: natural cycles have played a role but so has the changing landscape due to a greater human footprint and climate change.

Table 1. Trends among migratory tundra herds since recent peak numbers. In this table increasing and decreasing were assigned if there was a trend for 3 surveys in a row. Herd codes are: Teshekpuk Lake (TLH), Central Arctic (CAH), Cape Bathurst (CBH), Bluenose West (BNW), Porcupine (PCH), Western Arctic (WAH), Taimyr (TAI), Bluenose East (BNE), Bathurst (BAH), Qamanirjuaq (QCH), Leaf River (LRH), George River (GRH), and Kangerlussuaq-Sisimiut (KSH). The significance of Sedimentary versus Precambrian Shield geology relates to contrasts in vegetation communities and surficial hydrology. The herds labeled as either Coastal or Inland spend their calving and post-calving seasons in coastal or inland ranges, respectively.

	Sedimentary Geology						Precambrian Shield Geology						
	Coastal Calving/Post-calving						Inland Calving/Post-calving						
	Peak < 100,000				Peak > 100,000								
Year	TLH	CAH	CBH	BNW	PCH	WAH	TAI	BNE	BAH	QCH	LRH	GRH	KSH
2024													
2023													
2022													
2021													
2020													
2019													
2018													
2017													
2016													
2015													
2014													
2013													
2012													
2011													
2010													
2009													
2008													
2007													
2006													
2005													
2004													
2003													
2002													
2001													
2000													
1999													
1998													
1997													
1996													
1995													
1994													
1993													
1992													
1991													
1990													
1989													
1988													
1987													
1986													

Legend	
No survey	
Stable	
Increase	
Decline	
Peak	
Pre-peak	

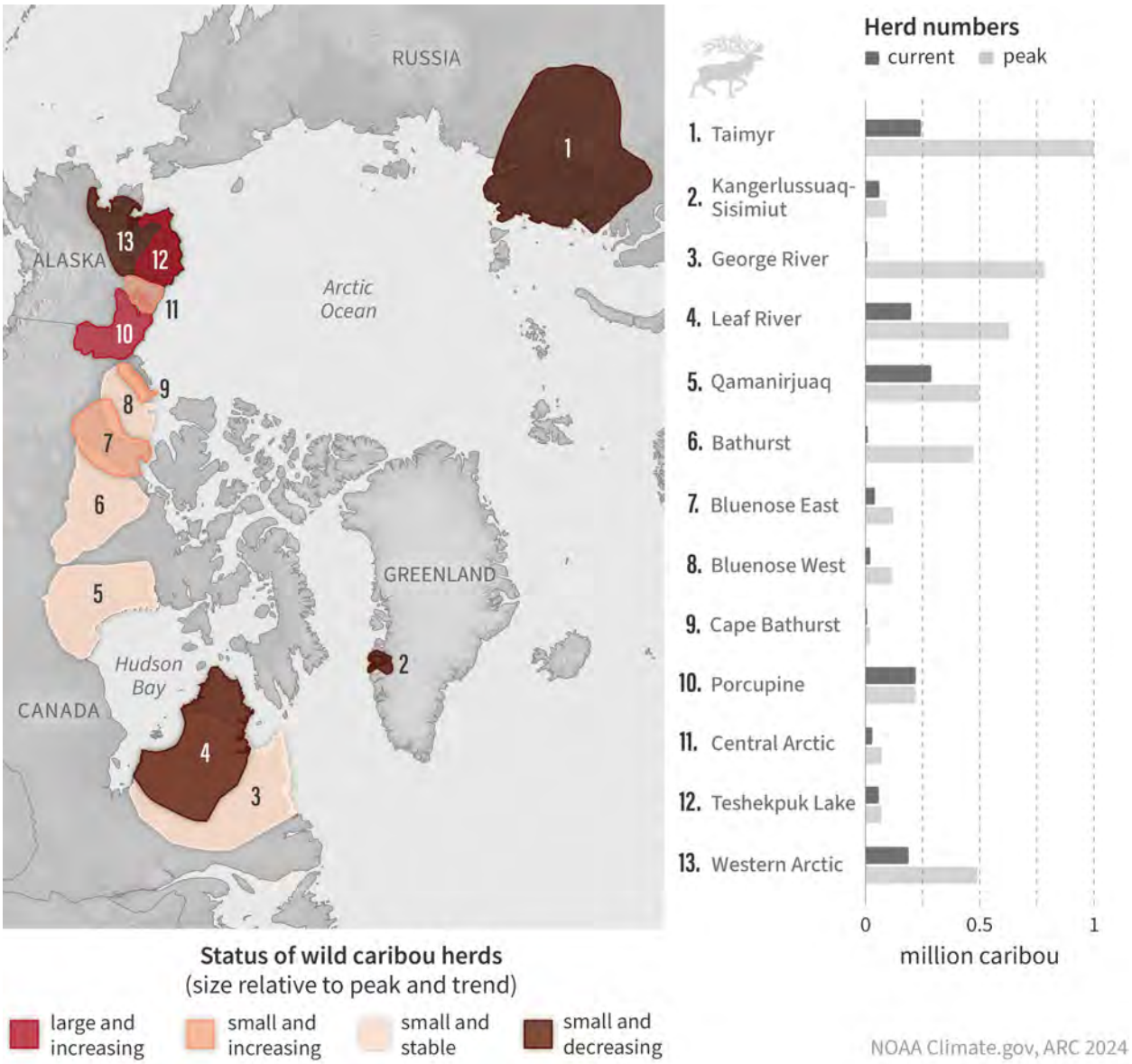

Fig. 1. Trends and herd size status among migratory tundra caribou herds since peak numbers in the 1990s and early 2000s.

Current and projected signals of the warmer climate for caribou

Since 1980, the fall warming trend across the Arctic is the most consistent climate signal (Russell et al. 2024). Warmer falls are correlated with increased risk of icing on winter ranges. The western coastal herds have earlier and warmer springs while the central continental herds have drier and warmer summers. Warmer and drier summers reduce adult survival (Russell et al. 2024) and Indigenous Knowledge emphasizes that caribou are healthy during cool, wet summers (Tłı̨chǫ Government 2022). The Western Arctic Herd in western Alaska has declined 70% since numbering 490,000 in 2003, which harvesters attribute partly to climate change. Although the herd has a maritime arctic climate, the herd calves and summers inland from the coast (Fig. 2). Communities have observed that reduced summer snow patches have impacted the herd's ability to avoid insect harassment. On the winter ranges, days with freezing rain and rain-on-snow will likely increase as the fall temperature increases. Ice layers can

lock away terrestrial forage that overwintering caribou rely upon, impacting body condition and survival. For example, for the Western Arctic herd, an extreme midwinter thaw with rain in December 2005 left many caribou in poor body condition and cow survival declined to 70%.

Fig. 2. Caribou in fall range of the Western Arctic Herd of Alaska. Photo credit: K. Joly.

To project what a warmer climate may mean, we applied an existing model (Russell et al. 2021) for a coastal herd (Fig. 1; Central Arctic Herd), an interior continental herd (Bathurst Herd), and the central Siberian Taimyr Herd (Russell and Gunn 2024). Under the optimistic scenario (global temperature increases <1.5°C by 2100), the Russian and Alaskan coastal herds' summer range temperatures by 2100 remain between the historic mean daily and historic maximum daily temperature (historic period as 1980-2019) while the interior Bathurst Herd's average summers will be as hot as the historic maximum daily mean. Specifically, the annual average number of days >19°C is projected to increase from the historic period 14 days to 38 days by 2100 on the Bathurst Herd's summer range compared to 7 to 11 days for the Central Arctic Herd and 3 to 6 days for the Taimyr Herd. The hotter days cause caribou to reduce their forage intake partly in response to mosquito harassment but also to reduce internal heat generated by digestion (Trondrud et al. 2023). Resulting daily forage intake would be 8% less for the Bathurst Herd, 2% less for the Taimyr Herd, and unchanged for the Central Arctic Herd (Russell and

Gunn 2024). Forage intake impacts cow body weight in the fall, which dictates pregnancy rates and calf survival. For the optimistic scenario, the additional costs of climate change are that the Bathurst and Taimyr herds would decline to 71% and 67% of current herd size, respectively, but the Central Arctic herd would slightly increase (4% higher). However, under the pessimistic 2100 scenario (~4.4°C global warming by 2100), all three herds are projected to decline by 64%, 32%, and 9% of current levels for the Bathurst, Taimyr, and Central Arctic herds, respectively (Russell and Gunn 2024).

A warmer climate and the people who depend on caribou

Arctic caribou are adapted to annually variable weather, but projections of when their adaptability could be exceeded are uncertain, especially as there are other cumulative impacts on caribou seasonal ranges. For example, a warmer climate, landscape changes (including mining, roads, and railways), and increasing predation are driving reindeer herding in Finland toward tipping points when adaptive mechanisms reach their limits (Landauer et al. 2021). Adaptive mechanisms include caribou avoiding extremes in weather, such as icing on their winter ranges, by shifting their migratory pathways, but they are at risk if roads and railways limit their free passage. The observations of people who share the caribou's landscape emphasize that a warmer climate is already part of a changing landscape creating threats for caribou health and productivity and adding to the food security threats faced by the people who have long depended on them. Caribou will shift their ranges to adapt to a changing climate but that can have unexpected impacts when they encounter other uses of the landscapes. Inuit hunters are observing unexpected shifts in the Qamanirjuaq Herd's calving grounds after decades of calving in a relatively fixed location. The location of calving is partly tied to vegetation green up, which is now progressively earlier (Mallory et al. 2020; Cameron et al. 2020). Inuit hunters reported that the shift brought calving to the edge of an operational gold mine (NIRB 2023), which was unanticipated and a strong concern for the neighboring communities who depend on the Qamanirjuaq herd.

Indigenous Elders are afraid for the future of the Bathurst Herd, which they have depended on for thousands of years. They identify how the herd's hotter climate, mining, and associated roads are changing the herd's movements. The herd has declined 97% since the mid-1990s and the Wek'èezhìi Renewable Resources Board, a co-management body, has worked with communities, Indigenous governments, and the Government of the Northwest Territories to eliminate caribou harvesting and increase wolf harvests. The decline was partly a natural cycle but warmer summers, roads, traffic, and mines have contributed. Alarmingly, conservation actions have not led to herd recovery, which raises fears for its future given the predictions of a hotter climate across its interior range.

While the hotter climate projections are not encouraging for the long-term health and vitality of many of the Arctic caribou herds, the signals of a warmer climate are already measurable on the Arctic caribou ranges. Understanding when caribou reach the limits of their adaptability will require the observations and knowledge of people who share the ranges, as well as scientific monitoring. Sharing knowledge among all stakeholders is essential for the bodies charged with looking after caribou as they endeavor to contribute to the resilience for caribou and people across the Arctic landscapes.

Methods and data

We used estimates of caribou abundance from aerial surveys 1970 to 2023 (Gunn 2016; Russell et al. 2018; unpublished CARMA database). We derived seasonal herd-specific climates from the National Aeronautics and Space Administration's Modern Era Retrospective Analysis for Research and

Applications climate indicators clipped to herd-specific ranges (Russell et al. 2013). For future climates, we focused on average monthly temperature projections for late spring to fall for mid-century (2050) and end-century (2100) from the Coupled Model Intercomparison Project Phase 6 (CMIP6) global climate models with an optimistic SSP1-1.9 scenario (below 1.5°C global warming by 2100) and the pessimistic SSP5-85 (high emissions; ~4.4°C global warming by 2100) scenarios. We applied relationships of climate, population dynamics, and forage ecology for spring to fall to quantify climate change impacts using an existing integrative Caribou Cumulative Effects model (White et al. 2014; Russell et al 2021; Russell and Gunn 2024). Russell and Gunn (2024) presents a novel quantification of the regional impacts and the authors will make the report, the data inputs, and model output available on request. A journal publication of this report is in preparation.

Acknowledgments

We thank the Government of the Northwest Territories and the World Wildlife Fund (WWF Global Arctic Programme) for financial support. This review would not be possible without Indigenous Knowledge holders sharing their understanding of caribou ecology and the work of many scientists engaged in caribou conservation across North America. We thank Matthew Druckenmiller and Rick Thoman for their review comments.

References

Callaghan, T. V., R. Cazzolla Gatti, and G. Phoenix, 2022: The need to understand the stability of arctic vegetation during rapid climate change: An assessment of imbalance in the literature. *Ambio*, **51**, 1034-1044, https://doi.org/10.1007/s13280-021-01607-w.

Cameron, M. D., K. Joly, G. A. Breed, C. P. H. Mulder, and K. Kielland, 2020: Pronounced fidelity and selection for average conditions of calving area suggestive of spatial memory in a highly migratory ungulate. *Front. Ecol. Evol.*, **8**, 564567, https://doi.org/10.3389/fevo.2020.564567.

Gunn, A., 2003: Voles, lemmings and caribou – population cycles revisited? *Rangifer*, **23**(5), 105–111, https://doi.org/10.7557/2.23.5.1689.

Gunn, A., 2016: Rangifer tarandus. The IUCN Red List of Threatened Species 2016: e.T29742A22167140, accessed September 2024, https://dx.doi.org/10.2305/IUCN.UK.2016-1.RLTS.T29742A22167140.en.

Landauer, M., S. Rasmus, and B. Forbes, 2021: What drives reindeer management in Finland towards social and ecological tipping points? *Reg. Environ. Change*, **21**, 32, https://doi.org/10.1007/s10113-021-01757-3.

Mallory, C. D., S. N. Williamson, M. W. Campbell, and M. S. Boyce, 2020: Response of barren-ground caribou to advancing spring phenology. *Oecologia*, **192**, 837-852, https://doi.org/10.1007/s00442-020-04604-0.

Nunavut Impact Review Board (NIRB), 2023: Reconsideration report and recommendations for the Meliadine Extension Proposal Related to Agnico Eagle Mines Limited's Meliadine Gold Mine Project Certificate No. 006 NIRB File No. 11MN034. Accessed September 2024, https://www.nirb.ca/portal/pdash.php?appid=125684.

Russell, D., and A. Gunn, 2024: Arctic Conservation Forecast project (ARCON4): assessing vulnerability of migratory tundra caribou to climate change. Report prepared for World Wildlife Fund Global Arctic Programme (available on request to the authors and WWF).

Russell, D. E., A. Gunn, and S. Kutz, 2018: Migratory tundra caribou and wild reindeer. *Arctic Report Card 2018*, E. Osborne, J. Richter-Menge, and M. Jeffries, Eds., https://www.arctic.noaa.gov/report-card.

Russell, D., A. Gunn, and R. White, 2021: A decision support tool for assessing cumulative effects on an Arctic migratory tundra caribou population. *Ecol. Soc.*, **26**(1), 4, https://doi.org/10.5751/ES-12105-260104.

Russell D., R. White, and A. Gunn, 2024: Understanding productivity of North American Migratory tundra caribou (Rangifer tarandus): role of vital rates and climate. Government of Northwest Territories, Department of Environment and Natural Resources, Manuscript Report 318. Yellowknife, Northwest Territories, Canada.

Russell, D. E., P. H. Whitfield, J. Cai, A. Gunn, R. G. White, and K. Poole, 2013: CARMA's MERRA-based caribou range climate database. *Rangifer*, **33**(2), 145-152, https://doi.org/10.7557/2.33.2.2535.

Tłı̨chǫ Government, 2022: Ekwǫ Nàxoèhdee K'è 2022 Results. Tłı̨chǫ Research and Training Institute 2023, accessed September 2024, https://research.tlicho.ca/research/bootsontheground.

White, R. G., D. E. Russell, and C. J. Daniel, 2014: Simulation of maintenance, growth and reproduction of caribou and reindeer as influenced by ecological aspects of nutrition, climate change and industrial development using an energy-protein model. *Rangifer*, **34**(2), 1-126, https://doi.org/10.7557/2.34.2.3269.

December 5, 2024

Arctic Terrestrial Carbon Cycling

https://doi.org/10.25923/0gpp-mn10

S. M. Natali[1], B. Rogers[1], E. A. G. Schuur[2], V. Romanovsky[3], H. Alcock[4], K. Arndt[1], E. S. Euskirchen[5,6], G. Falvo[2], G. Fiske[1], G. Hould-Gosselin[4], J. Hung[1], A. Kholodov[3], S. Potter[1], O. Sonnentag[4], and A. -M. Virkkala[1]

[1]Woodwell Climate Research Center, Falmouth, MA, USA
[2]Center for Ecosystem Science and Society, Northern Arizona University, Flagstaff, AZ, USA
[3]Geophysical Institute, University of Alaska Fairbanks, Fairbanks, AK, USA
[4]Département de Géographie, Université de Montréal, Montréal, QC, Canada
[5]Institute of Arctic Biology, University of Alaska Fairbanks, Fairbanks, AK, USA
[6]Department of Biology and Wildlife, University of Alaska Fairbanks, Fairbanks, AK, USA

Headlines

- When including wildfire emissions, the Arctic tundra region has shifted to a carbon dioxide (CO_2) source and is a consistent methane (CH_4) source.
- In 2024, permafrost temperatures were the highest on record at nearly half of Alaska long-term monitoring stations. On average, the year represented the second-warmest permafrost temperatures on record for Alaska.
- Wildfires in North American permafrost regions have increased since the mid-20th century, and circumpolar wildfire emissions have averaged 207 teragrams of carbon (Tg C) per year since 2003. 2024 was the second highest year for wildfire emissions north of the Arctic Circle.

Introduction

The terrestrial Arctic region has been a carbon sink for thousands of years, meaning that there has been a net removal of carbon dioxide (CO_2) from the atmosphere by plants and storage as organic carbon in soils and permafrost (perennially frozen ground). Climate warming can stimulate plant productivity and growth (see essay *Tundra Greenness*), resulting in enhanced rates of CO_2 removal from the atmosphere. At least 1.4 to 1.6 trillion tonnes of carbon (Hugelius et al. 2014; Schuur et al. 2022) have accumulated in terrestrial soils and permafrost across the region. Despite increased plant growth and CO_2 uptake, recent indicators suggest that some locations in the Arctic are becoming a net source of carbon to the atmosphere. Increasing surface air temperatures (see essay *Surface Air Temperature*) are causing permafrost to warm and thaw (Smith et al. 2024). Once thawed, permafrost carbon can be decomposed by microbes and released into the atmosphere as greenhouse gasses, CO_2 and methane (CH_4). In addition to changes in plant and microbial processing of carbon, disturbances, such as wildfire, are resulting in pulse releases of CO_2 and CH_4 that may shift the Arctic from a net carbon sink to a source.

Here, we describe trends in permafrost temperatures, wildfire, and carbon cycling (CO_2 and CH_4) at select long-term terrestrial monitoring sites and across the Arctic. Our discussion of the Arctic region considers all tundra and boreal lands within the northern permafrost region (Brown et al. 2002; Fig. 1), which covers 16.6 x 10^6 km^2.

Fig. 1. The Arctic study domain for this essay includes all tundra and boreal biome regions within the northern permafrost region (shaded areas). Shaded triangle symbols represent a subset of Arctic carbon flux monitoring sites (open circles) that were included in the site-level analysis.

Permafrost temperature trends

Permafrost temperatures have been monitored across the Arctic for almost half a century, providing a long-term record of climate change impacts. Deeper permafrost temperatures (≥ 15 m), which are reported here, are less sensitive to seasonal temperature fluctuations than surface measurements, and thus, these long-term trends are good indicators of permafrost response to climate change. Here, we report trends in deep permafrost temperatures across Alaska, which, similar to permafrost temperatures across the Arctic, have been increasing for the past several decades (Smith et al. 2024). These warming trends are also associated with a deepening of the seasonally thawed soils, which can have important implications for carbon cycling.

Permafrost temperatures in 2024 were the highest on record at 9 of 20 long-term monitoring sites across Alaska. Over the past four decades, the average increase in permafrost temperature ranged from 0.3 to 0.7°C per decade in colder permafrost in Northern Alaska (i.e., North Slope) and from 0.02 to 0.3°C per decade in warmer permafrost in Interior Alaska (Fig. 2). Greater permafrost warming rates at higher latitudes compared to lower latitudes are partly due to greater air temperature increases at higher latitudes. Additionally, permafrost with temperatures close to 0°C—such as those in lower latitudes in Interior Alaska—require energy (i.e., latent heat) to melt ground ice before temperatures can continue rising, bringing about reduced permafrost warming rates.

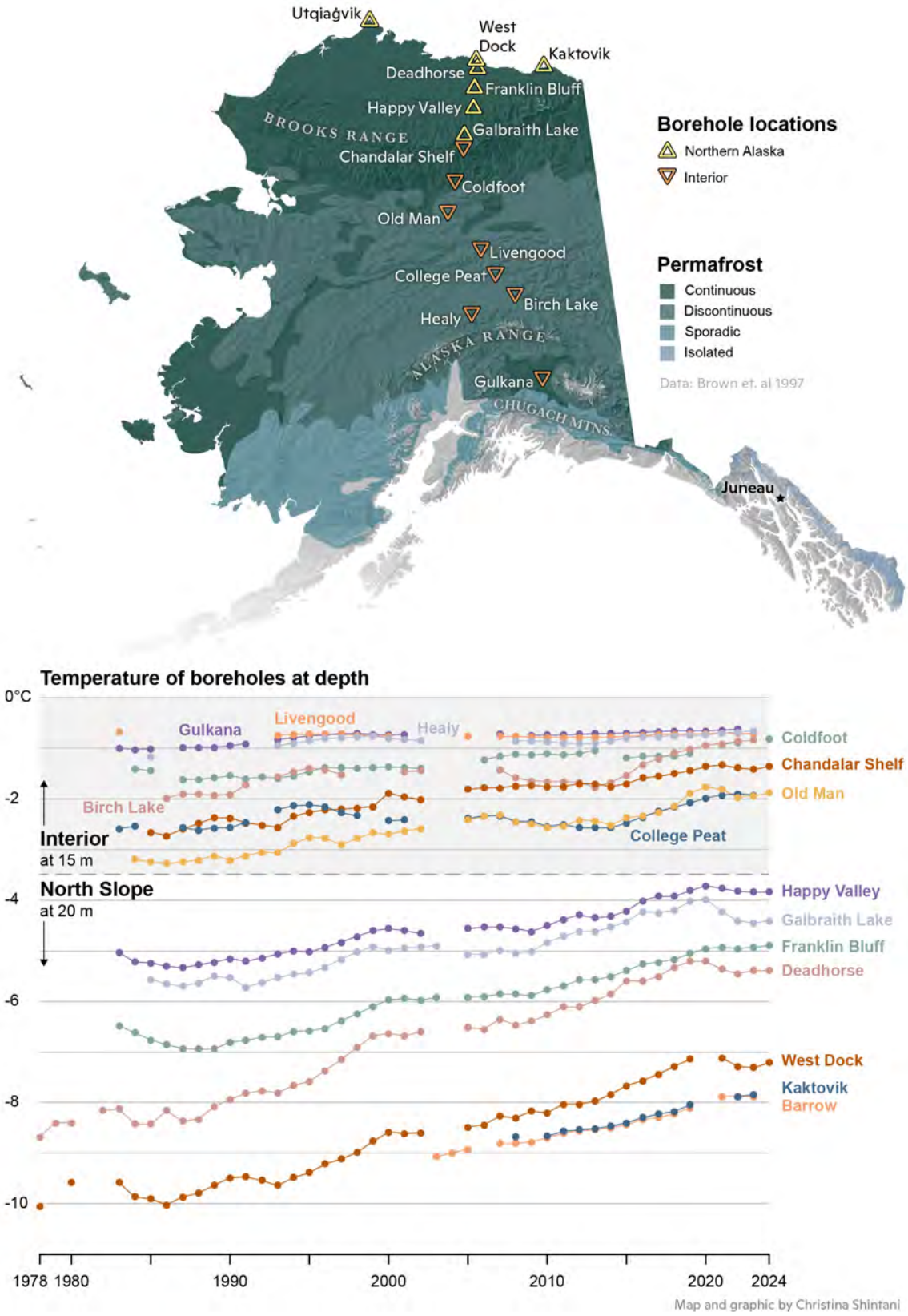

Fig. 2. Mean annual ground temperature (°C) at depths of 15 m (Interior Alaska) or 20 m (North Slope) below the surface at measurement sites across Alaska. (Figure prepared by Christina Shintani).

Site-level carbon fluxes

Published observations from several long-term carbon flux monitoring sites have shown that some ecosystems have already shifted from carbon sinks to carbon sources (Schuur et al. 2021; Euskirchen et al. 2024). Here, we report net CO_2 and CH_4 exchange between ecosystems and the atmosphere through August 2024 for 13 locations (Fig. 1) in the North American and European permafrost region, each having between 6 and 17 years of data (Fig. 3). It is important to note that the fluxes from these sites do not directly correspond to the average fluxes for the entire biomes they fall within or the region as a whole. For the 12-month period of September 2023 to August 2024, the three boreal forest sites were on average a net sink of CO_2, taking up 17 g CO_2-C/m^2/y from the atmosphere, which was slightly less CO_2 uptake than their long-term average. During the same 12-month period, the six tundra sites took up an average of 19 g CO_2-C/m^2/y, which was similar to their long-term average uptake. The four wetland sites were stronger CO_2 sources than in previous years, releasing an average of 46 g CO_2-C/m^2/y; however, larger data compilations demonstrate wetlands to be on average CO_2 sinks (Ramage et al. 2024). The six sites that measured CH_4 fluxes (three wetland, two tundra, one boreal forest) were on average net emitters of CH_4 (7 g CH_4-C/m^2/y) during this period. Fire, logging, and other disturbances at the regional scale, which may cause these biomes to become net carbon sources, are not included in these site-level assessments.

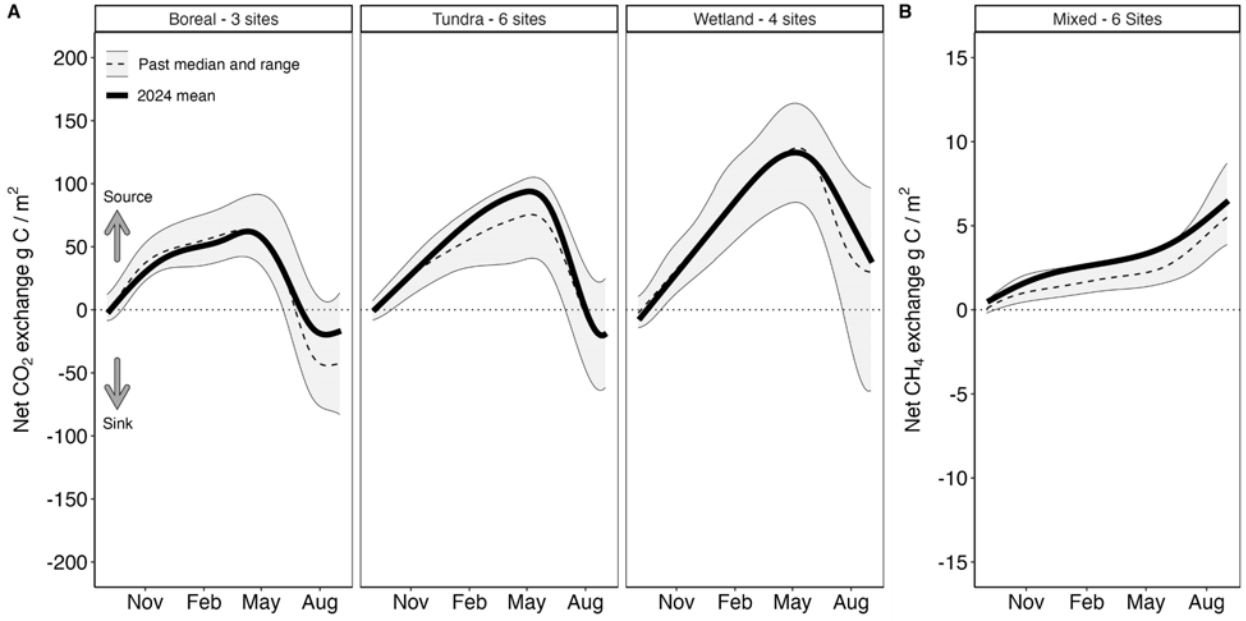

Fig. 3. (A) Cumulative net CO_2 exchange for 2024 (solid line) and previous years (shading; data records range from 6-17 years depending on site) across 13 North American and European eddy covariance sites. (B) Cumulative net CH_4 exchange for six eddy covariance sites (3 wetland, 2 tundra, 1 boreal forest). Positive values indicate a flux from the land to the atmosphere (carbon source) and negative values indicate a flux from the atmosphere to the land (carbon sink).

Wildfire

Climate change has been intensifying high-latitude fire regimes, resulting in increased burned area, fire intensity, and carbon emissions. Vegetation regrowth after wildfire often re-sequesters CO_2 from the atmosphere over decades following fire, but more frequent and severe fires, combustion of below-

ground carbon, and long-term impacts of fire on ground thaw from combustion of vegetation and organic soils are resulting in net carbon emissions to the atmosphere over large spatial scales.

Given the high interannual variability in permafrost-region fires, it is not possible to detect trends across the entire Arctic (Fig. 1) over the previous two decades alone, which is when robust satellite-based fire products are available (Fig. 4, top panel). During this period, the largest carbon emissions from fire occurred in 2003 (343 Tg C) and 2023 (478 Tg C) due to large fires in southern Siberia and Canada, respectively. Fires in Canada's permafrost region in 2023 burned more than twice the area of any previous year on record and emitted 381 Tg C. Over a longer multi-decadal time frame, Alaskan and Canadian permafrost regions have experienced a clear upward trend in burned area since the mid-20th century (Fig. 4, bottom panel); burned area over the last 20 years (2004-23) is 28% higher than the 1981-2000 average and 62% higher than the 1971-90 average. Fire emissions have also been increasing at higher rates north of the Arctic Circle compared to permafrost regions below the Arctic Circle. North of the Arctic Circle the three years with the largest fire emissions during the last 20 years are 2019 (39.2 Tg C), 2024 (42.3 Tg C), and 2020 (60.5 Tg C). Across the entire pan-Arctic permafrost region, 2024 was a moderately high fire year, with 7.5 Mha burned and 335 Tg C emitted (Scholten et al. 2024; Copernicus Atmosphere Monitoring Service 2022).

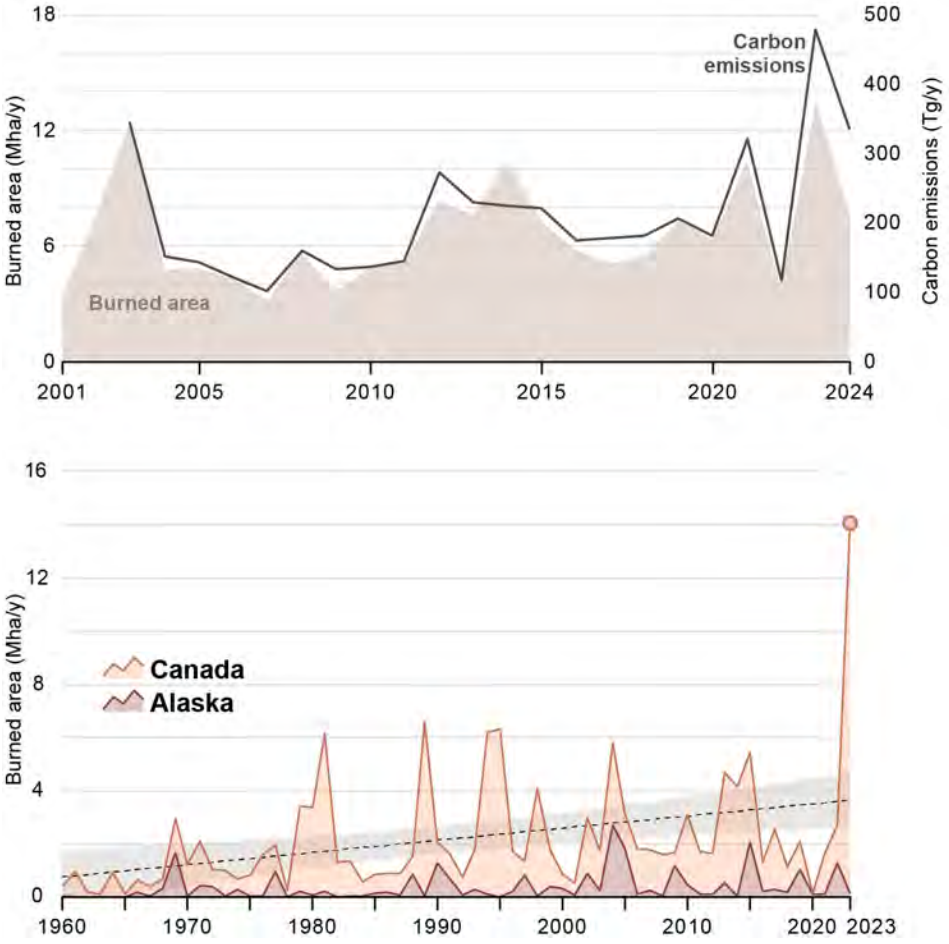

Fig. 4. Burned area (2001-24) and direct fire carbon emissions (2003-24) across the circumpolar permafrost domain (top) and burned area (1960-2023) across the permafrost region within Alaska and Canada (bottom). Bottom panel shows an ordinary least squares regression line and 95% confidence intervals. Note that separate data products were used for burned area and emissions, and for the two time periods presented, as described in the *Methods and data* section.

Regional carbon cycling trends

Across the Arctic region (Fig. 1), warmer temperatures over the past two decades (see essay *Surface Air Temperature*) were associated with more CO_2 uptake during the growing season (Virkkala et al. 2024a, 2024b), but CO_2 emitted from microbial respiration during the non-growing season offset growing season uptake (See et al. 2024; Virkkala et al. 2024a, 2024b). The pan-Arctic region was CO_2 neutral during 2001-20 (budget: -24 ± 123 Tg C/yr; Virkkala et al. 2024a, 2024b) when considering net ecosystem exchange (i.e., plant CO_2 uptake through photosynthesis and plant and microbial CO_2 release through respiration) and fire. However, the tundra region has shifted from a CO_2 sink—which it has been for millenia—to a small CO_2 source, while the boreal region remains a CO_2 sink (Hugelius et al. 2024; Ramage et al. 2024; Virkkala et al. 2024a; Fig. 5). The permafrost region is a CH_4 source, releasing 15 to 39 Tg CH_4-C/yr during 2000-20 (Hugelius et al. 2024).

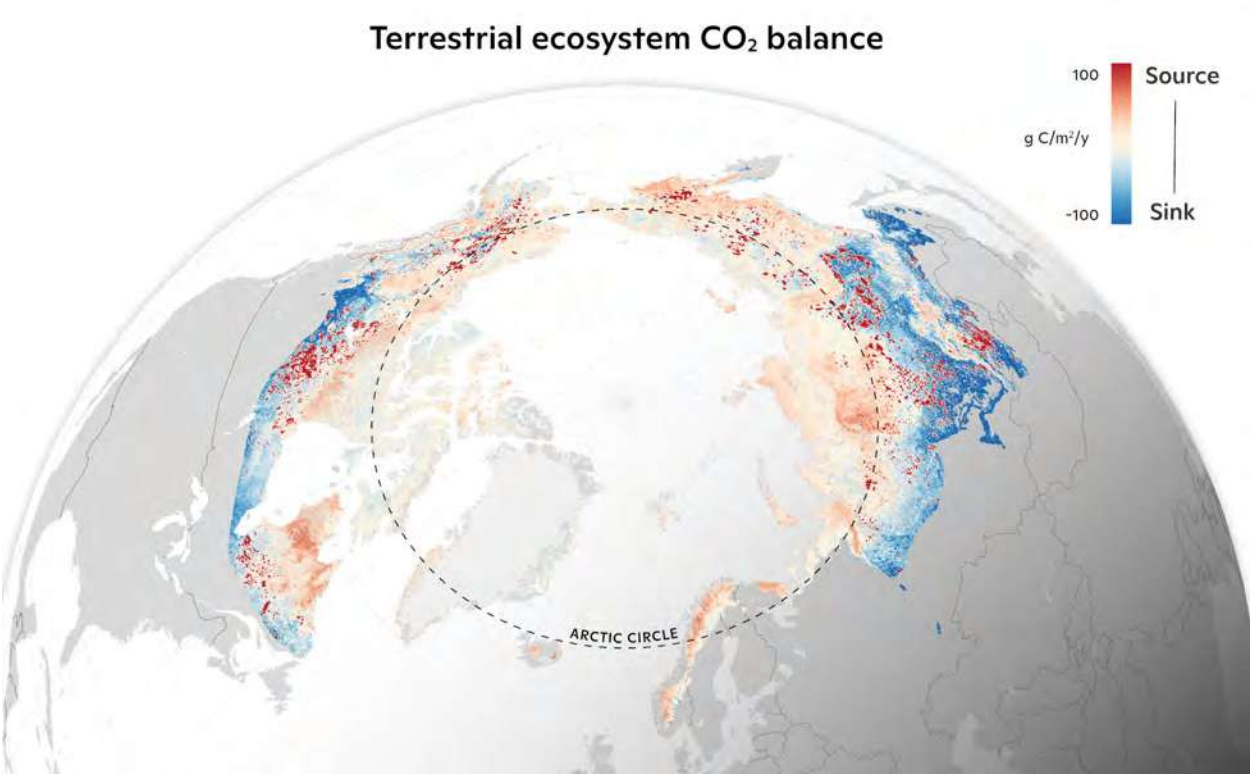

Fig. 5. Terrestrial ecosystem CO_2 fluxes with direct fire emissions (red shading) for the northern permafrost region (2002-20 average), showing areas that are CO_2 sources in pink and red and CO_2 sinks in blue. (Figure data from Virkkala et al. 2024b).

Methods and data

Site-level carbon fluxes were measured using the eddy covariance technique and gap-filled using Marginal Distribution Sampling or Random Forest methods (e.g., Euskirchen et al. 2024). Data were acquired through 31 August 2024 from public databases and site principal investigators (Lundin et al. 2024; NEON 2024). The shading in Fig. 3 denotes the 2.5%, 50%, and 97.5% quantiles of previous years' data and were generated using a generalized additive model. The long-term (6-17 year) mean fluxes were calculated using a linear mixed effect regression model with land cover as the fixed effect and site as the random intercept.

Burned area data from 2001-24 were taken from the MODIS-based MCD64A1 product (Giglio et al. 2018), and fire carbon emissions from 2003-24 were derived from the Copernicus Atmosphere Monitoring Service (2022). Due to lags in data latency, we used burned area information from the VIIRS active fire-based product (Scholten et al. 2024) for the months of August, September, and October in 2024. Data for 2024 were updated as of 15 October 2024 for both fire emissions and burned area. We also provide information on longer-term patterns in burned area in North America's permafrost region using the Canadian National Fire Database (Stocks et al. 2002; Canadian Forest Service 2021) and the Alaska Large Fire Database (Kasischke et al. 2002; Alaska Interagency Coordination Center 2024). Note these data sources are less reliable during the earlier decades.

References

Alaska Interagency Coordination Center, Wildland Fire Predictive Services Maps. Alaska Fire Service Bureau of Land Management, accessed 22 October 2024, https://fire.ak.blm.gov/predsvcs/maps.php.

Brown, J., O. Ferrians, J. A. Heginbottom, and E. Melnikov, 2002: Circum-Arctic Map of Permafrost and Ground-Ice Conditions, Version 2. NASA National Snow and Ice Data Center Distributed Active Archive Center, Boulder, CO, USA, accessed 20 January 2017, https://doi.org/10.7265/skbg-kf16.

Canadian Forest Service, 2021: Canadian National Fire Database. Natural Resources Canada, Canadian Forest Service, Northern Forestry Centre, accessed 22 October 2024, https://cwfis.cfs.nrcan.gc.ca/ha/nfdb.

Copernicus Atmosphere Monitoring Service, 2022: CAMS global biomass burning emissions based on fire radiative power (GFAS). Atmosphere Data Store, accessed 22 October 2024, https://ads.atmosphere.copernicus.eu/datasets/cams-global-fire-emissions-gfas?tab=overview.

Euskirchen, E. S., and Coauthors, 2024: Persistent net release of carbon dioxide and methane from an Alaskan lowland boreal peatland complex. *Glob. Change Biol.*, **30**(1), e17139, https://doi.org/10.1111/gcb.17139.

Giglio, L., L. Boschetti, D. P. Roy, M. L. Humber, and C. O. Justice, 2018: The Collection 6 MODIS burned area mapping algorithm and product. *Remote Sens. Environ.*, **217**, 72-85, https://doi.org/10.1016/j.rse.2018.08.005.

Hugelius, G., and Coauthors, 2014: Estimated stocks of circumpolar permafrost carbon with quantified uncertainty ranges and identified data gaps. *Biogeosciences*, **11**, 6573-6593, https://doi.org/10.5194/bg-11-6573-2014.

Hugelius, G. and Coauthors, 2024: Permafrost region greenhouse gas budgets suggest a weak CO_2 sink and CH_4 and N_2O sources, but magnitudes differ between top-down and bottom-up methods. *Global Biogeochem. Cy.*, **38**(10), e2023GB007969, https://doi.org/10.1029/2023GB007969.

Kasischke, E. S., D. Williams, and D. Barry, 2002: Analysis of the patterns of large fires in the boreal forest region of Alaska. *Int. J. Wildland Fire*, **11**(2), 131-144, https://doi.org/10.1071/WF02023.

Lundin, E., P. Crill, H. Grudd, J. Holst, A. Kristoffersson, A. Meire, M. Mölder, and N. Rakos, 2024: ETC L2 Fluxes, Abisko-Stordalen Palsa Bog, 2021-12-31-2024-08-31. ICOS RI, https://hdl.handle.net/11676/pPnlUbSqmjVMEf0SjkOpoUCX.

NEON (National Ecological Observatory Network), 2024: Bundled data products – eddy covariance (DP4.00200.001), provisional data, accessed 12 September 2024, https://data.neonscience.org/data-products/DP4.00200.001.

Ramage, J., and Coauthors, 2024: The net GHG balance and budget of the permafrost region (2000-2020) from ecosystem flux upscaling. *Global Biogeochem. Cy.*, **38**(4), e2023GB007953, https://doi.org/10.1029/2023GB007953.

Scholten, R. C., S. Veraverbeke, Y. Chen, and J. T. Randerson, 2024: Spatial variability in Arctic-boreal fire regimes influenced by environmental and human factors. *Nat. Geosci.*, **17**, 866-873, https://doi.org/10.1038/s41561-024-01505-2.

Schuur, E. A. G., and Coauthors, 2021: Tundra underlain by thawing permafrost persistently emits carbon to the atmosphere over 15 years of measurements. *J. Geophys. Res.:-Biogeo.*, **126**(6), e2020JG006044, https://doi.org/10.1029/2020JG006044.

Schuur, E. A. G., and Coauthors, 2022: Permafrost and climate change: Carbon cycle feedbacks from the warming Arctic. *Annu. Rev. Env. Resour.*, **47**, 343-371, https://doi.org/10.1146/annurev-environ-012220-011847.

See, C. R., and Coauthors, 2024: Decadal increases in carbon uptake offset by respiratory losses across northern permafrost ecosystems. *Nat. Climate Change*, **14**, 853-862, https://doi.org/10.1038/s41558-024-02057-4.

Smith, S. L., V. E. Romanovsky, K. Isaksen, K. E. Nyland, N. I. Shiklomanov, D. A. Streletskiy, and H. H. Christiansen, 2024: Permafrost. State of the Climate in 2023. *Bull. Amer. Meteor. Soc.*, **105**(8), S314-S317, https://doi.org/10.1175/BAMS-D-24-0101.1.

Stocks, B. J., and Coauthors, 2002: Large forest fires in Canada, 1959-1997. *J. Geophys. Res.-Atmos.*, **107**, 8149, https://doi.org/10.1029/2001JD000484.

Virkkala, A. -M., and Coauthors, 2024a: An increasing Arctic-boreal CO_2 sink offset by wildfires and source regions. *bioRxiv*, https://doi.org/10.1101/2024.02.09.579581.

Virkkala, A. -M., B. M. Rogers, J. D. Watts, K. Arndt, S. Potter, I. Wargowsky, and S. Natali, 2024b: Machine learning-based Arctic-boreal terrestrial ecosystem CO2 fluxes, 2001-2020. ORNL DAAC, Oak Ridge, TN, USA, https://doi.org/10.3334/ORNLDAAC/2377.

January 8, 2025

Ice Seals of Alaska

https://doi.org/10.25923/4488-8843

L. Quakenbush[1], A. Bryan[1], J. Crawford[1], J. Olnes[1], and R. Stimmelmayr[2,3]

[1]Arctic Marine Mammal Program, Alaska Department of Fish and Game, Fairbanks, AK, USA
[2]North Slope Borough, Department of Wildlife Management, Utqiaġvik, AK, USA
[3]Institute of Arctic Biology, University of Alaska, Fairbanks, AK, USA

Headlines

- Ice seal populations in the Pacific Arctic (ringed, bearded, spotted, and ribbon seals) remain healthy.
- Monitoring the subsistence harvest since the 1960s shows no sustained change in body condition, a stable or younger age of maturity, high pregnancy rates, and pup survival past weaning.
- As predicted with warmer water, fewer ringed seals are eating Arctic cod, and more are eating saffron cod; however, no concurrent changes in health are evident.

Introduction

Climate change in the Arctic is expected to affect sea ice-associated seal populations, or “ice seals,” by reducing sea ice extent and the length of time sea ice is available for resting, pupping, pup rearing, and molting (see essay *Sea Ice*). Four species of ice seals occupy the Bering, Chukchi, and Beaufort Seas, west and north of Alaska, and are harvested by Alaska Natives for subsistence: ringed (*Pusa hispida*), bearded (*Erignathus barbatus*), spotted (*Phoca largha*), and ribbon seals (*Histriophoca fasciata*) (Nelson et al. 2019; Fig. 1). Ringed and bearded seals were listed as ‘Threatened’ under the Endangered Species Act (ESA) in 2012 due to concerns with predicted sea ice decline over the next century (U.S. Federal Register 2012a,b). Current populations of all four species are large (>100,000s) and the subsistence harvest for all four species is sustainable (Nelson et al. 2019).

Fig. 1. Map of communities where ringed, bearded, spotted, and ribbon seal samples were collected from the Alaska Native subsistence harvest since the 1960s and used in these analyses. The dotted lines denote the 200 m depth contours marking the north and south boundaries of the continental shelf. Seal photographs were taken by the Alaska Department of Fish and Game pursuant to NMFS ESA/MMPA Permit No.15324.

Sampling of the annual ice seal harvest, coordinated by the Alaska Department of Fish and Game, has provided important information regarding seal population health and status since the 1960s. Coastal Indigenous communities that harvest seals provide measurements and tissues used to assess diet, body condition, age of maturity, pregnancy rate, and proportion of pups in the harvest (Fig. 1). The longevity of this biomonitoring program allows for comparisons over time that provide insight into individual and population level responses to recent environmental changes.

Diet

Changes in seal prey availability may occur as sea ice decreases and ocean temperatures increase (see essay *Sea Surface Temperature*), which may cause shifts in seal diet. For example, stomach contents from ringed seals, collected since 2010, suggest changes in their winter (December-May) diet are occurring. Arctic cod, saffron cod, rainbow smelt (*Osmerus mordax*), and Pacific herring (*Clupea pallasii*) are the four most common fish identified in ringed seal stomachs in winter. Fewer ringed seals ate Arctic cod during the 2010s than 2000s, whereas more ate saffron cod, rainbow smelt, and Pacific herring (Fig. 2). Walleye pollock were not identified in seal stomachs in the 2000s but have been identified at low frequency in the 2010s (Fig. 2).

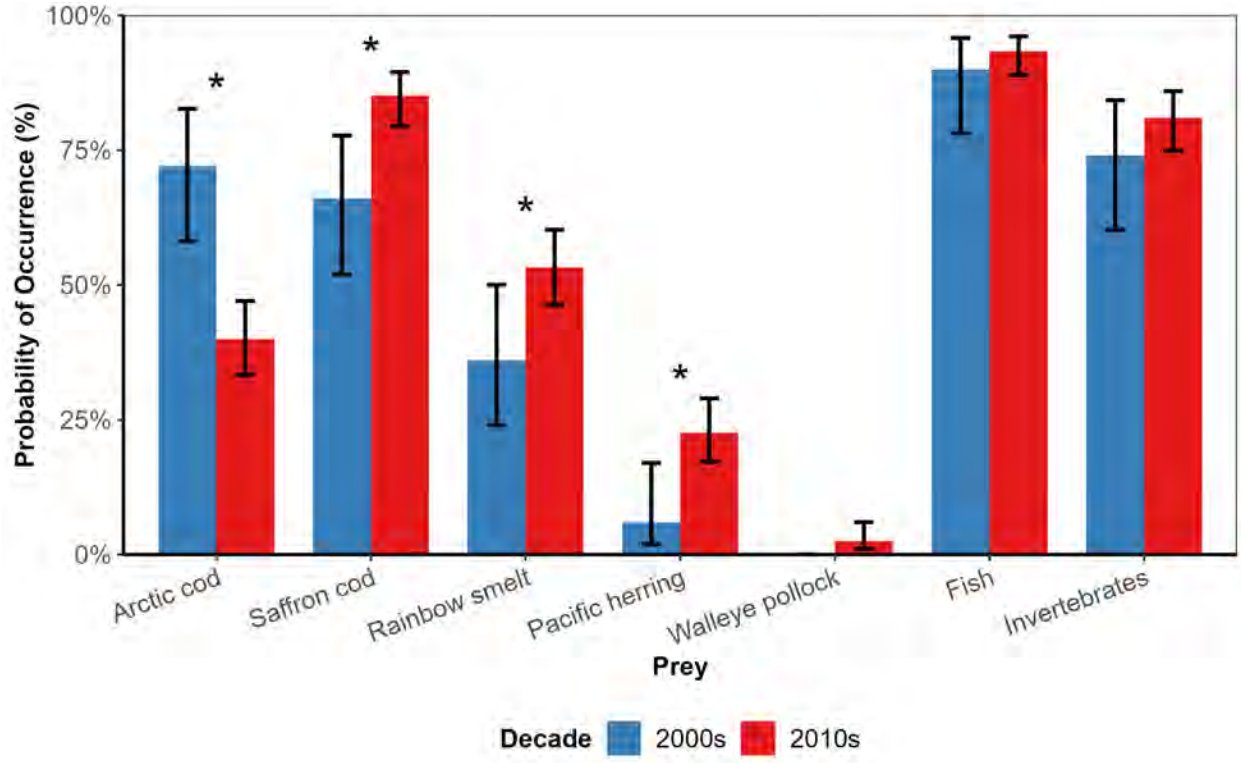

Fig. 2. The percent probability of occurrence (%PO ± 95% confidence intervals) of the four most common fish prey species (and walleye pollock) identified in the stomach contents of ringed seals ≥1 year of age collected during December-May in the 2000s and 2010s. Fish and Invertebrate categories represent all fish and invertebrates consumed. Statistically significant differences in %PO, based on logistic regression, between decades are indicated with an asterisk ("*", p <0.05).

These shifts in diet fit with known and predicted changes in fish distribution. Arctic cod (*Boreogadus saida*) have shifted their range northwards and are predicted to become less available on the continental shelf (waters <200 m deep), and therefore less available to seals (Marsh and Mueter 2020). Saffron cod (*Eleginus gracilis*) and walleye pollock (*Gadus chalcogrammus*) are predicted to become more available due to their preference for warmer waters (Stevenson and Lauth 2019; Deary et al. 2021). This change in diet is predicted to have negative effects on the energetics, body condition, and productivity of seals because saffron cod contain less energy by mass than Arctic cod (Florko et al. 2021).

Body condition

Blubber thickness was used as an index of body condition (Crawford et al. 2015) to determine if seal health has responded to changes in environmental conditions over time. It is important to account for known seasonal fluctuations and other sources of variability in blubber thickness when considering trends (Quakenbush 2020), before we can determine if there were decades when seals were on average thinner (unhealthy) or fatter (healthy). In general, the average blubber thickness of all four seal species has not undergone sustained negative changes since the 1960s (Fig. 3). Blubber thickness values dipped slightly for ringed, bearded, and spotted seals in the 2010s, a decade that included two unusual mortality events (UMEs). One primarily occurred in 2011 and 2012 when 657 seals were sickened by an unknown disease (NOAA Fisheries 2024a) and another in 2018 and 2019 when 275 seals were found dead. The later UME was attributed to malnutrition caused by extremely warm ocean temperatures in the Bering Sea during the consecutive winters of 2017/18 and 2018/19 (NOAA Fisheries 2024b). However, average blubber thickness rebounded in the early 2020s and was above average for spotted seals.

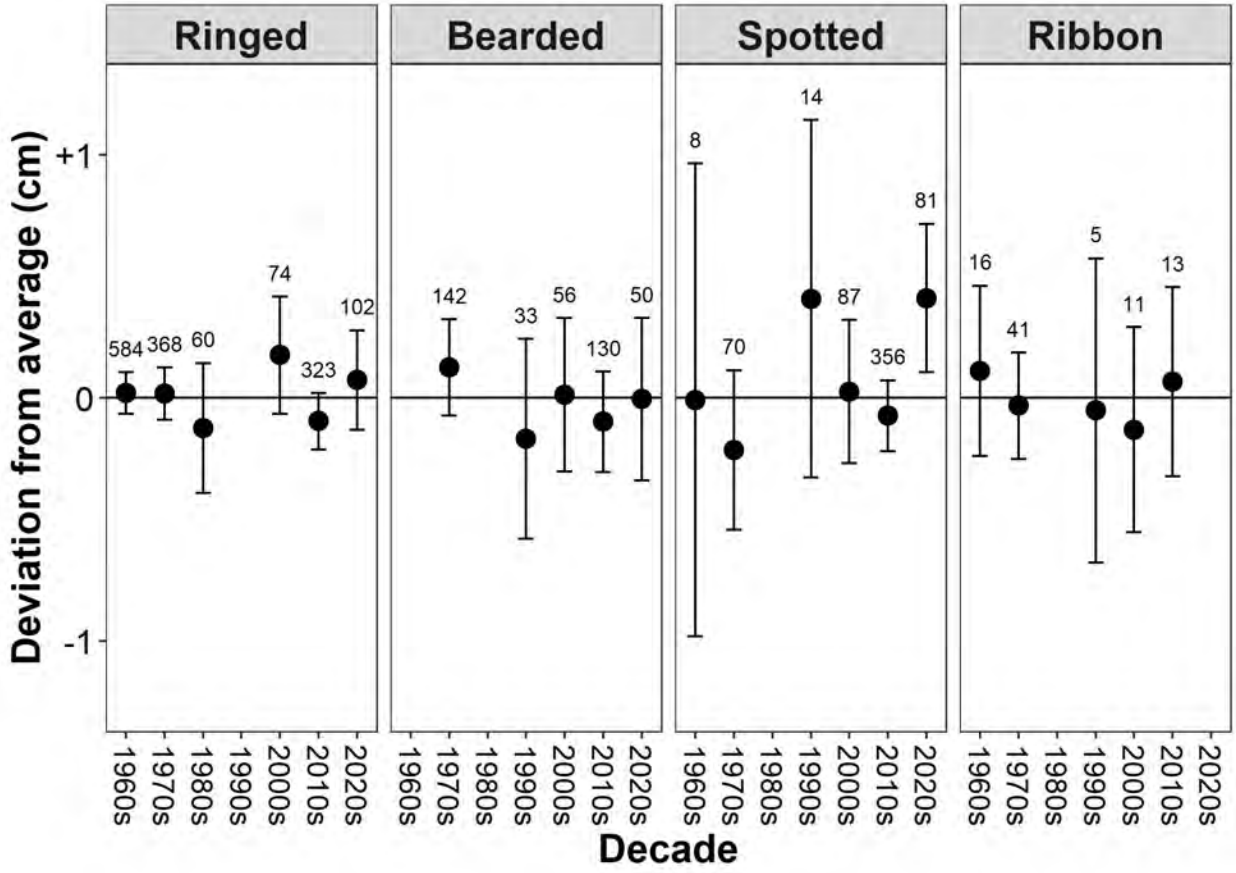

Fig. 3. Blubber thickness by decade, shown as deviations from the average across all decades after accounting for seasonal fluctuations and seal length. Positive values are above average and negative values are below average. The number of seals analyzed each decade is shown above the 95% confidence intervals. Some decades lacked data for some seal species.

Productivity

When resources are limited, it takes longer to acquire the energy needed to grow, and females mature at an older age (Laws 1956). When resources are not limited, seals grow quickly and mature at a younger age. The age of maturity has been consistent (spotted and ribbon) or occurred at a younger age in recent decades (ringed and bearded) for all species over the sampled period (Fig. 4a).

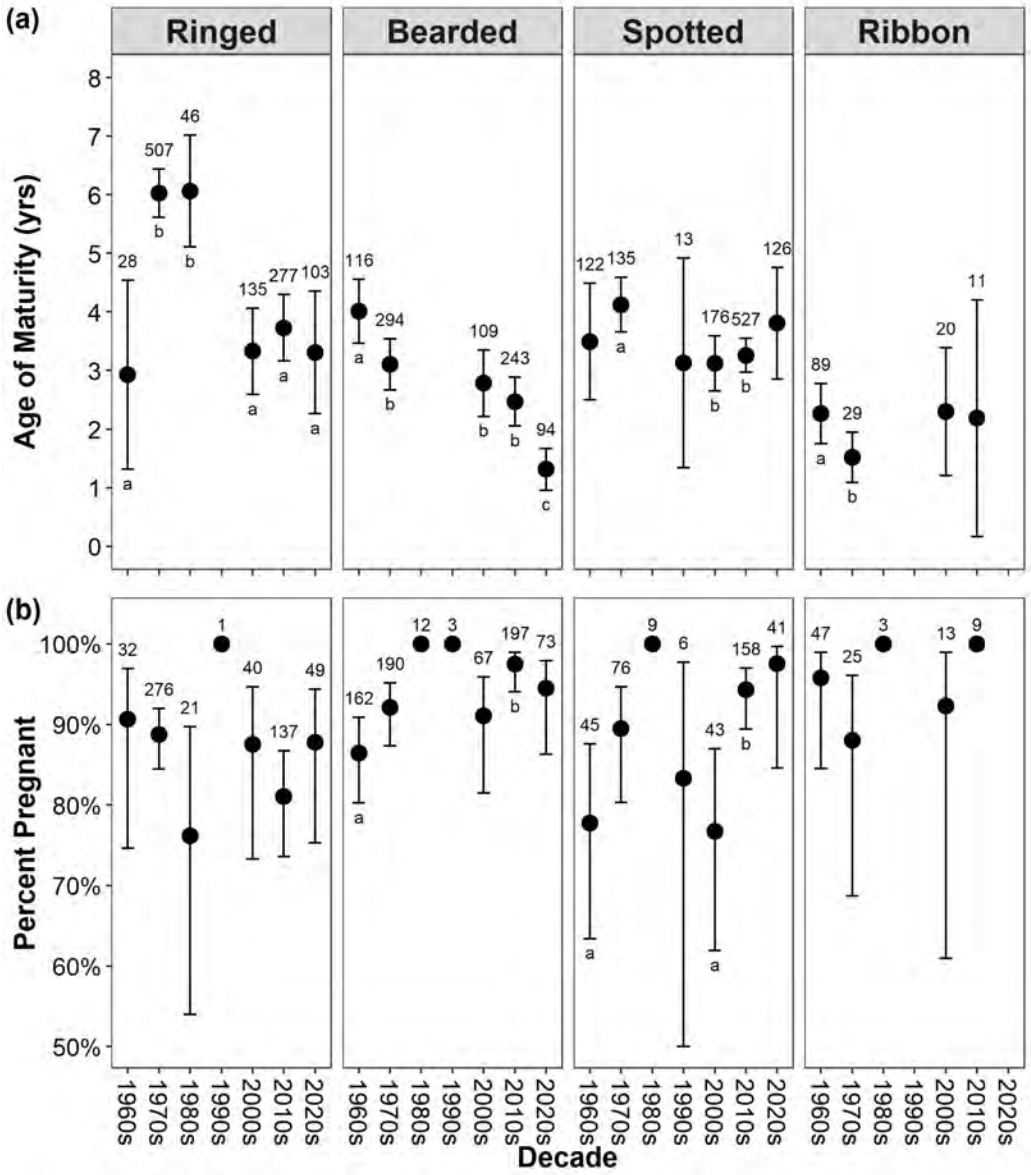

Fig. 4. (a) Mean age of maturity for ringed, bearded, spotted, and ribbon seals by decade, and (b) pregnancy rates for mature ringed, bearded, spotted, and ribbon seals by decade. The number of seals analyzed each decade is shown above the 95% confidence intervals (CIs); different letters below CIs indicate significant differences (p <0.05) and no letter indicates the decade is not significantly different from any others. For example, using the bearded seal age at maturity, the 1960s is labeled with the only "a" and therefore is significantly different (higher) from all other decades. 1970s, 2000s, and 2010s are labeled "b" and so are not significantly different from each other but are significantly lower than "a" and significantly higher than "c". 2020s is labeled "c" and therefore is significantly different (lower) from all other years. In panel (b) for some decades with low sample sizes all mature females were pregnant, therefore no CIs could be calculated. Some decades lacked data for some seal species.

Once mature, and when conditions are good, females can give birth to one pup per year (Riedman 1990). The percentage of adult females that are pregnant each decade is used to indicate good or poor reproductive decades. Pregnancy rate has remained high (>75%) for all four species throughout the study period (Fig. 4b).

Proportion of pups in the harvest

Although female body condition and pregnancy rates are currently high, and maturation is occurring at a younger age, if pups do not survive, the population will eventually decline. Females nurse their pups on the sea ice; therefore, it is important for sea ice to remain stable until pups are weaned. As sea ice becomes less stable in the spring and recedes earlier (see essay *Sea Ice*), the nursing period could become shorter, making it harder for pups to survive. Because the harvest in Alaska occurs after pups are weaned, and seals are harvested opportunistically without deference to age, we can use the proportion of pups relative to other ages in the harvest to know that pups are being born and surviving past weaning. The proportion of pups in the harvest has remained high (>40%) and increased over time for ringed, bearded, and spotted seals since the 1970s (Fig. 5).

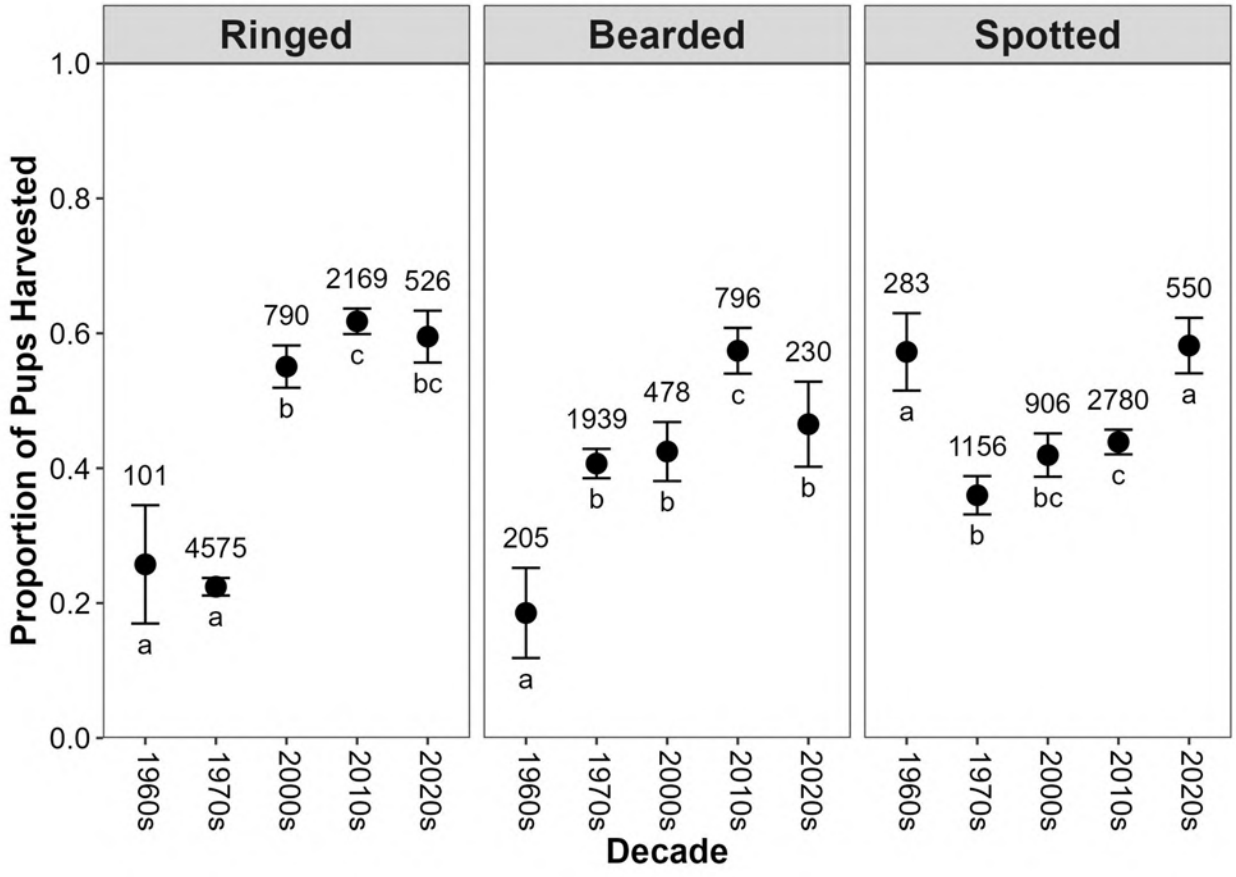

Fig. 5. The mean proportion of seal pups by species in the sampled subsistence harvest from 10 villages of the Alaskan Bering, Chukchi, and Beaufort Seas during the 1960s, 1970s, 2000s, 2010s, and 2020s (2020-23). Sample sizes of harvested ribbon seals are too low to reliably estimate the proportion of pups harvested. The number of seals analyzed each decade is listed above the 95% confidence intervals (CIs). Different letters shown below CIs designate significant differences (p <0.05). See Figure 4 for more detail on letters.

In summary, information analyzed from the ice seal subsistence harvest in Alaska indicates that all four species are as healthy and productive in the early 2020s as they have been in past decades. Stomach contents have shown some changes in diet between the 2000s and 2010s, such as fewer ringed seals consuming Arctic cod and more consuming saffron cod and other fish. Changes in diet are likely indicative of broader ecosystem changes affecting prey species composition and distributions. Despite less sea ice and potential shifts in prey availability and quality, integrated health indices such as body condition, productivity, and pup survival are stable or above average, leading us to conclude that the changes in the Pacific Arctic marine environment through 2023 have not resulted in long-term negative impacts to ice seals. Our conclusion agrees with observations from the seal hunters that provide samples; they report seals are generally healthy.

Methods and data

Samples and morphometric data were collected from seals harvested for Alaska Native subsistence purposes during 1998-99, 2000s, 2010s, and 2020-23 at communities under a biological monitoring program conducted by Alaska Department of Fish and Game (ADF&G). See Crawford et al. (2015) and Quakenbush (2020) for detailed methods. Data from this period were compared to data previously collected by ADF&G from the subsistence harvest and research cruises during 1962-69, 1970s, 1980-82, 1984-85, and 1990-91. In the analysis of body condition, we also included blubber thickness data from 1,282 ringed seals harvested near Point Hope as part of the Cape Thompson Project Chariot study (1960-61; Johnson et al. 1966).

Data for each seal included collection date, species, sex, standard length, and blubber thickness. Tissues include the stomach, female reproductive tract, and a tooth or claw for aging. Samples from all locations and seasons were pooled by decade (except for diet, which were from December-May only) to compare changes over time. Seal age was determined by counting annual growth rings in a tooth or claw. Stomach contents were identified using taxonomic keys to the lowest taxonomic level. Changes in prey categories over time were analyzed using logistic regression models. Blubber thickness was measured over the sternum between the front flippers and changes by decade were analyzed using linear mixed effects models that accounted for known sources of variability, including seasonal variation in blubber thickness, seal length, and sex. The remaining unexplained variability, also known as the model residuals, can then be plotted by decade to determine if there were periods when seals were on average thinner or fatter. Female reproductive tracts were evaluated for reproductive status and condition to evaluate productivity using changes in the age of maturity and pregnancy rate by decade. Age of maturity was estimated as the age at which 50% of females had ovulated at least once and analyzed using probit regression models (DeMaster 1978). Pregnancy rate was defined as the proportion of mature females with a corpora lutea in the year of harvest, except that seals with a corpora lutea but no fetus by 1 November were considered not pregnant. Pregnancy rate data were analyzed using logistic regression models. We assessed changes in the proportion of pups harvested using logistic regression models.

Acknowledgments

These data are available due to sample contributions by subsistence hunters from their ice seal harvests, and the support of their communities and Tribal Councils. Support is provided by the North Slope Borough Department of Wildlife Management (NSB) and the Ice Seal Committee. J. Burns, K. Frost, and the late L. Lowry established this biomonitoring program and collected and maintained data prior to

2000. Many biologists, technicians, and college interns have helped with sample collection and processing. The late W. Walker identified many fish to species using otoliths. Funding was provided by the National Oceanic and Atmospheric Administration, National Marine Fisheries Service (NMFS, Projects NA05NMF4391187, NA08NMF4390544, NA11NMF4390200, and NA22NMF4390239). Samples were collected under NMFS research permits 358-1787, 15324, 20466, and 26254 issued to ADF&G and permits 814-1899, 17350, 21386, and 26667 issued to NSB.

References

Crawford J. A., L. T. Quakenbush, and J. J. Citta, 2015: A comparison of ringed and bearded seal diet, condition and productivity between historical (1975-1984) and recent (2003-2012) periods in the Alaskan Bering and Chukchi seas. *Prog. Oceanogr.*, **136**, 133-150, https://doi.org/10.1016/j.pocean.2015.05.011.

Deary, A. L., C. D. Vestfals, F. J. Mueter, E. A. Logerwell, E. D. Goldstein, P. J. Stabeno, S. L. Danielson, R. R. Hopcroft, and J. T. Duffy-Anderson, 2021: Seasonal abundance, distribution, and growth of the early life stages of polar cod (*Boreogadus saida*) and saffron cod (*Eleginus gracilis*) in the US Arctic. *Polar Biol.*, **44**, 2055-2076, https://doi.org/10.1007/s00300-021-02940-2.

DeMaster, D. P., 1978: Calculation of the average age of sexual maturity in marine mammals. *J. Fish. Res. Board Can.*, **35**(6), 912-915, https://doi.org/10.1139/f78-148.

Florko, K. R. N., T. C. Tai, W. W. L. Cheung, S. H. Ferguson, U. R. Sumaila, D. J. Yurkowski, and M. Auger-Méthé, 2021: Predicting how climate change threatens the prey base of Arctic marine predators. *Ecol. Lett.*, **24**(12), 2563–2575, https://doi.org/10.1111/ele.13866.

Johnson, M. L., C. H. Fiscus, B. T. Ostenson, and M. L. Barbour, 1966: Marine mammals. *Environment of the Cape Thompson Region, Alaska*, N. J. Wilimovsky and J. N. Wolfe, Eds., U.S. Atomic Energy Commission, Oak Ridge, TN, 877-924.

Laws, R. M., 1956: Growth and sexual maturity in aquatic mammals. *Nature*, **178**, 193-194, https://doi.org/10.1038/178193a0.

Marsh, J. M., and F. J. Mueter, 2020: Influences of temperature, predators, and competitors on polar cod (*Boreogadus saida*) at the southern margin of their distribution. *Polar Biol.*, **43**, 995-1014, https://doi.org/10.1007/s00300-019-02575-4.

Nelson, M. A., L. T. Quakenbush, B. D. Taras, and Ice Seal Committee, 2019: Subsistence harvest of ringed, bearded, spotted, and ribbon seals in Alaska is sustainable. *Endangered Species Res.*, **40**, 1-16, https://doi.org/10.3354/ESR00973.

NOAA Fisheries, 2024a: Diseased ice seals and unusual mortality events: UMEs for ice seals in the Bering and Chukchi Seas of Alaska. Last updated by Alaska Regional Office on 08/28/2024, https://www.fisheries.noaa.gov/alaska/marine-life-distress/diseased-ice-seals-and-unusual-mortality-events#2018%E2%80%932020-unusual-mortality-event.

NOAA Fisheries, 2024b: 2018-2019 Ice Seal Unusual Mortality Event in Alaska (CLOSED): NOAA Fisheries closed the investigation into the Unusual Mortality Event affecting stranded bearded, ringed, and

spotted seals in Alaska. Last updated by Alaska Regional Office on 08/28/2024, https://www.fisheries.noaa.gov/alaska/marine-life-distress/2018-2019-ice-seal-unusual-mortality-event-alaska-closed.

Quakenbush, L., 2020: *Biological monitoring of ice seals in Alaska to determine health and status of populations-diet, disease, contaminants, reproduction, body condition, growth, and age at maturity*. Alaska Department of Fish and Game, final report to NOAA, award number NA16NMF4390029. 47 pp + appendices, https://www.adfg.alaska.gov/static/research/programs/marinemammals/pdfs/biomonitoring_biology_adfg_2020_pinniped_research_ice_seals_report.pdf.

Riedman, M., 1990: *The Pinnipeds: Seals, Sea Lions, and Walruses*. University of California Press. 439 pp.

Stevenson, D. E., and R. R. Lauth, 2019: Bottom trawl surveys in the northern Bering Sea indicate recent shifts in the distribution of marine species. *Polar Biol.*, **42**, 407-421, https://doi.org/10.1007/s00300-018-2431-1.

U.S. Federal Register, 2012a: Threatened status for the Arctic, Okhotsk, and Baltic subspecies of the ringed seal and endangered status for the Ladoga subspecies of the ringed seal; Final Rule. FR 77 (249):76706-76738 (28 December 2012). National Marine Fisheries Service, National Oceanic and Atmospheric Administration, Department of Commerce, Washington, DC.

U.S. Federal Register, 2012b: Threatened status for the Beringia and Okhotsk distinct population segments of the *Erignathus barbatus nauticus* subspecies of the bearded seal; Final Rule. FR 77 (249): 76740-76768 (28 December 2012). National Marine Fisheries Service, National Oceanic and Atmospheric Administration, Department of Commerce, Washington, DC.

November 12, 2024

The Original Researchers: Hunters are Scientists Deserving Sustained Support

https://doi.org/10.25923/af21-r537

S. Fox[1] and M. Jaypoody[1]

[1]Ittaq Heritage and Research Centre, Kangiqtugaapik (Clyde River), NU, Canada

Headlines

- Inuit hunters are the original researchers of their homelands. Observation, monitoring, and research skills are all integral parts of being a hunter or harvester.
- The Ittaq Heritage and Research Centre in Kangiqtugaapik (Clyde River), Nunavut, Canada runs the Angunasuktiit program, a full-time land-based program that teaches all aspects of hunting and harvesting to the next generations.
- Supporting the participation and leadership of Indigenous Peoples in broader Arctic research must include the sustained support of Indigenous ways of life on the land and generating knowledge.

Introduction

Over the history of Arctic research, Indigenous Peoples have not been equitably included and call for systemic change (Ellam Yua et al. 2022). In Canada, we have seen growing recognition and action toward increasing Indigenous self-determination in research (e.g., ITK 2018; Wilson et al. 2020).

One of the most exciting areas of change and action is at the community level, where there is an increase in projects and programs demonstrating new directions in Indigenous science and collaboration (e.g., Simonee et al. 2021; Ljubicic et al. 2022). At the Ittaq Heritage and Research Centre (Ittaq) in Kangiqtugaapik, Nunavut, Canada, our mission is to support Inuit self-determination through the promotion of Inuit knowledge, language, and culture, and building a more Inuit-centered economy (https://ittaq.ca/). Through our core themes of Inuit-led research, culture and heritage, multimedia, and land programming, we advance our mission. Here, we focus on our flagship land program, Angunasuktiit ("hunters"). This program demonstrates how Inuit hunters are, among their many roles, the original researchers of their homelands and deserve to be recognized and supported so they cannot only benefit their communities with critical observations and knowledge, but the wider scientific community as well.

The Angunasuktiit Program

The Angunasuktiit Program is a full-time land-based program based out of Ittaq, a division of Ilisaqsivik Society, an Inuit-led not-for-profit located in Kangiqtugaapik, Nunavut (Fig. 1). In this year-round program, five expert Inuit hunter-instructors take community participants on the land to gain knowledge and learn skills, language, and values related to all aspects of hunting and harvesting and being on the land. Participants range in age from 14 years on up and learn skills such as hunting, sea ice travel, navigation, and tool making. Learning how to observe the environment is core and constant, a critical

skill taught and learned in all activities. To be safe and successful on the land, keen observation and monitoring skills are essential. Mastering observational skills, and practicing them consistently over time and space, is part of being a hunter. Some ways the Angunasuktiit make environmental observations include using cutting edge technologies such as custom-programmed InReach devices, digital photos and video, and drones, and they assist with maintaining the community-based weather station network (Fig. 1).

Fig. 1. Location map of Kangiqtugaapik (Clyde River, orange dot), Nunavut, Canada and station locations (green dots) for the Kangiqtugaapik Weather Station Network (www.clyderiverweather.org).

Here, we highlight the research role of Angunasuktiit and the observations and monitoring they practice based on their own knowledge and expertise as hunters. This knowledge and these observations cannot be separated from the people and the land they come from. We emphasize that while the wider scientific community has increasingly recognized the observations and knowledge of hunters, at the same time, there must be more concrete recognition, and on the hunters' terms. Increased funding investments from the scientific community into hunters' activities, including programs like the Angunasuktiit, would support the creation, on-going transmission, and sharing of the knowledge that western science is seeking to learn from.

Hunters are the original Arctic researchers

Hunters have always researched their environment. If we define it in western science terms, hunters *are* scientists, and Inuit knowledge and hunting practices hold many of the elements of scientific inquiry as most visiting scientists would understand them, including observation, data collection, evaluation and analysis, communication, and adapting tools, equipment, and practices (Pfeifer 2018). While hunters are scientists, at the same time, we need to see beyond considering their knowledge and expertise in comparison to western scientific models. We must understand that this science is its own way of

knowing. Hunters are highly educated professionals with expertise in a living system of knowledge (Fig. 2).

Fig. 2. Angunasuktiit teach all aspects of hunting, harvesting, and being on the land. Photo: Apiusie Apak.

When the knowledge of hunters and other Indigenous experts is included in western science-led projects and writing, observations are usually distilled into statements that fit a western scientific framework of understanding and communication. For example, observations about changes in ice, weather, winds, storms, and vegetation are usually separated out, used alongside western science and often presented as complementary evidence that advances our collective understanding of climate and environmental change. This approach has brought some recognition to Indigenous knowledge in the Arctic research space, but it separates the knowledge from the people, land, language, and methods that generated it. In our experience, this means that much of the knowledge and understanding behind the observations has been left out. There needs to be space, time, and funding to support hunters and Indigenous experts to practice, apply, and share their own knowledge according to their own methods, in their own language, and for their own purposes. This includes knowledge closely tied to things such as original Inuit laws, Inuit worldview, and values.

Watching the Angunasuktiit work, we can see that their knowledge, and the knowledge they are teaching to the next generations, is founded on relationships. The hunters have deep, close relationships with the environment, with the animals, and with each other. Knowledge is a practice. It cannot be separated from the people, culture, language, and land, and it cannot always be adequately expressed in western scientific terms. For example, each day the Angunasuktiit usually start with observing the weather and the conditions (ocean, ice, land, travel routes, etc.). They consider the season, different locations, the recent patterns and changes in the environment and in the animals and compare those to previous years. They decide and plan where they will go, why, when, and with whom, considering everything from safety to equipment needs, to what is happening in the community, to where participants may be within their learning journey. On the land, teaching and learning includes the vast technical skills of travel and harvesting (e.g., safe ice travel, navigation, observing animals, proper harvesting techniques, butchering, food preparation and transport). Through their own observations and methods, they log weather, ice, and trail conditions. Over time, and using their expert analysis, this information provides unparalleled environmental monitoring. Their observing, teaching, and learning on the land also includes so much more, such as the meaning and history of placenames and of families

where they are travelling, visiting old travel routes or camping areas and describing previous ways of living or stories of what happened there, practicing proper terminology, traditions related to treatment of animals, the catch, and sharing of food. These are only a few examples, but all and more go into the construction, sharing, practice, and understanding of knowledge. We have seen youth participants in the program learn through observing and doing and transform from brand new learners to increasingly independent hunters, providing for their families and community. And it is not only youth who benefit, but adults and Elders are part of the program, with opportunities to visit places they may have not been in many years after moving into the community. All these aspects of being on the land are part of their research process and critical aspects of the observations of these knowledge-holders. We need to recognize that the ways of life and activities those observations come from need to be supported and sustained so knowledge can continue in future generations (Fig. 3).

Fig. 3. Teaching and learning about hunting includes a research process. Also, hunting not only involves the harvest of animals, but all of the related knowledge, skills, and methods that go with being on the land, including tool making, maintaining equipment, fixing machinery, and activities like cabin building. Photo: Mike Jaypoody.

Sustained support for hunters and their way of life is sustained support for Arctic research

Arctic Indigenous hunters and other Indigenous expert knowledge-holders have been sharing their knowledge with the broader Arctic scientific community for decades (e.g., ACIA 2005; Reed et al. 2024). In our experience, the Angunasuktiit and other harvesters we work with have been open and generous

with sharing their knowledge, observations, and expertise with visiting scientists when they have an opportunity to build trusting research relationships and there are clear benefits for their community. At the same time, there is a deep interest in strengthening Inuit practices in research, practices that are directly tied to consistent time and relationships on the land. It is all tied together. For Inuit communities and knowledge-holders to continue to build meaningful participation and leadership in broader Arctic research when they choose, they need to continue to build their own knowledge and experience, with full control, expression, and on their own terms.

Programs like the Angunasuktiit are training the next generations of hunters, and in turn, the next generations of researchers. Indigenous Guardians programs, Elder-youth camps, and other land-based initiatives are similar (e.g., see the Indigenous Leadership Initiative and the Young Hunters Program, Aqqiumavvik Society). Since hunters are researchers, then programs like the Angunasuktiit are research programs. These initiatives depend on and deserve adequate and sustained support from research funding agencies regarding infrastructure, funding, and recognition as critical sources of knowledge production, teaching, and learning. More recognition of the importance of maintaining full-time, consistent access to the land in the context of supporting long-term Arctic research and monitoring may open doors to additional research funding support. If this is done in a way where resources and authority (e.g., regarding research methods, program design, and data sovereignty) are kept in the hands of hunters and communities, then we will continue to make transformation in the research world that will see Inuit and Indigenous knowledge lead and thrive.

For more information on the Angunasuktiit, please visit the Ittaq website and view videos about the program online (shorter video and longer video).

References

ACIA, 2005: Arctic Climate Impact Assessment. *ACIA Overview report*, Cambridge University Press, 1020 pp, accessed 8 September 2024, https://www.amap.no/documents/doc/arctic-arctic-climate-impact-assessment/796.

Ellam Yua, J. Raymond-Yakoubian, R. A. Daniel, and C. Behe, 2022: A framework for co-production of knowledge in the context of Arctic research. *Ecol. Soc.*, **27**(1), 34, https://doi.org/10.5751/ES-12960-270134.

ITK, 2018: National Inuit strategy on research. Inuit Tapiriit Kanatami (ITK), Ottawa, accessed 4 September 2024, https://www.itk.ca/wp-content/uploads/2018/04/ITK_NISR-Report_English_low_res.pdf.

Ljubicic, G. J., R. Mearns, S. Okpakok, and S. Robertson, 2022: Nunami iliharniq (Learning from the land): Reflecting on relational accountability in land-based learning and cross-cultural research in Uqšuqtuuq (Gjoa Haven, Nunavut). *Arctic Sci.*, **8**(1), 252-291, https://doi.org/10.1139/as-2020-0059.

Pfeifer, P., 2018: From the credibility gap to capacity building: An Inuit critique of Canadian Arctic research. *Northern Public Affairs*, **6**(1), 29-34.

Reed, G., and Coauthors, 2024: For Our Future: Indigenous Resilience Report. *Canada National Climate Assessment*, Ottawa, Ontario, accessed 8 September 2024,

https://changingclimate.ca/site/assets/uploads/sites/7/2024/03/Indigenous-Resilience-Report_Final_EN.pdf.

Simonee, N., J. Alooloo, N. A. Carter, G. Ljubicic, and J. Dawson, 2021: Sila Qanuippa? (How's the weather?): integrating Inuit Qaujimajatuqangit and environmental forecasting products to support travel safety around Pond Inlet, Nunavut, in a changing climate. *Weather Climate Soc.*, **13**, 933-962, https://doi.org/10.1175/WCAS-D-20-0174.1.

Wilson, K. J., T. Bell, A. Arreak, B. Koonoo, D. Angnatsiak, and G. J. Ljubicic, 2020: The Sikumiut Model: Changing the role of non-Indigenous research partners in practice to support Inuit self-determination in research. *Arctic Sci.*, **6**(3), 127-153, https://doi.org/10.1139/as-2019-0021.

November 15, 2024

Authors and Affiliations

H. Alcock, Département de Géographie, Université de Montréal, Montréal, QC, Canada

K. Arndt, Woodwell Climate Research Center, Falmouth, MA, USA

T. G. Askjaer, Danish Meteorological Institute, Copenhagen, Denmark

J. J. Assmann, Department of Evolutionary Biology and Environmental Studies, University of Zurich, Zurich, Switzerland

T. J. Ballinger, International Arctic Research Center, University of Alaska Fairbanks, Fairbanks, AK, USA

L. T. Berner, School of Informatics, Computing and Cyber Systems, Northern Arizona University, Flagstaff, AZ, USA

U. S. Bhatt, Geophysical Institute, University of Alaska Fairbanks, Fairbanks, AK, USA

S. Bigalke, Department of Geography, Portland State University, Portland, OR, USA

A. Bliss, Goddard Space Flight Center, NASA, Greenbelt, MD, USA

J. E. Box, Geological Survey of Denmark and Greenland, Copenhagen, Denmark

B. Brettschneider, National Weather Service Alaska Region, NOAA, Anchorage, AK, USA

A. Bryan, Arctic Marine Mammal Program, Alaska Department of Fish and Game, Fairbanks, AK, USA

L. W. Cooper, Chesapeake Biological Laboratory, University of Maryland Center for Environmental Science, University of Maryland, Solomons, MD, USA

A. Crawford, Department of Environment and Geography, University of Manitoba, Winnipeg, MB, Canada

J. Crawford, Arctic Marine Mammal Program, Alaska Department of Fish and Game, Fairbanks, AK, USA

B. Decharme, Centre National de Recherches Météorologiques, Météo-France, Toulouse, France

C. Derksen, Climate Research Division, Environment and Climate Change Canada, Toronto, ON, Canada

D. Divine, Norwegian Polar Institute, Fram Centre, Tromsø, Norway

M. L. Druckenmiller, National Snow and Ice Data Center, Cooperative Institute for Research in Environmental Sciences, University of Colorado Boulder, Boulder, CO, USA

A. Elias Chereque, Department of Physics, University of Toronto, Toronto, ON, Canada

H. E. Epstein, Department of Environmental Sciences, University of Virginia, Charlottesville, VA, USA

E. S. Euskirchen, Institute of Arctic Biology, University of Alaska Fairbanks, Fairbanks, AK, USA; Department of Biology and Wildlife, University of Alaska Fairbanks, Fairbanks, AK, USA

G. Falvo, Center for Ecosystem Science and Society, Northern Arizona University, Flagstaff, AZ, USA

S. Farrell, Department of Geographical Sciences, University of Maryland, College Park, MD, USA

R. S. Fausto, Geological Survey of Denmark and Greenland, Copenhagen, Denmark

G. Fiske, Woodwell Climate Research Center, Falmouth, MA, USA

B. C. Forbes, Arctic Centre, University of Lapland, Rovaniemi, Finland

S. Fox, Ittaq Heritage and Research Centre, Kangiqtugaapik (Clyde River), NU, Canada

K. E. Frey, Graduate School of Geography, Clark University, Worcester, MA, USA

G. V. Frost, Alaska Biological Research, Inc., Fairbanks, AK, USA

C. Garcia, Arctic Research Program, Global Ocean Monitoring and Observing Program, NOAA, Silver Spring, MD, USA

S. Gerland, Norwegian Polar Institute, Fram Centre, Tromsø, Norway

S. J. Goetz, School of Informatics, Computing and Cyber Systems, Northern Arizona University, Flagstaff, AZ, USA

J. M. Grebmeier, Chesapeake Biological Laboratory, University of Maryland Center for Environmental Science, University of Maryland, Solomons, MD, USA

A. Gunn, CircumArctic Rangifer Monitoring and Assessment (CARMA), Whitehorse, YT, Canada

E. Hanna, Department of Geography and Lincoln Climate Research Group, University of Lincoln, Lincoln, UK

S. Hendricks, Alfred Wegener Institute, Helmholtz Centre for Polar and Marine Research, Bremerhaven, Germany

G. Hould-Gosselin, Département de Géographie, Université de Montréal, Montréal, QC, Canada

J. Hung, Woodwell Climate Research Center, Falmouth, MA, USA

M. Jaypoody, Ittaq Heritage and Research Centre, Kangiqtugaapik (Clyde River), NU, Canada

K. Joly, National Park Service, Fairbanks, AK, USA

L. Kaleschke, Alfred Wegener Institute, Helmholtz Centre for Polar and Marine Research, Bremerhaven, Germany

S. R. Karlsen, NORCE Norwegian Research Centre AS, Tromsø, Norway

A. Kholodov, Geophysical Institute, University of Alaska Fairbanks, Fairbanks, AK, USA

S. -J. Kim, Korea Polar Research Institute, Incheon, Republic of Korea

Z. M. Labe, Geophysical Fluid Dynamics Laboratory, NOAA, Princeton, NJ, USA

R. Lader, International Arctic Research Center, University of Alaska Fairbanks, Fairbanks, AK, USA

M. J. Lara, Department of Plant Biology, University of Illinois, Urbana, IL, USA; Department of Geography, University of Illinois, Urbana, IL, USA

B. D. Loomis, Goddard Space Flight Center, NASA, Greenbelt, MD, USA

E. López-Blanco, Department of Ecoscience and Arctic Research Centre, Aarhus University, Roskilde, Denmark

K. Luojus, Arctic Research Centre, Finnish Meteorological Institute, Helsinki, Finland

M. J. Macander, Alaska Biological Research, Inc., Fairbanks, AK, USA

R. Í. Magnússon, Plant Ecology and Nature Conservation Group, Wageningen University & Research, Wageningen, Netherlands

K. D. Mankoff, Goddard Institute of Space Studies, NASA, New York, NY, USA; Autonomic Integra, New York, NY, USA

L. Manzo, Kivalliq Inuit Association, Rankin Inlet, NU, Canada

B. C. Medley, Goddard Space Flight Center, NASA, Greenbelt, MD, USA

W. N. Meier, National Snow and Ice Data Center, Cooperative Institute for Research in Environmental Sciences, University of Colorado Boulder, Boulder, CO, USA

P. M. Montesano, Goddard Space Flight Center, NASA, Greenbelt, MD, USA; ADNET Systems, Inc., Bethesda, MD, USA

T. A. Moon, National Snow and Ice Data Center, Cooperative Institute for Research in Environmental Sciences, University of Colorado Boulder, Boulder, CO, USA

T. L. Mote, Department of Geography, University of Georgia, Athens, GA, USA

H. Motrøen Gjelten, Norwegian Meteorological Institute, Oslo, Norway

L. R. Mudryk, Climate Research Division, Environment and Climate Change Canada, Toronto, ON, Canada

S. M. Natali, Woodwell Climate Research Center, Falmouth, MA, USA

C. S. R. Neigh, Goddard Space Flight Center, NASA, Greenbelt, MD, USA

J. Olnes, Arctic Marine Mammal Program, Alaska Department of Fish and Game, Fairbanks, AK, USA

J. E. Overland, Pacific Marine Environmental Laboratory, NOAA, Seattle, WA, USA

J. Pellissey, Wek'èezhìi Renewable Resources Board, Yellowknife, NT, Canada

D. Perovich, Thayer School of Engineering, Dartmouth College, Hanover, NH, USA

A. Petty, Earth System Science Interdisciplinary Center, University of Maryland, College Park, MD, USA

G. K. Phoenix, School of Biosciences, University of Sheffield, Sheffield, UK

K. Poinar, University at Buffalo, Buffalo, NY, USA

S. Potter, Woodwell Climate Research Center, Falmouth, MA, USA

L. Quakenbush, Arctic Marine Mammal Program, Alaska Department of Fish and Game, Fairbanks, AK, USA

R. Ricker, NORCE Norwegian Research Centre, Tromsø, Norway

B. Rogers, Woodwell Climate Research Center, Falmouth, MA, USA

V. Romanovsky, Geophysical Institute, University of Alaska Fairbanks, Fairbanks, AK, USA

D. Russell, CircumArctic Rangifer Monitoring and Assessment (CARMA), Whitehorse, YT, Canada

E. A. G. Schuur, Center for Ecosystem Science and Society, Northern Arizona University, Flagstaff, AZ, USA

M. C. Serreze, National Snow and Ice Data Center, Cooperative Institute for Research in Environmental Sciences, University of Colorado Boulder, Boulder, CO, USA

B. E. Smith, University of Washington, Seattle, WA, USA

O. Sonnentag, Département de Géographie, Université de Montréal, Montréal, QC, Canada

R. Stimmelmayr, North Slope Borough, Department of Wildlife Management, Utqiaġvik, AK, USA; Institute of Arctic Biology, University of Alaska, Fairbanks, AK, USA

L. V. Stock, Cryospheric Sciences Laboratory, Goddard Space Flight Center, NASA, Greenbelt, MD, USA

M. Tedesco, Lamont-Doherty Earth Observatory, Columbia Climate School, Columbia University, Palisades, NY, USA

R. L. Thoman, Alaska Center for Climate Assessment and Policy, University of Alaska Fairbanks, Fairbanks, AK, USA; International Arctic Research Center, University of Alaska Fairbanks, Fairbanks, AK, USA

X. Tian-Kunze, Alfred Wegener Institute, Helmholtz Centre for Polar and Marine Research, Bremerhaven, Germany

M. -L. Timmermans, Department of Earth and Planetary Sciences, Yale University, New Haven, CT, USA

H. Tømmervik, Norwegian Institute for Nature Research, FRAM – High North Research Centre for Climate and the Environment, Tromsø, Norway

J. Tulagak, Kivalliq Inuit Association, Rankin Inlet, NU, Canada

A. -M. Virkkala, Woodwell Climate Research Center, Falmouth, MA, USA

C. Waigl, University of Alaska Fairbanks, Fairbanks, AK, USA

D. A. Walker, Institute of Arctic Biology, University of Alaska Fairbanks, Fairbanks, AK, USA

J. E. Walsh, Alaska Center for Climate Assessment and Policy, University of Alaska Fairbanks, Fairbanks, AK, USA; International Arctic Research Center, University of Alaska Fairbanks, Fairbanks, AK, USA

M. Wang, Cooperative Institute for Climate, Ocean, and Ecosystem Studies, University of Washington, Seattle, WA, USA; Pacific Marine Environmental Laboratory, NOAA, Seattle, WA, USA

M. Webster, Polar Science Center, Applied Physics Laboratory, University of Washington, Seattle, WA, USA

A. V. Whiting, Native Village of Kotzebue, AK, USA

D. Yang, Environmental Sciences Division and Climate Change Science Institute, Oak Ridge National Laboratory, Oak Ridge, TN, USA